CROSS-LINKED POLYBENZIMIDAZOLE MEMBRANES FOR HIGH TEMPERATURE PEM FUEL CELLS

A THESIS SUBMITTED TO

THE GRADUATE SCHOOL OF NATURAL AND APPLIED SCIENCES

OF

MIDDLE EAST TECHNICAL UNIVERSITY

BY

YAĞMUR ÖZDEMİR

IN PARTIAL FULLFILMENTS OF THE REQUIREMENTS

FOR

THE DEGREE OF MASTER OF SCIENCE

IN

POLYMER SCIENCE AND TECHNOLOGY

JUNE 2018

Approval of the thesis:

CROSS-LINKED POLYBENZIMIDAZOLE MEMBRANES FOR HIGH TEMPERATURE PEM FUEL CELLS

submitted by **YAĞMUR ÖZDEMİR** in partial fulfillment of the requirements for the degree of **Master of Science in Polymer Science and Technology Department, Middle East Technical University** by,

Prof. Dr. Halil Kalıpçılar
Dean, Graduate School of **Natural and Applied Sciences** _____

Prof. Dr. Necati Özkan
Head of Department, Supervisor, **Polymer Science and Technology** _____

Assoc. Prof. Dr. Yılser Devrim
Co-Supervisor, **Energy Systems Eng. Dept., Atılım University** _____

Examining Committee Members:

Prof. Dr. Göknur Bayram
Chemical Engineering Dept., METU _____

Prof. Dr. Necati Özkan
Polymer Science and Technology Dept., METU _____

Assoc. Prof. Dr. Yılser Devrim
Energy Systems Engineering Dept., Atılım University _____

Prof. Dr. Cevdet Kaynak
Metallurgical and Materials Engineering Dept., METU _____

Assoc. Prof. Dr. Can Özgür Çolpan
Mechanical Engineering Dept., Dokuz Eylül University _____

Date: 05.06.2018

I hereby declare that all information in this document has been obtained and presented in accordance with academic rules and ethical conduct. I also declare that, as required by these rules and conduct, I have fully cited and referenced all material and results that are not original to this work.

Name, Last name: Yağmur Özdemir

Signature:

ABSTRACT

CROSS-LINKED POLYBENZIMIDAZOLE MEMBRANES FOR HIGH TEMPERATURE PEM FUEL CELLS

Yağmur Özdemir,

M.S., Department of Polymer Science and Technology

Supervisor: Prof. Dr. Necati ÖZKAN

Co-Supervisor: Assoc. Prof. Dr. Yılser DEVRİM

June 2018, 107 pages

Literature studies have shown that it is desirable to increase operation temperature of Proton Exchange Membrane Fuel Cells (PEMFCs) due to the reasons like reduced fuel impurity sensitivity, fast electrode kinetics, simple thermal and water management. However, during fuel cell operation at high temperatures, the PEM suffers from inevitable leaching out of the doped acid, which can have deteriorating effect on the membrane performance. Thus, there is always a need to minimize this problem by making ways so that the PBI based membrane can retain sufficient acid even at elevated temperatures.

In this study, developing cross-linked PBI membranes for High Temperature PEMFC (HT-PEMFC) membranes with enhanced acid retention capability and better HT-PEMFC performance is the primary goal.

Significant progress was made regarding the understanding of polybenzimidazole (PBI) chemistry. Extensive work has been conducted concerning preparation and characterization of covalently cross-linked PBI

membranes. PBI membranes cross-linked by BADGE, DBpX, EGDE and TPA were prepared and their properties and performances were studied comperatively along with pristine PBI membrane. Membranes were characterized using acid doping, and acid leaching, proton conductivity, extraction in DMAc, SEM, TGA, and FTIR analyses in order to investigate the influences of cross-linking. The membranes prepared with TPA, BADGE and DBpX were tested in a single cell HT-PEMFC test unit. The membranes prepared with EGDE cross-linker was not studied further after the observation of nonpromising results. HT-PEMFC tests were conducted with dry air and H_2 as reactants, at 165^0C. The pristine PBI membrane based MEA reached to 0.085 $W.cm^{-2}$ maximum power density and 0.081 $A.cm^{-2}$ current density at 0.6 V. PBI-TPA-5 has shown the poorest performance among all the membranes with 0.051 $W.cm^{-2}$ maximum power density and 0.048 $A.cm^{-2}$ current density. PBI-DBpX-3 membrane gave 0.106 $W.cm^{-2}$ power density and 0.100 $A.cm^{-2}$ current density. The current density for PBI-BADGE-5 was found to be 0.121 $A.cm^{-2}$ and maximum power density was determined as 0.123 $W.cm^{-2}$. This is the highest performance obtained in this study.

PBI-BADGE membranes were further investigated in order to determine the influence of cross linker content. Two additional sets of membranes with different cross linker content (2.5 and 7.5%) were prepared, characterized and tested. PBI-BADGE-7.5 showed maximum power density of 0.019 $W.cm^{-2}$, while PBI-BADGE-2.5 showed maximum power density of 0.027 $W.cm^{-2}$. After these results, PBI-BADGE-5 was found as the best performing membrane.

Keywords: Polybenzimidazole, Fuel Cell, Cross-linked membrane, PEM, High Temperature PEMFC

ÖZ

YÜKSEK SICAKLIK PEM YAKIT PİLLERİ İÇİN ÇAPRAZ BAĞLI POLİBENZİMİDAZOL MEMBRANLAR

Yağmur Özdemir,

Yüksek Lisans, Polimer Bilim ve Teknolojisi Departmanı

Tez Yöneticisi: Prof. Dr. Necati Özkan

Ortak Tez Yöneticisi: Assoc. Prof. Dr. Yılser DEVRİM

Haziran 2018, 107 sayfa

Son yıllarda yapılan literatür araştırmaları göstermiştir ki, Polimer Elektrolit Membran Yakıt Pillerinde (PEMYP) operasyon sıcaklığının arttırılması yakıt safsızlığına daha yüksek tolerans, iyileştirilmiş elektrot kinetiği, kolaylaştırılmış su ve ısı yönetimi gibi avantajlar sağlamaktadır. Ancak yüksek sıcaklık çalışmalarında, membranların kaçınılmaz bir şekilde asit kaybına uğradığı ve bu sebeple yüksek sıcaklıkta performans kaybının yaşandığı gözlemlenmiştir. Dolayısıyla, yüksek sıcaklıklarda asit kaybının engellenmesi için yeni yöntemlerin geliştirilmesi bir gereklilik halini almıştır. Bu çalışmada, yüksek sıcaklık PEMYP'ler (YS-PEMYP) için geliştirilmiş özelliklere sahip çapraz bağlanmış PBI bazlı membranların hazırlanması amaçlanmıştır. Bu özelliklerin başında düşük asit kayıp oranları ve yüksek YS-PEMYP performansı sayılabilir.

Çapraz bağlanmış polibenzimidazol membranlar bu tez kapsamında geliştirilmiş ve polibenzimidazol kimyasının anlaşılması açısından önemli gelişmeler kaydedilmiştir. Bu çalışmada, BADGE, DBpX, EGDE ve TPA kullanılarak hazırlanan kovalent çapraz bağlanmış PBI bazlı membranlar performansları ve diğer özellikleri açısından incelenmiş ve karşılaştırılmıştır. Membran karakterizasyonu için asit yükleme, asit kaybı, proton iletkenlik, DMAc içinde çözülme, SEM, TGA, ve FTIR analizleri yürütülmüştür ve çapraz bağlanmanın etkisi analiz edilmiştir. TPA, BADGE ve DBpX çapraz bağlayıcıları ile hazırlanan membranlar tek hücreli YS-PEMYP test istasyonunda test edilmiştir. EGDE çapraz bağlayıcısı ile hazırlanan membran, karakterizasyonlar sonucunda yetersiz bulunduğu için yakıt pili testlerinde kullanılmamıştır. YS-PEMYP testlerinde kuru H_2 ve hava gazları kullanılarak 165^0C'de gerçekleştirilmiştir. PBI membran 0.6 V'da sırasıyla 0.085 W.cm^{-2} maksimum güç yoğunluğuna ve 0.081 A. cm^{-2} akım yoğunluğuna ulaşmıştır. PBI-TPA-5 tüm membranlar içindeki en düşük performansı gösteren membran olmuştur. 0.6 V'da 0.051 W.cm^{-2} maksimum güç yoğunluğu ve 0.048 A.cm^{-2} akım yoğunluğuna ulaşabilmiştir. PBI-DBpX-3 membranı ise 0.106 W.cm^{-2} maksimum güç yoğunluğu ve 0.100 A.cm^{-2} akım yoğunluğuna ulaşarak en yüksek ikinci performansı göstermiştir. Bu çalışmada elde edilen en yüksek akım, 0.121 A.cm^{-2}, ve güç yoğunluğu, 0.123 W.cm^{-2} , PBI-BADGE-5 membran ile elde edilmiştir.

Çapraz bağlayıcı etkisinin incelenmesi amacı ile ağırlıkça % 7.5 ve % 2.5 BADGE çapraz bağlayıcısı kullanılarak ikinci bir membran seti hazırlanarak yakıt pili performansları belirlenmiştir. PBI-BADGE-7.5 ve PBI-BADGE-2.5 membranlarının sırasıyla 0.019 W.cm^{-2} ve 0.027 W.cm^{-2} güç yoğunluklarına ulaştığı gözlemlenmiştir. Bu testler sonucunda, PBI-BADGE-5 membranın yüksek sıcaklık yakıt pili uygulamalarında en iyi performansı gösterdiği belirlenmiştir.

Anahtar Kelimeler: Polibenzimidazol, Yakıt Pili, Çapraz bağlı membran, PEM, Yüksek Sıcaklık PEM Yakıt Pili

To My Family

ACKNOWLEDGMENTS

The author wishes to express her deepest gratitude to her supervisor Prof. Dr. Necati Özkan and cosupervisor Assoc. Prof. Dr. Yılser Devrim for their guidance, advice, criticism, encouragements and insight throughout the research.

The author would also like to thank Prof. Dr. İnci Eroğlu for her suggestions and comments.

Special thanks to the TEKSİS Company (to Hüseyin Devrim, Kübra Pehlivanoğlu and Ömer Erdemir) for their support and preparing MEAs. Also the author would like to thank to the lab collegues Yağmur Budak and Nurhan Öztürk for their support and friendship.

This study was supported by The Scientific and Technological Research Council of Turkey (TUBITAK) under project TUBITAK 1001-214M301. The author gratefully acknowledges TEKSIS (METU Technopolis, TURKEY) for their support during MEA preparation. Some of the characterizations (SEM, thermal anlysis, and mechanical testing**)** of the polymer membranes were carried out in Central Laboratory at Middle East Technical University.

TABLE OF CONTENTS

ABSTRACT v
ÖZ vii
ACKNOWLEDGMENTS x
LIST OF FIGURES xiii
LIST OF TABLES xvi
LIST OF ABBREVIATIONS xvii
CHAPTERS
1. INTRODUCTION 1
1.1. Fuel Cells: History and Applications 1
1.2. Mechanism of Fuel Cell Operation 5
1.3. Types of Fuel Cells, an introduction to PEMFC and HT-PEMFCs 6
1.4. Introduction to PBIs 8
2. PROTON EXCHANGE MEMBRANE FUEL CELLS (PEMFCS) 13
2.1. Main Components and Processes of PEMFCs 13
2.2. Operation of PEMFCs 19
2.3. Proton Exchange Membranes 26
2.4. Proton Conduction Mechanisms in PEMs 29
2.5. Acid Doped Polybenzimidazoles in High Temperature PEMFCs 31
3. EXPERIMENTAL STUDIES 37
3.1. Materials 37
3.2. Polybenzimidazole Synthesis 37
3.3. Membrane Preparation 40
3.4. Acid Doping of the Membranes 43
3.5. Preparation of Membrane Electrode Assembly 44
3.6. Characterization of PBI Polymer 44
3.7. Characterization of the Membranes 46
3.8. HT-PEMFC Performance Tests 52
4. RESULTS AND DISCUSSION 55
4.1. Characterization of the Synthesized PBI Polymer 56
4.1.2. Determination of Molecular Weight 56
4.2. Characterization of the Membranes 58

4.3. HT-PEMFC Test Results.....81
5. CONCLUSIONS AND RECOMMENDATIONS.....87
REFERENCES.....91
APPENDIX A 105
APPENDIXB……. 107

LIST OF FIGURES

FIGURES

Figure 1 First Fuel Cell, Sir William Groove's Gas Battery 2
Figure 2 Fuel cell development milestones. (Data adapted from [1])..... 3
Figure 3 Comparison of fuel cell performance with other possible energy conversion systems[3] 4
Figure 4 Conceptual operation of a fuel cell. 5
Figure 5 Fuel Cell Types [7] 6
Figure 6 Polybenzimidazole synthesis by solution polycondensation. Data retrieved from [11] 9
Figure 7 Main cell components of a PEMFC stack [30] 14
Figure 8 Schematic illustration of the ideal hydrogen-oxygen fuel cell operation. 20
Figure 9 Fuel cell polarization curve with major losses [46]. 24
Figure 10 PEMFC membrane classification according to the materials used [50]. 26
Figure 11 Chemical structures of perflourinated PEM (reprinted from [52]) 28
Figure 12 Solution Polymerization of PBI 38
Figure 13 Experimental set-up for PBI synthesis 39
Figure 14 PBI fibers and crushed PBI polymer 40
Figure 15 Schematic representation of membrane casting 42
Figure 16 Cross-linking mechanism of (a) PBI-BADGE, (b) PBI-DBpX, (c) PBI-TPA, (d) PBI-EGDE [23,25,93] 43
Figure 17 Instron 3367 tensile machine and a representative apparatus[103] 47

Figure 18 ZIVE SP2 Electrochemical Workstation 49
Figure 19 Randel's Circuit Model 50
Figure 20 Experimental set-up for proton conductivity analysis. 51
Figure 21 HT-PEMFC Test Station Set-up 54
Figure 22 ^{13}C-NMR spectra of PBI polymer 56
Figure 23 Reduced and inherent viscosity vs. concentration graphs. 57
Figure 24 The cross-sectional SEM images of the pristine PBI membrane at x2000, x5000 and x50000 magnifications (a,b,c); the EDX analysis of pristine PBI membrane (d).....59
Figure 25 The cross-sectional SEM images of thr PBI-DBpX-3 membrane at x2000, x5000 and x50000 magnifications (a,b,c); the EDX analysis of the PBI-DBpX-3 membrane (d) 60
Figure 26 The SEM cross-sectional images of the PBI-TPA-5 membrane at x2000, x5000 and x50000 magnifications (a,b,c); the EDX analysis of PBI-TPA-5 membrane (d).....61
Figure 27 The SEM cross-sectional images of the PBI-BADGE-5 membrane at x2000, x5000 and x50000 magnifications (a,b,c), the EDX analysis of PBI-BADGE-5 membrane (d).....62
Figure 28 The cross-sectional SEM images of the PBI-EGDE-5 membrane from cross-section at x2000, x5000 and x50000 magnification (a,b,c); the EDX analysis of PBI-EGDE-5 membrane (d) 63
Figure 29 TGA graph of PBI membranes with different cross-linkers 64
Figure 30 TGA graph of PBI membranes with BADGE cross-linker at different amounts.....65
Figure 31 FTIR spectrums for pristine PBI, PBI-BADGE-5, PBI-TPA-5, PBI-DBpX-3, and PBI-EGDE-5.....66
Figure 32 FTIR spectrums of pristine PBI, PBI-BADGE-2.5, PBI-BADGE-5 and PBI-BADGE-7.5.....67
Figure 33 Nyquist plot for PBI 72
Figure 34 Nyquist plot for PBI-BADGE-5 73
Figure 35 Nyquist plot for PBI-DBpX-3.....74
Figure 36 Nyquist plot for PBI-EGDE-5 75

Figure 37 Nyquist plot for PBI-TPA-5 76
Figure 38 Proton conduction by Grotthus mechanism in PBI-H3PO4 system. 79
Figure 39 The HT-PEMFC performance curves of base PBI and PBI-BADGE-5, PBI-DBpX-3, PBI-EGDE-5 and PBI-TPA-5 membranes (First set of membranes). Operating conditions: H2 and air stoichiometry of 1.5 and 2.5, respectively; H2 and air RH of 0; 1650C cell temperature 83
Figure 40 OCV values (V) of cross-linked PBI membranes (1st set of membranes) and pristine PBI membrane 83
Figure 41 The HT-PEMFC performance curves of base PBI and PBI-BADGE-5, PBI-DBpX-3, PBI-EGDE-5 and PBI-TPA-5 membranes (First set of membranes). Operating conditions: H2 and air stoichiometry of 1.5 and 2.5, respectively; H2 and air RH of 0; 165^0C cell temperature 85
Figure 42 The OCV values (V) of PBI-BADGE cross-linked membranes (2nd set of membranes) and pristine PBI membrane 85
Figure 43 Spectrum map for bond responses [128] 107
Figure 44 FTIR Spectrum of BADGE [129] 107

LIST OF TABLES

TABLES

Table 1.1. Fuel Cell Types

Table 3.1. Nomenclature of Membranes Prepared

Table 3.2. HT-PEMFC Single Cell Properties

Table 4.1. Extraction in DMAc test results for 1st set of cross-linked membranes and pristine PBI

Table 4.2. Extraction in DMAc test results for 2nd set of cross-linked membranes and pristine PBI

Table 4.3. Proton conductivity results of cross-linked PBI membranes prepared with different cross-linkers (BADGE, EGDE, TPA and DBpX) and cross- linked PBI membranes prepared with different amounts of BADGE cross-linker.

Table 4.4. Mechanical test results for PBI, PBI-DBpX-3 and PBI-BADGE-5

LIST OF ABBREVIATIONS

AFC: Alkaline Fuel Cell

DMFC: Direct Methanol Fuel Cells

PAFC: Phosphoric acid fuel cells

MCFC Molten Carbonate Fuel Cells

SOFC: Solid Oxide Fuel Cells

PEM: polymer electrolyte membrane

PEMFC: proton exchange (polymer electrolyte) membrane fuel cell

ICE: Internal Combustion Engine

CHP: Combined Heat and Power

DAB: Diaminobenzidine

DAB.4HCl.2H2O: diaminobenzidine tetrahydrochloride

DMAc: N,N-dimethylacetamide

H_3PO_4: Phosphoric Acid

BADGE: diglycidil ether bisphenol-A

DBpX: α-dibromo-p-xylene

EGDE: Ethylene glycol diglycidil ether

TPA: Terephtaldehyde

OCV: Open Circuit Voltage

EDX: Energy dispersive X-ray analysis

FTIR: Fourier transform infrared spectroscopy

GDL: gas diffusion layer

IPA: isophthalic acid

MEA: membrane electrode assembly

PBI: polybenzimidazole(poly[2,2’-(m-phenylene)-5,5’-bibenzimidazole)]

NMR: nuclear magnetic resonance

sPEEK: sulfonated polyetheretherketone

PFSA: perflorosulfonic acid

PPA: polyphosphoric acid

PVDF: polyvinylidene fluoride

RH: relative humidity

RU: repeating unit

SEM: scanning electron microscopy

TGA: thermogravimetric analysis

α: transfer coefficient [dimensionless]

ΔG: change in Gibbs free energy due to the electrochemical reaction

[J/mol]

ΔVact: activation polarization [V]

ΔVconc: concentration polarization [V]

ΔVohm: ohmic losses [V]

ηinh: inherent viscosity [dl/g]

ηint: intrinsic viscosity [dl/g]

ηred: reduced viscosity [dl/g]

ηrel: relative viscosity [dimensionless]

ηsp: specific viscosity [dimensionless]

CHAPTER 1

INTRODUCTION

1.1. Fuel Cells: History and Applications

The decomposition of water into hydrogen and oxygen was observed at the end of the 18th century by two dutchmen, Adriaan Paets van Troostwijk and Johan Rudolph Deiman. Extracting electric current by recombining oxygen and hydrogen was suggested by Sir William Groove in 1839 ,**Figure *1***. He constructed a setup, keeping hydrogen and oxygen in two different containers with a platinized electrode for each container. When he immersed it in sulphuric acid, he observed a constant current flowing between the electrodes. ‘’Gaseous Voltaic Battery’’ was the name of the device which in fact was the first fuel cell.

Many researchers studied on fuel cells in the late 19th century resulting in the better understanding of the working principles of the system, development of different types of electrodes and electrolytes. However, till the day Sir Francis T. Bacon constructed first prototype of a fuel cell in 1953, fuel cells remained without a practical application. Based on Sir Francis T. Bacon’s studies, NASA decided to use alkaline fuel cells as power generator for their Apollo missions. Apollo missions were important for a pratical application of fuel cells and many applications were done in the following years. In 1959, Herry K. Igrih used alkaline fuel cells as a power source for agricultural tractors [1].

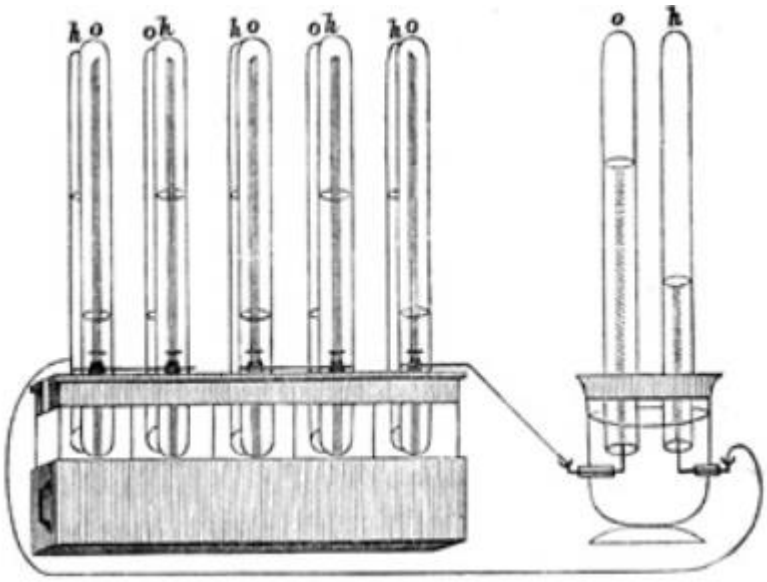

Figure 1 First Fuel Cell, Sir William Groove's Gas Battery

In its currect form, PEMFCs were invented by Willard T. Grub from General Electric Company. These cells had 50 $W.cm^{-2}$ power output and used in Gemini flights for the first time. After intense researches, PEMFCs have gained a great importance as power sources for transportation. Many researchers are trying to develop a competitive PEMFC system as an alternative to current ICE systems. In general, many different types of fuel cells are being used for different applications worldwide. Fuel cell applications can be classified as stationary and mobile applications. Combined generation for electricity and heat for smart buildings, stand-by generators or industrial facilities is the most common usage area of stationary fuel cell systems while transportation applications are more common in mobile fuel cell systems. The objective of both systems is the same, higher efficiency and lower emissions. System designs for both applications are also similar, but they differ from each other by choice of fuel, power conditioning and heat rejection [2]. In **Figure *2***. a few of the key milestones of fuel cell technology history is summarized.

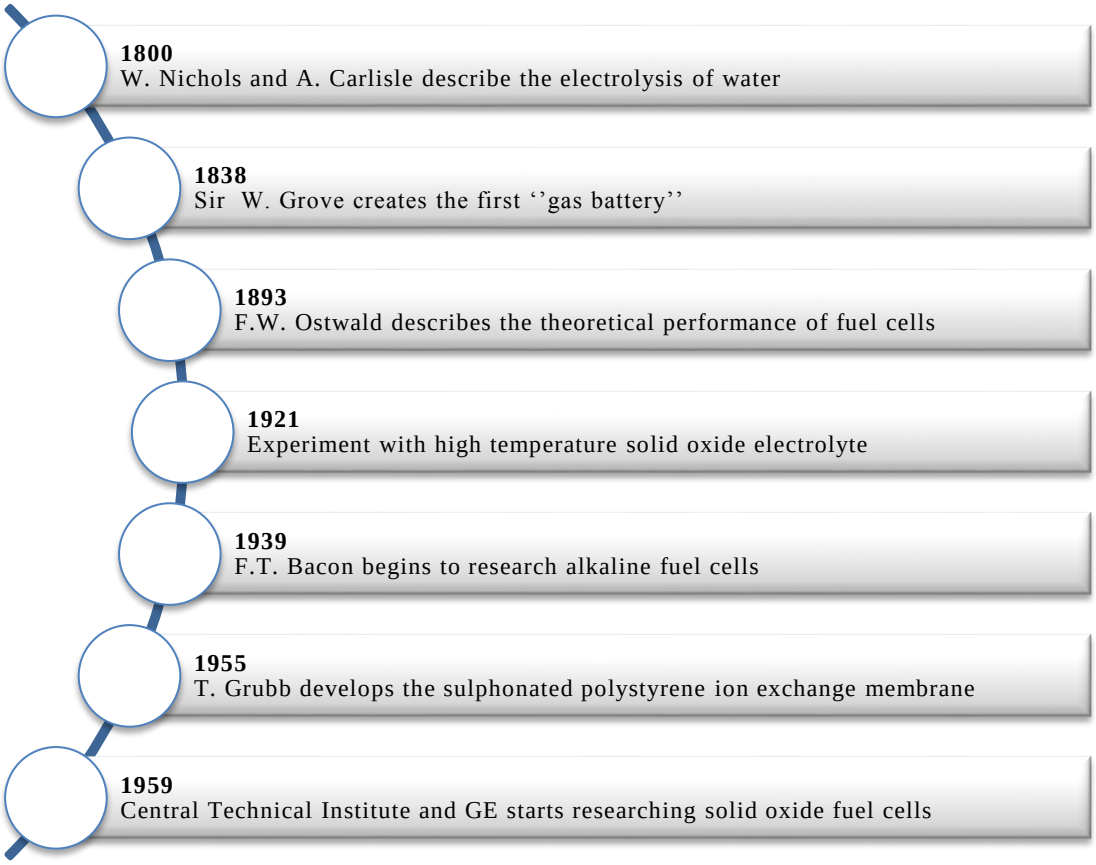

Figure 2 Fuel cell development milestones. (Data adapted from [1])

Parallel to historical development of fuel cell technology, the interest in fuel cell systems has been increased both in academic and industrial environment. As establishing hydrogen infrastructure and developing efficiently operating large scale systems are challenging, fuel cells are expected to be a part of our daily life with mobile applications first in the near future.

Fuel cell technologies have attracted much attention in recent decades owing to their high efficiencies and low emissions. Fuel cell efficiency can reach as high as 60% in electrical energy conversion and 80 % overall in co-generation of electrical and thermal energies. The efficiency of a fuel cell is normally higher than that of commercial internal combustion engines because fuel cells are not restricted by Carnot limitation. In **Figure 3** it can be seen that fuel cells

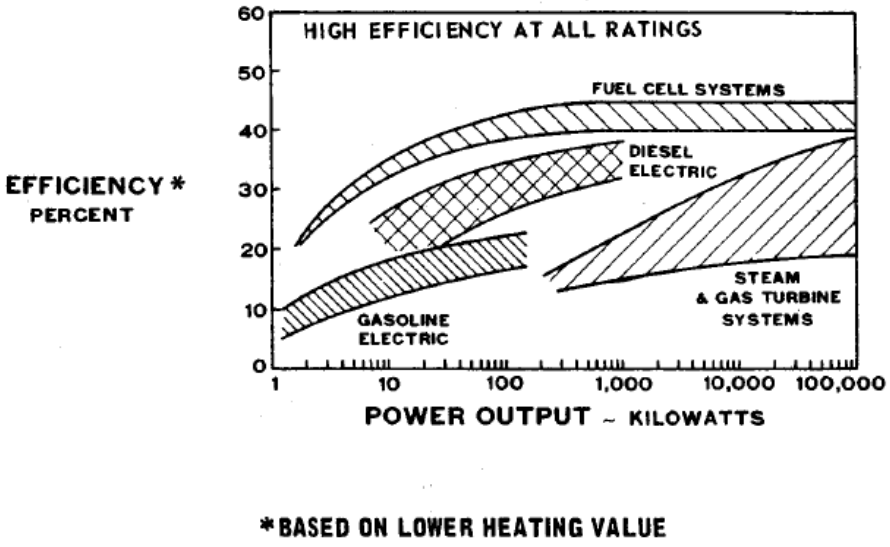

Figure 3 Comparison of fuel cell performance with other possible energy conversion systems*[3]*

have higher efficiency than any other energy conversion systems. Fuel cells use hydrogen as fuel, oxygen/air as oxidant and produce water as the final product, as a result, they can be regarded as environmentally friendly. Furthermore, they are very quiet, reliable and modular. They have no moving parts, and they can be nearly instantaneously recharged which is a significant advantage over batteries. Fuel cells can generate a wide range of power from watts to kilowatts as long as the reactant gasses are fed to the system. Thus they can be used in many applications such as busses, boats, trains, planes, scooters, bicycles etc. However, fuel cells are not panacea for every energy conversion system being used around the world. Before fuel cells are commercialized and conversion from internal combustion engines to fuel cells occurs, there are some major technical challenges that must be handled. Major limitations that are common for every fuel cell system are;

- Alternative construction methods and materials should be developed to reduce the cost of a fuel cell powered system.
- Reliability and durability must be ensured. The performance of every fuel cell system degrades within time. In order to use fuel cell systems for powering of automobiles, fuel cell must perform with high durability under harsh environmental conditions and under repetitive start up/shut down cycles.

- Suitable power density and energy output must be achieved.
- Fuel storage, generation and delivery technology must meet safety limitations if the hydrogen is used as pure.
- Sensors and online control systems for fuel cells are needed [4].

Researchers aim to address and handle the above mentioned problems one by one. Although great efforts have been made with many breakthroughs achieved, another 10-15 years is anticipated being required for fuel cells to be introduced in our daily lives in a safe, efficient and economic way.

1.2. Mechanism of Fuel Cell Operation

Fuel cells are the systems that convert chemical energy directly into electrical energy. While doing so, various interrelated and complex phenomena occur during fuel cell operation including heat/mass transfer, electrochemical reactions and ionic/electronic transport [5]. The fundamental physical structure of a fuel cell consists of an electrolyte layer sandwiched between porous anode and cathode layers. **Figure *4***. shows a schematic representation of operation basics of fuel cell with components common to all types of fuel cells.

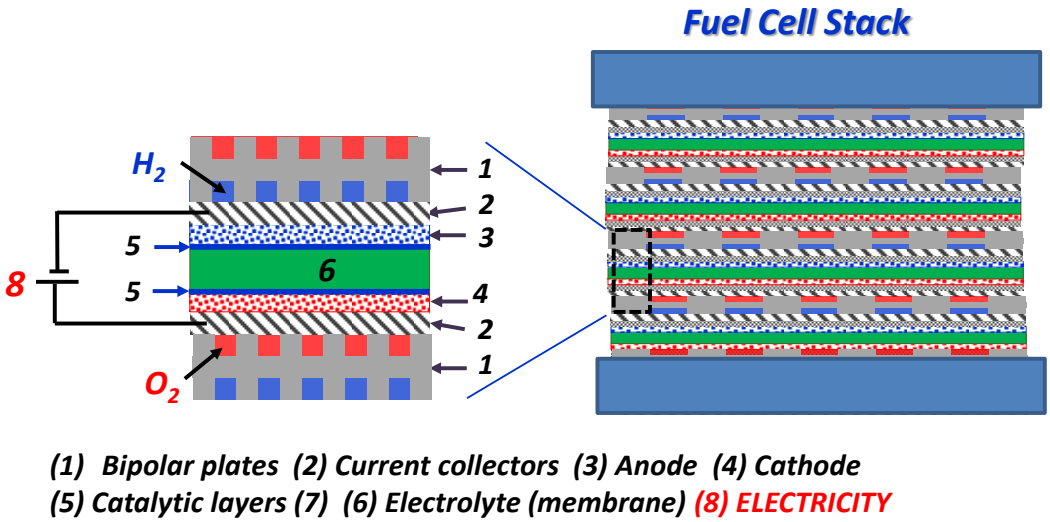

(1) Bipolar plates (2) Current collectors (3) Anode (4) Cathode
(5) Catalytic layers (7) (6) Electrolyte (membrane) (8) ELECTRICITY

Figure 4 Conceptual operation of a fuel cell.

Fuel cells function on the principals of electrolytic charge exchange between a positively charged anode plate and negatively charged cathode plate. As the fuel is hydrogen, reverse hydrolysis takes place and water and heat is produced while chemical energy is converted into electrical energy.

Separate gas or liquid phase fuel and oxidizer streams flows through the flow channels separated by electrode/electrolyte assembly. Reactants are transported to the catalyst layer mainly by diffusion. Electrochemical reactions take place at the catalyst layer to generate a current. At the anode electrode, oxidation of the fuel produces electrons that flow through the bipolar plate to the external circuit, while the ions generated migrate through the electrolyte to complete the circuit. The electrons in the external circuit drive the load and return to the cathode catalyst where they recombine with the oxidizer [4].

1.3. Types of Fuel Cells, an introduction to PEMFC and HT-PEMFCs

Fuel cells are generally categorized by the electrolyte they use. The characteristics of this material decide on the operation conditions mostly. Fuel cells can be grouped according to their operation temperature. Low temperature and high temperature. The low temperature includes PEMFC, AFC, DMFC and PAFC. High temperature fuel cells are the MCFC and SOFC. High temperature fuel cells always require a complete heat and power generation and fuel processing system [1]. **Figure 5**. summarizes the fuel cell types, operating temperatures and application areas.

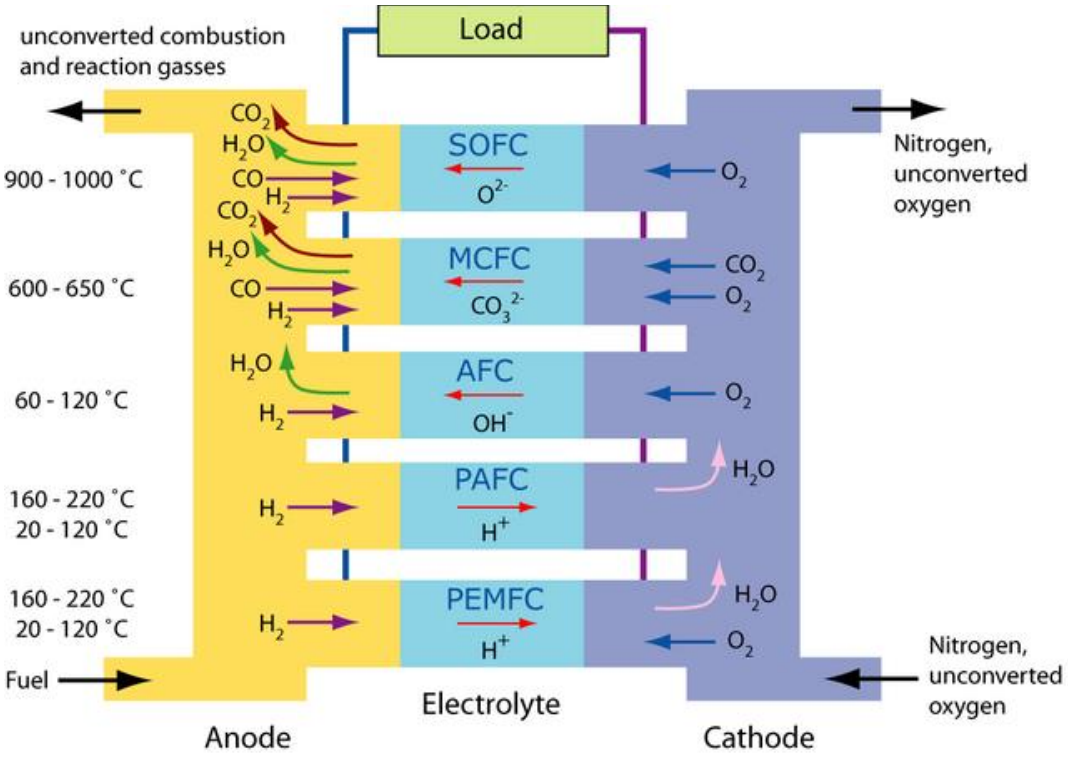

Figure 5 Fuel Cell Types [7]

As mentioned earlier, PEM fuel cells were invented in 1959 by General Electric for NASA. In 1960ies, Dupont invented a new polymer, Nafion, as a stable membrane material. It is now the most common membrane material that is used for PEMFCs. In PEMFCs, electrolyte is a polymer based membrane that is non-conducting to electrons, conducting protons only. This proton conductive membrane is sandwiched between gas diffusion electrodes that are covered by platinum catalyst. Operation temperature of PEMFCs differs as the according to the electrolyte membrane type. For the most common Nafion type membranes, operation temperature of a PEMFC is 60-80^{0}C. Low operating temperature enables fast start-up time and very little waste heat. The latter makes PEMFCs unsuitable for CHP systems. The cells are compact with simple mechanical design, have a fast response time and ease of maintenance so they are excellent candidates as a replacement for ICEs for transportation sector.

The main disadvantage of the PEMFCs is that they are intolerant to CO, thus the fuel must be pure hydrogen only. Additionally, Nafion is a polymer that conducts protons only when it is fully hydrated. Water management problem arises as a result of hydration of Nafion membrane. An increase in operating temperature from 80 to 150^{0}C leads to an increase of the water vapor pressure from 0.47 to 4.8 bars. As a result, membrane dries out and this results in loss of conductivity. Additionally, membrane softening also occurs at elevated temperatures. Cooling becomes a vital point for durable operation and this means extra auxiliary units.

HT-PEMFCs have been a significant field of research for more than two decades. A PEMFC system operates at 80^{0}C, while HT PEMFC systems can operate at elevated temperatures up to 200^{0}C. Since these temperatures are very high in engineering point of view, HT PEMFCs still belong to class of low temperature fuel cells. Even though, the temperature range for HT PEMFCs is not very high, due to the nature of polymeric materials, elevated temperatures tend to be very challenging in terms of development of chemically, thermally and mechanically stable polymer matrix. However, operating at slightly elevated temperatures has certain advantages. Key drivers for the development of high temperature PEMFCs are as follows:

- Fuel impurity is more tolerable at higher temperatures. In other words, carbon monoxide poisoning of Pt catalyst starts at higher concentrations when the temperature is higher. At 80 ^{0}C, a carbon monoxide content as low as 20 ppm (0.002 %) in the fuel stream results in a significant loss in cell performance, but at 160 ^{0}C, even 0.5–1 % carbon monoxide has only a minor effect. This enables reformer gas usage as fuel.
- Easy or no water management.
- Easy thermal management since higher temperatures compared to the surroundings makes cooling easier.
- A higher quality of waste heat [8].

1.4. Introduction to PBIs

Nafion based PEMFCs have temperature limitations as mentioned above. Polymers with high glass transition temperatures are needed for high temperature applications. PBI (poly [2,2 -(m-phenylene)- 5,5 – bi benzimidazole]), has been introduced as a possible alternative for Nafion. PBI refers to amorphous thermoplastic polymers with linear heterocyclic polymers containing benzimidazole nuclei as a repeat unit [9]. It has very high thermal stability (T_g= 425-436^{0}C), high chemical resistance, retention of stiffness and toughness. PBI is not a conducting polymer, impregnated with H_3PO_4 it becomes a good proton conductor since the phosphoric acid molecules in the membrane matrix build up a proton conducting bridge.

PBI was first synthesized by Vogel and Marvel by melt polycondensation in 1961[10]. Iwakura et al.[11] later proposed solution polycondensation for high molecular weight PBI production. Temperature control was found to be easier in the latter method since PPA was used as the solvent and reaction temperature was lower, around 170-200^{0}C. This method is an excellent route for preparation of laboratory or small scale PBI polymer.

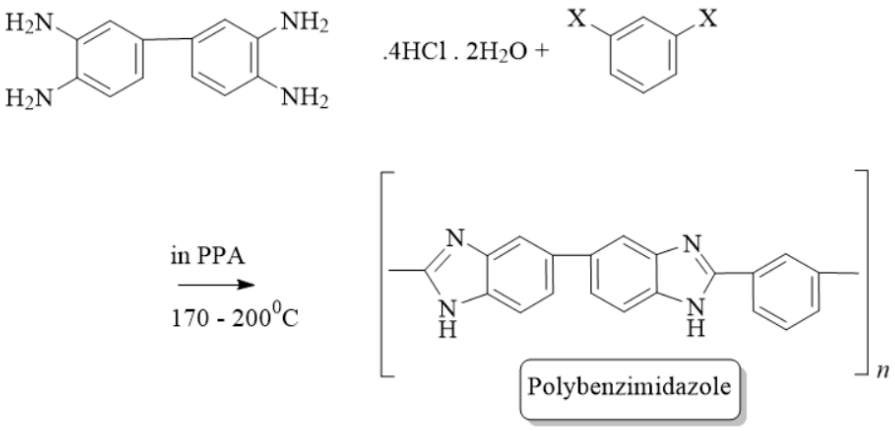

Figure 6 Polybenzimidazole synthesis by solution polycondensation. Data retrieved from [11]

*X: -COOH, -$COOCH_3$, -$CONH_2$ or –CN

PBI polymer can be solved in different organic solvents. DMAc is the one of the most common solvents used for PBI membrane preparation. Solvent casting method for membrane preparation includes solving PBI polymer in DMAc completely, then pouring the solution onto a flat surface and drying. The concentration of solution varies between 2.5-20 wt. %. When the concentration is too low, the collapse of polymer chains of PBI is not sufficient to form robust membranes, and if the solution is too concentrated, it becomes impossible to obtain a homogeneous solution [12]. H_3PO_4 doped PBI membranes were firstly used as polymer electrolyte membranes (PEMs) by Wainright et al. in 1995 [13]. Over the twenty years passed, intensive researches were conducted to improve acid doped PBIs as commercial PEMs. Acid doping level is one of the most important aspects deciding on the performance of PBI membrane as a PEM. After membrane casting completed, nonconducting PBI membranes are doped with H_3PO_4 as mentioned before in order to make the membranes proton conductive. At the end of the acid doping procedure, the amount of acid absorbed decides on the proton conductivity of the membrane, which is a key aspect in PEMFCs. As the proton conductivity gets higher, performance of the fuel cell also gets better. However, if the acid doping level of the membrane is too high, mechanical stability of the membrane decreases, which affects membrane performance adversely. Thus, acid doping level should be chosen wisely. Another significant disadvantage of H_3PO_4 doped PBI membranes is

that the acid doped in the membrane can bleed out as the membrane gets in direct contact with water or water vapor. This leads to loss of proton conductivity in the membrane and severe corrosion problems [14]. Several strategies have been developed to eliminate these problems. Cross-linking is one of the most commonly researched strategies in the literature. Studies focus on three types of cross-linking mechanism for PBI based membranes: 1) ionic cross-linking 2) covalent cross-linking and 3) organic-inorganic PBI hybrid membranes. Ionic cross-linking can be defined as preparation of polymeric acid-base blend membranes. This type of cross-linking was studied by mixing PBI with a polymeric sulfonic acid [15,16] as well as phosphonic acid [17]. Sulfonated PBI was also prepared and studied in the literature [18–20]. Covalent cross-linking refers to a procedure in which crosslinking of PBI can be achieved by thermal treatment [21] or an amide type [22] linkage between imidazole groups of the polymer. In this type of cross-linking reaction, functional group(s) crosslinkers react with the imidazole groups to form covalently crosslinked structures. In the literature, there are studies on DBpX [23], dicloromethyl phosphoric acid [24], BADGE [25,26], 1,3-bis(2,3-epoxypropoxy)-2,2-dimethylpropane [27]. These studies showed that covalently cross-linked PBIs exhibit better thermal stabilities than ionically cross-linked PBIs; however, fewer papers have reported fuel cell performance of covalently cross-linked membranes [28].

In the past two decades, there is a paucity of literature covering the performance of cross-linked PBI membranes in terms of acid leaching from the membrane and its effects on HT-PEMFC performance. In this study, cross-linked PBI membranes were prepared by blending PBI with four different cross-linkers, BADGE, EGDE, TPA and DBpX. It is pointed out that there is a paucity of literature covering the comparison of the above mentioned cross-linked membranes in terms of investigating acid leaching from the membranes and its effects on HT-PEMFC performance. In the present study, PBI membranes prepared with BADGE, EGDE, TPA and DBpX were compared in terms of their proton conductivity, acid retention capabilities, and HT-PEMFC performances. The effect of cross-linking on the thermal, morphological and mechanical properties was studied using TGA, SEM and mechanical test

measurements. Special attention was paid to measure the acid leaching percentages for temperatures between 95^0C–110^0C so that observing membrane behavior when in contact with water vapor could be possible. The conductivity of phosphoric acid doped PBI and cross-linked PBI membranes were measured at 140^0C, 165^0C and 180^0C. HT-PEMFC performance tests were carried out at 165^0C.

CHAPTER 2

PROTON EXCHANGE MEMBRANE FUEL CELLS (PEMFCS)

2.1. Main Components and Processes of PEMFCs

The PEMFC takes its name from the electrolyte it uses, which is a special type of polymer that conducts protons only. Membrane electrode assembly (MEA) is the heart of a PEMFC that combines electrodes and electrolyte, generates electric power when supplied with reactant gases. Thin gas difusion layers on each side of the electrolyte membrane are covered with electrocatalyst, on which electrochemical reactions take place [29]. The MEA is sandwiched between the collector/separator plates. In a multicell configuration, these plates connect cathode of the one cell to the anode of the adjacent cell both physically and electrically, and that is why they are also called as bipolar plates very often. Reactant gases flow through the flow fields craved on bipolar plates. The pattern of the flow fields drastically affects the performance of the PEMFC. **Figure 7** shows the main cell components and processes for PEMFCs.

Following processes take place inside the fuel cell.

1. Reactant gases flow through the channels.
2. Reactant gases diffuse through the porous media, catalyst layer.
3. Electrochemical reactions take place.
4. Protons transport through proton conductive polymer electrolyte.
5. The electrons that could not pass the proton conductive materials, conducts by means of electrically conductive cell components.
6. Water transports through proton conducting membrane mainly with two important mechanisms: drag and back diffusion.

7. Water transports from first catalyst layer and then gas diffusion layers.
8. Water droplets leaves the cell due to the excess reactant gases carrying water droplets (two-phase flow).
9. In a PEMFC, main heat transfer mechanisms are conduction due to the solid cell components, free convection with air, and forced convection including [2] cooling medium and reactant gases that fed to the cell with a certain mass flow rate.

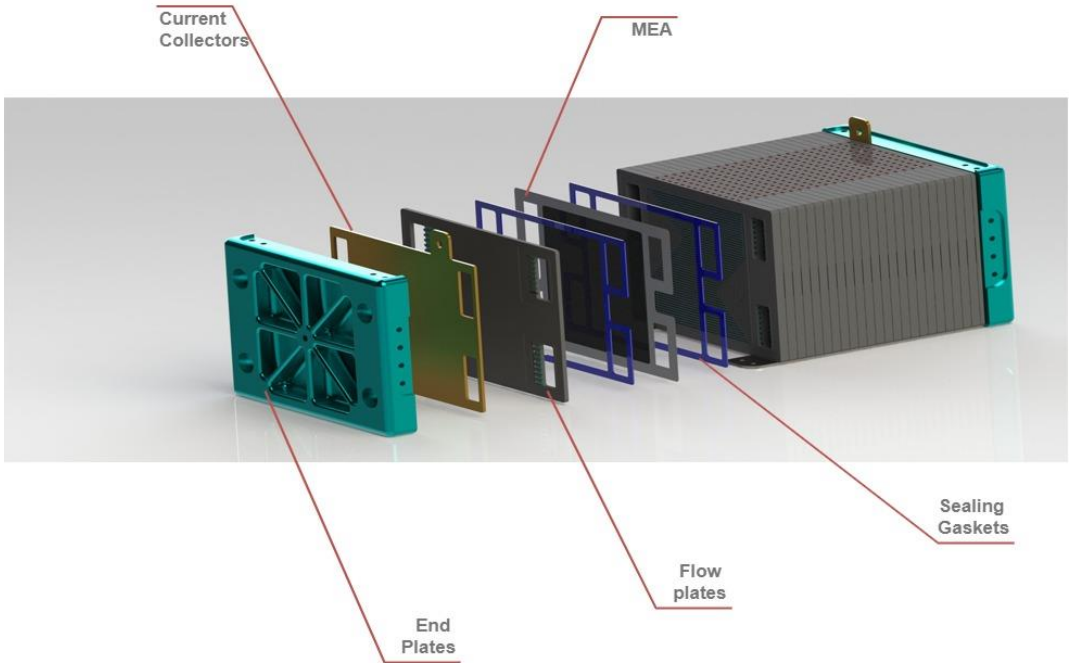

Figure 7 Main cell components of a PEMFC stack [30]

Properties of the materials used, the design of the components and the process parameters must be optimized to obtain minimum obstruction during operation of the fuel cell. All the components must be chosen according to the operation temperature and corrosive nature of the chemicals must be taken into consideration in fuel cell design. Although the fuel cell seems to be a very simple device, complicated processes takes place simultaneously. Thus, understanding the processes and the importance of the components helps to increase the fuel cell performance.

2.1.1. Electrolyte: Membrane

The strong interest in PEMFCs stems from the significant advantages of solid polymer electrolyte. Solid polymer electrolytes allow high cell and stack power densities which makes PEMFCs ideal candidates for automotive applications. The proton conducting membrane, as the "heart of the fuel cell," has to fulfill several demanding requirements simultaneously: high proton conductivity and good electrical isolation; adequate mechanical, thermal and chemical stability; low fuel permeability in order to prevent mixing of the reactant gases; and very good water management characteristics over wide temperature and humidity ranges [31]. Typically, membranes for PEMFCs are made of perfluorocarbon-sulfonic acid ionomer (PSA). The most common and best-known membrane material is Dupont's Nafion® which uses perfluoro-sulfonylfluoride ethyl-propyl-vinyl ether (PSEPVE) [2]. The conductivities of perfluorinated membranes such as Nafion® strongly depends on the hydration level of the membrane [32]. When proton exchange membranes with perfluorinated membranes operates temperatures above 80^0C, the conductivity of the membrane and thus the performance of the fuel cell drastically drops due to the dehydration. Pressurizing reactants to more than 1 to 2 bar is not practical since this would add to parasitic power requirement due to the compression. As a solution to these problems, many researches are taking place on Nafion® membranes with improved chemical and mechanical stabilities as well as higher water retention capabilities. Nafion® composites [33,34] are being studied widely. Another solution to the above-mentioned problems would be a different polymer membrane material that has better thermal stability and higher conductivity values.

Sulfonated polyethersulphone (PES) or polyetherketone (SPEEK) are some alternative materials for PEMFCs [35]. Nanocomposites with different matrix polymers such as sulfonated polysulfone/titanium dioxide membranes [36], and phosphoric acid doped polybenzimidazole membranes that can operate up to 200^0C are the new focuses of the field.

2.1.2. Electrodes and Gas Diffusion Layers

Modern fuel cell electrodes are gas diffusion electrodes (GDEs) that consist of a gas porous catalyst layer and an electrically conducting gas diffusion layer.

Polymer electrolyte membrane is sandwiched between two similar electrodes, anode and cathode. These two electrodes allow the reactant gases reach to the reactive catalyst layer. Electrons and heat are conducted through the substrate layer, which forms a link with adjacent cells, cooling plates, or current collector plates.

Several materials have been used as substrates for fuel cell electrodes. Carbon based materials such as carbon fiber papers and woven carbon clothes are the most common backing layers for electrodes. They have high temperature stability, enough rigidity and excellent electronic conductivity [37]. Potential low-cost approach may be poorly conducting carbon web filled with electrical conducting fillers like carbon black.

The significance of GDEs relies on the catalyst layer since this is where the whole reactions take place and membrane-catalyst layer interaction decides the performance of the fuel cell. The performance of a membrane electrode assembly for a PEMFC depends on the reaction efficiency, thus catalytic activity of Pt catalyst particles supported on the carbon black electrodes. PEMFC reactions include hydrogen oxidation reaction (HOR), oxygen reduction reaction (ORR), and electro oxidation of CO with the use of Pt catalyst on the electrodes. The oxidation reaction occurs at the anode and involves liberation of electrons. These liberated electrons travel through the external circuit producing electrical energy by means of external load and when they arrived at the cathode part, they participate in reduction reaction. Reaction products are formed at the cathode of PEMFC [38]. Since the dominant polarization comes from the slow ORR at the cathode side, reducing the Pt loading particularly at the cathode side is a reasonable approach to increase cost efficiency without compromising fuel cell efficiency. In other words, novel catalyst design involves not only reducing the Pt amount but also increasing its catalytic activity and efficiency.

PEM fuel-cell electrocatalyst technology has relied almost exclusively on either Pt blacks or Pt nanoparticles, 2–5 nm in size, dispersed onto larger carbon black particles. Neither will meet the DOE 2017 performance and durability targets at PGM (platinium group metals) loadings that meet the cost targets. Durability issue of Pt/C catalysts is a severe problem hindering the

commercialization of PEMFCs. This problem affects particularly cathode side, where the ORR occurs. In order to meet performance and durability targets, four basic electrocatalyst approaches have been the main focus of the researchers [39]. Unsupported nanoparticles, low aspect-ratio nanoparticles dispersed on low-aspect ratio supports, extended surface area catalysts and Pt free catalysts.

Chen et al. studied supportless Pt and platinum alloy (PdPt) nanotubes with the aim of solving durability problems of Pt based catalysts [40]. By producing supportless catalysts, support corrosion problem is also eliminated.

A highly promising subcategory of catalyst researches is low aspect-ratio nanoparticles dispersed on low-aspect ratio supports. It has been pioneered in Brookhaven National Laboratory and these systems have been found to exhibit higher mass activities since Pt is eliminated from the core of the catalyst particles. Bliznakov et al. [41], recently published a good example of these type of catalysts, demonstrating Pt monolayer-shell on electrodeposited Pd nanorods/nanowires-cores. Pd nanostructes were electrodeposited on thin film with a high surface area oxidized carbon. The surface of these electrodeposited Pd nanostructures were modified by a monolayer of Pt. Kuttiyiel et al. [42] studied Au stabilized Pt monolayer PdNi core-shell nanoparticles. This study exhibits a good example of using Pt while overcoming its supply problems.

Nanostructured thin-film (NSTF) catalysts are the only practical extended surface area catalysts found so far [39]. The support in this structure is a thin monolayer of an oriented array of crystalline organic whiskers. An example for this structure was studied by Debe et al. [43] and presented in 2011 Annual Merit Review of DOE Hydrogen and Fuel Cells and Vehicle Technologies Programs. Another good example was studied by Van der Vliet et al. [44] Briefly, the desired metals were sputtered consecutively on a substrate web coated with perylene red whiskers. Of all catalysts measured by Van der Vliet et al., the group determined the most active catalyst to be the PtNi alloy with 55 wt% of platinum.

At the present level of understanding of electro-oxidation reactions in PEMFCs (PEMFCs), it is not practical to replace platinum from the anode side. However,

non-platinum and non-platinum group metals (non-PGM) catalysts for cathode side reached performance up to 40–50% of platinum catalysts [45]. One of the most promising non-precious metal electrocatalysts for ORR is transition metal–nitrogen–carbon (M–N–C) materials (M = Co, Fe, Ni, Mn, etc.), which have gained increasing attention due to their promising catalytic activity displayed towards the ORR, along with the utilization of abundant, inexpensive materials.

2.1.3. Bipolar Plates

Bipolar plates are the backbones of HT-PEMFCs. They collect and conduct electrons and they provide the flow of reactants, hydrogen and oxygen. Bipolar plates are also known as 'flow field plates'. Multicell configurations requires very well-functioning bipolar plates. Primary function of a bipolar plate is to supply reactant gases to the core of the fuel cell via flow channels. They also have to remove water effectively out.

The most common material used for bipolar plates is graphite. Graphite has excellent electrical conductivity, high corrosion resistance and lighter in weight compared to the materials such as steel or copper. These materials also can be used as bipolar plates however their corrosion resistance is low and density higher than graphite plates.

2.1.4. Gaskets

Gaskets are placed between MEAs and graphite plates. Their primary objective is to prevent gas leakage from the fuel cell core and by applying pressure, they make sure that the acidic electrolyte and the bipolar plate are not in direct contact. Gaskets can be produced from various materials such as silicone being the most widely used material for gaskets. Teflon and other thermoplastics are also can be used as efficient gaskets for PEMFCs. For High temperature applications, the most promising candidate for gaskets is viton sheet gasket. It has very high thermal resistance which ensures that at higher temperatures gaskets stays firm and leakage is prevented.

2.2. Operation of PEMFCs

In this section, a brief information about fuel cell thermodynamics, electrochemical kinetics, proton conductance and mechanism, and percolation theory are given. Fuel cell operation includes electrochemical reactions following the kinetic and thermodynamic principles.

2.2.1. Thermodynamic and Kinetic for PEMFCs

The reactions in a hydrogen/oxygen PEMFC system corresponds to a chemical process that contains two separate electrochemical reactions at the anode and the cathode. These reactions are given in 2.1, 2.2 and 2.3.

Anode Reaction: $H_2 \rightarrow 2H^+ + 2e^-$ (2.1)

Cathode Reaction: $\frac{1}{2}O_2 + 2H^+ + 2e^- \rightarrow H_2O$ (2.2)

Overall Reaction: $H_2 + \frac{1}{2}O_2 \rightarrow H_2O$ (2.3)

Number of electrons exchanged must be the same in both reactions to balance of the overall reaction.

Schematic illustration of the ideal hydrogen-oxygen fuel cell operation is given in the **Figure 8**

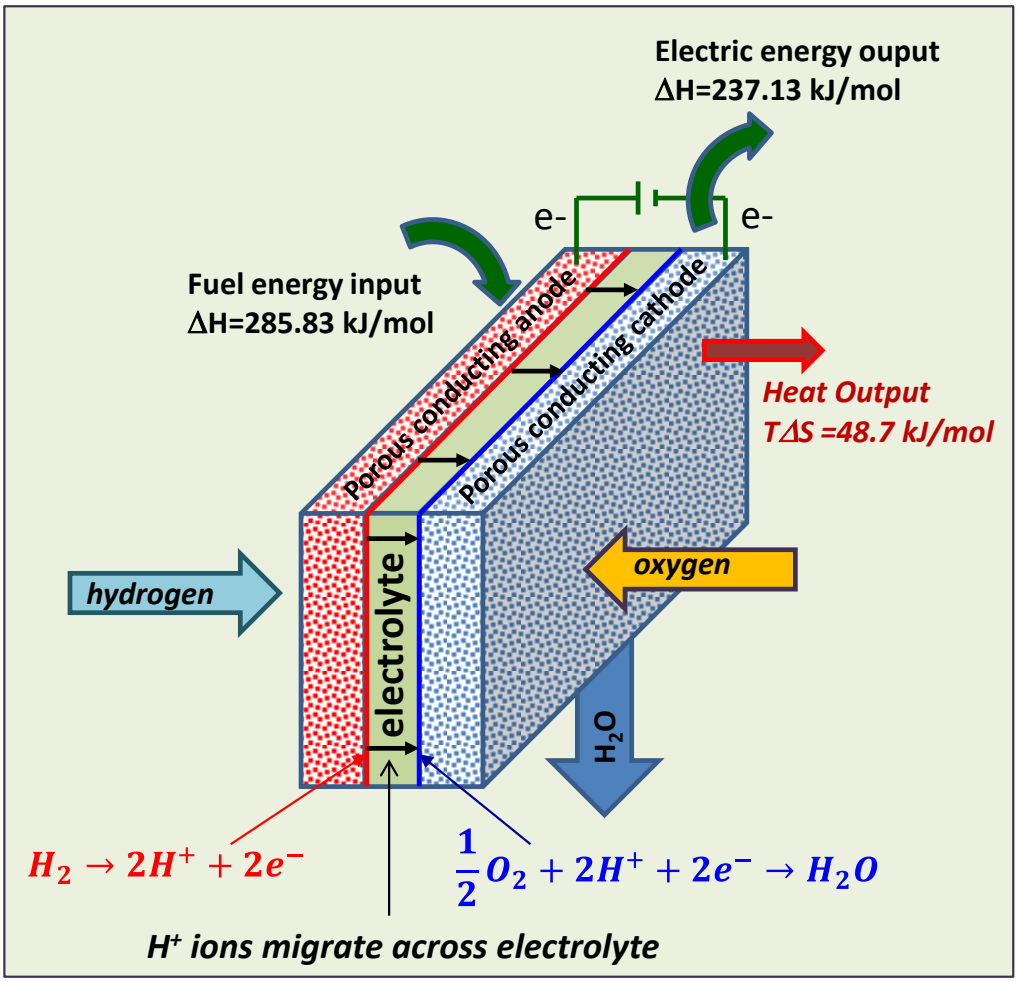

Figure 8 Schematic illustration of the ideal hydrogen-oxygen fuel cell operation.

The maximum energy available from a reaction, given by ΔG, and the electric work obtained, given by the electromotive force (emf) E, are related by equation 2.4. n is the number of electrons participating in the reaction and F is the Faraday's constant, their product giving the charge generated by the reaction. The negative sign is due to the convention of electric work obtained being positive number, but the work done by the system on the surroundings being negative by definition

The ΔG of the reactions given above can be determined by using the following equation:

$$\Delta G = -nFE = \Delta H - T\Delta S \qquad (2.3)$$

Assuming that all of the Gibbs free energy can be converted into electrical energy, the maximum possible theoretical efficiency (η_{theo}) of a fuel cell is the ratio between the change of Gibbs free energy and the change of enthalpy of reaction. η_{theo} can be calculated as in equation 2.4.

$$\eta_{theo} = \frac{\Delta G}{\Delta H} = \frac{237.13}{285.83} x100\% \cong 83\% \quad (2.4)$$

The maximum possible theoretical efficiency of PEMFC is much higher than other energy conversion systems that operate at low temperatures, which are limited by Carnot Cycle, typically in the range 20% - 40% at temperatures between 100^0C and 200^0C.

Because ΔG, n, and F are all known, the theoretical fuel cell potential of hydrogen/oxygen can also be calculated as in Equation 2.5 at 25^0C and atmospheric pressure (E).

$$E = \frac{-\Delta G}{nF} = \frac{237.13}{96485x2} = 1.23\ V \quad (2.5)$$

Theoretical reversible cell voltage, which depends on pressure and temperature, also known as Nerst voltage, is expressed as the following equation:

$$E_{T,P} = -\left(\frac{\Delta H}{nF} - \frac{T\Delta S}{nF}\right) + \frac{RT}{nF}\ln(P_{H_2}.\frac{{P_{O_2}}^{0.5}}{P_{H_2O}}) \quad (2.6)$$

Note that the previous equations are only valid for gaseous products and reactants. When liquid water is produced in a fuel cell, $P_{H_2O} = 1$ [2].

PBI based PEMFCs typically operate at temperatures higher than 120^0C, thus the potential can be considered as fitting the gaseous water condition which achieves approximately 1.118V.

The actual fuel cell potential (V_{cell}), and the actual efficiency are lower than the theoretical values due to the losses (ΔV_{loss}) related with kinetics and dynamics of the processes. The actual fuel cell potential is given in Equation 2.7 which is expressed in terms of E (OCV) and ΔV_{loss}.

$$V_{cell} = E - \Delta V_{loss} \tag{2.7}$$

The irreversible losses that affects the performance of the fuel cells are refered to as;

- Activation related losses (ΔV_{act}): Losses caused by activation energy needed for reactions to initiate. Also called as *activation polarization.* This type of loss is associated with sluggish electrode kinetics.
- Ohmic losses (ΔV_{ohm}): Losses at intermediate current densities as a result of ohmic losses. These losses are resulted from ionic resistance in electrolyte, electronic resistance in electrodes and also other conductive parts of the fuel cell.
- Mass transport related losses (ΔV_{conc}): Due to the mass transfer rate limitation of the reactants and depends highly on currents density. It is observable at higher current densities.
- Internal currents
- Crossover of reactants: Although the electrolyte, a polymer membrane, is not electrically conductive and is practically impermeable to reactant gases, some small amount of hydrogen will diffuse from anode to cathode, and some electrons may also find a “shortcut” through the membranes.

Cell voltage of PEMFC can be written in terms of these losses as:

$$V_{cell} = E - (\Delta V_{act} + \Delta V_{ohm} + \Delta V_{conc}) \tag{2.8}$$

At relatively high negative overpotentials (i.e., potentials lower than the equilibrium potential) such as those at the fuel cell cathode, the first term in

the Butler–Volmer equation (equation 2.9) becomes predominant, which allows for expression of potential as a function of current density.

$$\text{i}=i = i_0 \left\{ exp\left[\frac{-\alpha_{Rd}F(E-E_r)}{RT}\right] - exp\left[\frac{-\alpha_{Ox}F(E-E_r)}{RT}\right]\right\} \quad (2.9)$$

$$\Delta V_{act} = \frac{RT}{\alpha F}\ln(\frac{i}{i_0}) \quad (2.10)$$

Where R is the universal gas constant, T is the temperature, $\propto$ is the transfer coefficient, i and i_0 are current density and exchange current density, respectively.

Tafel equation can also be used to represent activation polarization as follows:

$$\Delta V_{act} = a + b\ log(i) \quad (2.11)$$

Where;

$$a = -2.3\frac{RT}{\propto F}\log(i_0) \quad (2.12)$$

$$b = 2.3\frac{RT}{\propto F} \quad (2.13)$$

The parameter 'b' is called as Tafel Slope.

ΔV_{ohm} can be represented with following equation:

$$\Delta V_{ohm} = iR_c \quad (2.14)$$

Where R_c is the total internal resistance.

Finally, ΔV_{conc} can be written according to Nerst Equation:

$$\Delta V_{conc} = \frac{RT}{nF}\ln(\frac{i_L}{i_L - i}) \quad (2.15)$$

Where i_L is the limiting current density.

Final form of the V_{cell} equation is written as:

$$V_{cell} = E - \frac{RT}{\propto F}\ln\left(\frac{i}{i_0}\right) - iR_c - \frac{RT}{nF}\ln\left(\frac{i_L}{i_L - i}\right) \quad (2.16)$$

Figure 9 represents the the cell voltage-current relationship showing all of the expected losses. This curve is widely known as a typical polarization curve of a fuel cell.

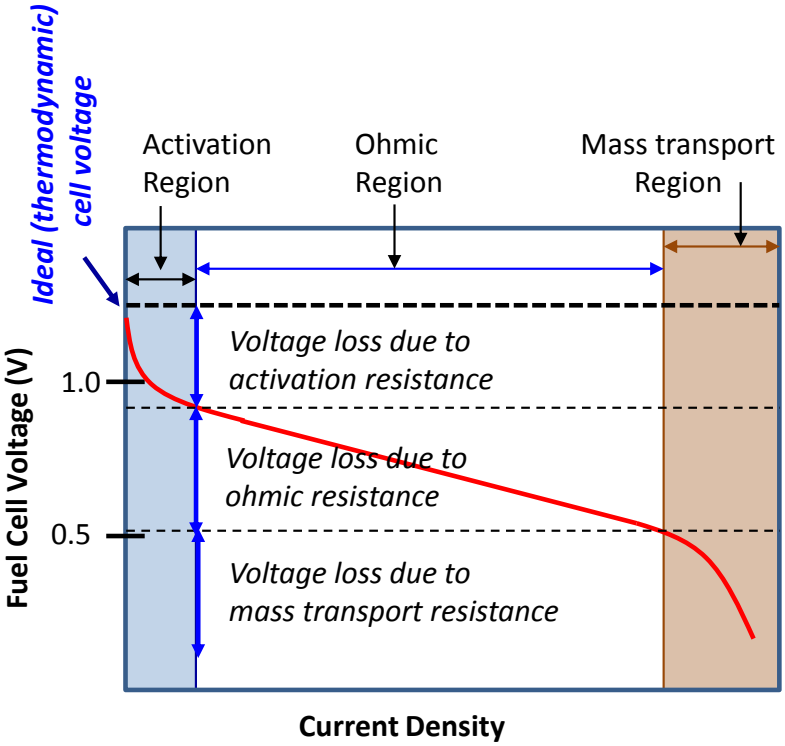

Figure 9 Fuel cell polarization curve with major losses [46].

In addition to these major losses, practical equilibrium and open circuit voltages (OCV) are affected by other significant factors such as hydrogen crossover, purity of the platinum coating on to the gas diffusion layers, the corrosion of the carbon electrode support etc.

To be able to have a better understanding on the effect of OCV on PEMFC performance, a more detailed explanation is needed.

Open Circuit Voltage, OCV, value is expressed as the voltage at zero current density, in other words at the open circuit condition without any power output. The values of OCV for PEMFC ranges between 0.9-1.1, which is lower than theoretical values, 1.23 V, due to the aforementioned major parameters, hydrogen crossover, temperature and mixed potentials, the impurities CH_x on carbon support and Pt coating.

Pt oxidation caused by mixed potential on cathode side is considered as one of the major factors for OCV drop in a PEMFC system. In literature, it was reported that Pt-O_2 reaction can cause up to 182 mV drop which proves that mixed potential has severe effects on OCV values. As the temperature increases up to 120^0C however, the voltage loss decreases drastically (from 182 to 96 mV) which proves the importance of operating at higher temperatures.

Hydrogen crossover refers to a phenomenon in which hydrogen and oxygen gets in direct contact and reacts without donating electron and proton. Even though the membranes are assumed to be impermeable to gases, it is not possible to prevent gases pass through the thin membrane without separating into hydrogen and electron. As the membrane thickness decreases, hydrogen crossover increases due to the higher gas permeability of the membrane, hence it results in lower OCV values.

OCV values ranged between 0.75-0.95 in this study. The reasons are discussed in detail in the following chapters.

2.2.2. HT-PEMFCs

As discussed in Chapter 1, most of the shortcomings of low-temperature PEMFC technology can be solved by developing alternative membranes that can operate at higher temperatures such as 100^0C. Hence, in the recent years, fuel cells that operate at higher temperatures in the range of 100^0C-400^0C has attracted the interest of researchers.

HT-PEMFCs offers some significant advantages compared to LT-PEMFCs such as:

- Kinetics for both electrodes will be enhanced [47,48].

- Catalyst poisoning is reduced as discussed in previous section. This higher tolerance to CO makes it possible for a fuel cell to use hydrogen that is obtained from a reformer unit [47].
- Fuel cell flooding caused by water at the exhaust is avoided.
- Cooling system is simplified.
- Non-noble metal catalysts are more feasible [49].

Hence, the development of HT-PEMFCs is of great importance for fuel cell literature, research and development.

2.3. Proton Exchange Membranes

As mentioned before, membrane is the key component of a PEMFC. Triple roles of the polymer based membranes in PEMFCs can be listed as follows:

- Charge carrier for protons
- Separation of reactant gases
- Preventing electrons to pass through.

In general, the materials used in synthesis of the PEMs can be classified into three vast groups: perflourinated ionomers, non-fluorinated hydrocarbons and acid-base complexes. In **Figure 9** membrane classification according to the materials used in synthesis has been shown.

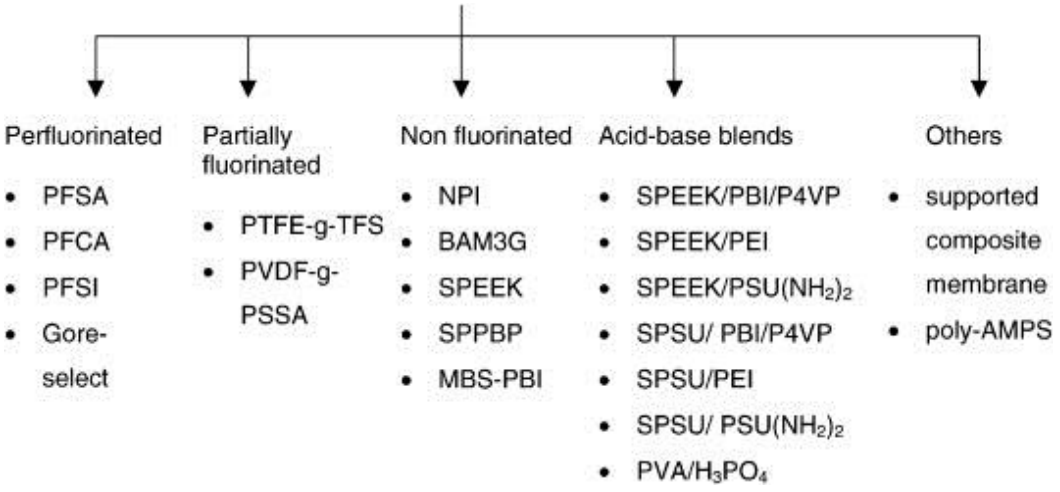

Figure 10 PEMFC membrane classification according to the materials used [50].

Perfluorinated membranes are selected due to their thermostability, chemical inertness and the enhanced acidity of the sulfonic groups. The most renowned

member of these membranes is Dupont's Nafion®. Similar polymers are Flemion® by Asahi Glass and Aciplex-S® by Asahi Chemical. Nafion, however, is considered to be superior to others due to its high proton conductivity, chemical stability and mechanical strength [51].

Another type of materials commonly used in PEMFCs are non-flourinated hydrocarbon polymer membranes which can be aromatic or aliphatic. These polymers have benzene rings in the backbone or in the bulky pendant groups from membrane polymeric backbone. Hydrocarbon polymers are widely being researched due to promising results obtained for high performance membrane production [52]. Hydrocarbons are less expensive, commercially available, and their structure is appropriate to addition of polar sites as pendant groupzs [53].

2.3.1. Perfluorosulphonic acid (PFSA) polymer membranes

In 1970s, DuPont developed a perfluorosulfonic acid called Nafion® that showed two fold improvements in the proton conductivity and fourfold increase in the lifetime of PEMFCs. It is now accepted as a standard and the most commonly used membrane type till today. The Dow Chemical Company and Asahi Chemical Company developed advanced perfluorosulfonic acids with shorter side chains and higher ratio of SO3H to CF2 groups [50].

Nafion® is composed of flouoro 3,6-dioxo 4,6-octane sulfonic acid with polytetra-fluorethylene (PTFE). Teflon backbone of this structure gives hydrophobic nature to the membrane while sulfonic acid groups adds hydrophilicity to the membrane. In this type of membranes, proton conductivity, which is the main parameter that affects PEMFC performance, is directly affected by hydration level of the membrane. **Figure 11** shows chemical structure of Nafion® and other famous perfluorinated electrolyte membranes.

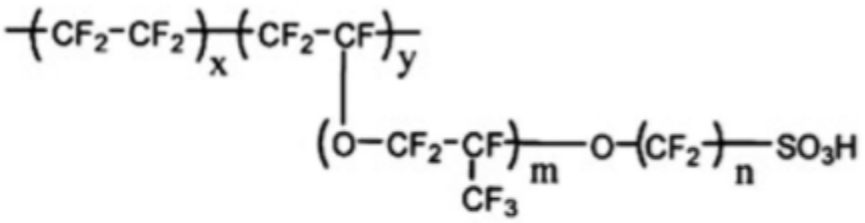

Nafion 117: m≥1, n=2, x=5-13.5, y=100
Flemion: m=0, 1; n=1-5
Aciplex: m=0, 3; n=2-5, x=1.4-14
Dow membrane: m=0, n=2, x=3.6-10

Figure 11 Chemical structures of perflourinated PEM (reprinted from [52])

2.3.2. Non-fluorinated hydrocarbon membranes

Recently, one of the most promising alternative membrane types for higher performance PEMFCs is the use of hydrocarbons in the polymer backbone. Hydrocarbon membranes are less expensive, commercially available, and their structure permits introduction of polar sites as pendant groups.

In order to enhance the membrane stability at elevated temperatures, aromatic hydrocarbons can be introduced to directly to the backbone of a hydrocarbon polymer or polymers with bulky groups added as modification. Polyaromatic amines have inflexible bulky groups and thus a T_g value greater than 200^0C. Polyether ketones (PEK), Polyether sulfones (PESF), poly (arylene ethers), polyesters and polyimides are significant examples of polyaromatics in the main chain.

2.3.3. Acid/Base polymer membranes

Acid–base complexes have been considered as a viable alternative for membranes that can maintain high conductivity at elevated temperatures without suffering from dehydration effects. In general, the acid–base complexes considered for fuel cell membranes involve incorporation of an acid component into an alkaline polymer base to promote proton conduction. In the absence of free water, pure sulfuric and phosphoric acids undergo self-ionization. Polymers involving basic sites such as alcohol, ether, imine, amide or imide groups that react with strong acids, increase acid dissociation. The polymer studied in the efforts of early years include poly ethylene oxides (PEO) [54], polyvinyl acetate (PVA) [55],

polyacrylamide (PAAM) [56], polyvinylpyridine (PVP), and linear & branched polyethyleneimine (L- or B-PEI) [57].

Phosphoric acid has a good conductivity and thermal stability, and it is known that is performing well in phosphoric acid fuel cells (PAFC) for intermediate temperatures ranging between 175^0C–200^0C. Conventional PAFCs on the other hand, have limited applications due to the disadvantages related to phosphoric acid electrolyte immobilization in certain matrices. The phosphoric acid-doped polybenzimidazole (PBI/H_3PO_4) system seems so far the most successful membrane for temperatures between 175^0C–200^0C. Fuel cell technologies based on PBI/H_3PO_4 system have been introduced successfully at these temperatures, under ambient pressure. Gas humidification is not needed and CO sensitivity of the Pt-based catalyst is higher at higher temperatures. Thus, PBI/H_3PO_4 systems are the most promising candidates as conventional membranes for HT-PEMFCs. Easy control of air flow rate and cell temperature are other operating features of the PBI-based fuel cells [50].

2.4. Proton Conduction Mechanisms in PEMs

Proton conduction phenomena have significant importance in many chemical reactions, biomolecular and electrochemical energy conversion processes. The very unique chemistry of protons suggests two mechanisms for proton conduction: the proton transfer by a carrying molecule (*vehicle mechanism*) or by means of a hydrogen bond chain with hopping from one site to another one (*Grotthus mechanism*) [8].

In vehicle mechanism, protons migrate with a molecular carrier. The transport of the proton through a vehicle does not utilize or require an infinite hydrogen bond web, thus follows Stokes Law. The most known proton solvent is the water. Proton conduction in aqueous media often involves migration of different hydrated proton complexes. PFSA membranes consist of a perflourinated backbone and perflourinated ether side chains with terminal sulfonic acid functional groups as mentioned in previous section. High electronegativity of fluorine, results in super strong bond between the sulfonic acid and perfluorinated backbone. It absorbs water, where protons solved in continuous hydrated domain created. The resultant hydrated protons are the protonic charge carriers [58]. Due to this phenomenon, proton conductivity of

PFSA membranes depends on vehicle mechanism mostly, and is very dependent on the hydration level of the membrane. Proton conductivity values of these membranes reach above 0.1 S cm^{-1} under fully hydrated conditions [8].

The Grotthus mechanism requires an infinite hydrogen bond web. Strength of the hydrogen bond is intermediate, around 10-30 kJ mol^{-1}. Since the bond strength is relatively low, hydrogen bond forming and breaking can be induced by many different triggers such as thermal energy. This dynamic forming-breaking hydrogen bonds is appropriate for hopping proton conduction mechanism. Hopping mechanism consists of breaking of an O-H bond in one molecule and forming the same type of bond with another. Each proton moves over very small distances; however, the resulting effective movement of a charge takes place through a longer distance. Activation energy of this process is lower compared to regular movement of the ions through viscous media. To achive higher temperature operations with PEMFCs, a membrane of this type of proton conduction mechanism is desired. Until today, the most successful data were collected by doping basic polymers with amphoteric acids, such as phosphoric acid doped PBI systems.

Studies showed that the conductivity of the membrane strongly depends on the nature of the two components on the acid content. Minimum conductivity is observed at the acid degree that leads to maximum protonation. Excess of the acid is needed to achieve higher conductivity values. This suggests that proton conduction proceeds primarily through the hydrogen-bonded anionic chain. For phosphoric doped PBI systems, overall proton conductivity of the acid-doped complex is lower significantly due to the presence of solid polymer matrix. PBI does not interrupt the hydrogen bond network that phosphoric acid established; however, it decreases the percolation inside of the phosphoric acid domain. Proton conducting mechanism stays same, mainly by Grotthus mechanism; however, rotational motion of phosphoric acid molecules needed for this mechanism is limited by PBI-H_3PO_4 interactions. This results in a loss of proton conductivity as protons are not transferred as effectively between the protonated imidazole (ImH^+) and H_3PO_4 [8].

2.5. Acid Doped Polybenzimidazoles in High Temperature PEMFCs

Poly(2,2'-(m-phenylene)-5,5'-bibenzimidazole, commercially named as PBI is first manufactured by Hoechst-Celanese to be used as a fire protection clothing. PBI is well known for its very high thermal and chemical stability. Also, it has god mechanical properties. Glass transition temperature of PBI (T_g) is between 425 – 436^{0}C and decomposition temperature around 600^{0}C since it has all aromatic structure. Owing to this aromatic structure, chains cannot move around easily and as a result PBI is a rigid polymer with very high T_g. PBI is an electronic and ionic insulator. When modified by acids it becomes a good conductor to ions. The pKa of the benzimidazole group is around 5.5, which facilitates the absorption of acids. Another common polybenzimidazole type is known as ABPBI, which has a very similar structure to PBI but it does not contain a connecting phenyl group.

The first fully aromatic polybenzimidazoles were prepared by Vogel and Marvel in 1961. Condensation of tetraamines and diacids was used to synthesize those polymers. Savinell et al. were the first to dope PBI with H_3PO_4, finding out that doped membranes exhibited a significantly high proton conductivity at elevated temperatures [13]. The doping processes involving imbibing the membrane in phosphoric acid yields 5-16 mol of H_3PO_4 per mole PBI repeat unit. These polymers have also been imbibed with other acids [59], bases [60,61] and inorganic proton conducting molecules [48,62]. Also sulfonated polybenzimidazoles have been studied in the literature widely [63–67]. These membranes are also used in sensors [68,69], supercapacitors[70], and electronic devices [71].

Morphology and microstructure of PBI membranes have not been studied deeply in the literature. Morphology control claimed to be directly affected by polymerization conditions and starting isomers by Kohama et al. [63] There are two main morphologies obtained as *para*- and *meta*- PBIs. Polymerization of DAB and benzene-1,4-dicarboxylic acid resulted in plate-like crystals of *para*-PBI which has high crystallinity. Polymerization of DAB with benzene-1,3-dicarboxylic acid diphenyl ester afforded of *para*-PBI fibers with good mechanical yields. Polymerization of meta-PBI, on the other hand, can be accomplished by condensation of DAB and benzene-1,3-dicarboxylic acid in

DBT, results in micrometric particles. Kohama et al. also claimed that *para*-PBIs have higher acid doping levels than *meta*-PBI membranes. Direct casted *para*-PBIs showed completely amorphous structure and higher acid doping levels compared to the solution casted PBIs [71].

2.5.1. Methods for Preparation of Phosphoric Acid Doped PBI

In fuel cells, a membrane serves as an ionic conducting electrolyte, an interface for electrode reactions, reactant separator and as a support for catalyst layers/electrodes. This is why it is important to prepare membranes with optimized gas permeability. For this purpose, the most widely used method to prepare dense PBI based membranes is based on casting from a PBI solution in DMAc [72] by evaporation of the solvent. Afterwards, the cast membranes are washed in boiling water to remove the solvent traces and then dried for 24 hours. Most conventional method to dope cast membranes with H_3PO_4 is to impregnate membranes by soaking them in concentrated phosphoric acid bath [13,73]. As the bath impregnation time increases, acid doping level increases simultaneously. The aimed ADL can be obtained faster by increasing the acid bath temperature [71]. In literature it was observed that after 10-11 hours of impregnation time, the conductivity raises drastically [59].

Another method is recently developed imbibing process, known as direct casting process, in which PBIs are polymerized and cast in polyphosphoric acid (PPA) solvent to produce PPA-cast PBI membranes or a mixture of phosphoric acid and trifluoroacetic acid (TFA) is used and TFA-cast membranes are produced [74].

In order to produce TFA-cast membranes, PBI powder is first mixed with TFA. Afterwards a certain amount of H_3PO_4 is added. The obtained solution is then filtered and cast into membranes on a glass plate under nitrogen atmosphere. Membranes are dried under room temperature, at vacuum conditions.

As for the PPA-cast membranes, a sol-gel method was developed by Xiao et al. [75,76] to fabricate PBI- H_3PO_4 membranes directly from the PBI solution in PPA at around 200^0C. After casting, hydrolysis of PPA by capturing moisture in the air results in phosphoric acid and induces a sol-gel transition which results in phosphoric acid doped PBI membranes.

The properties of the films produced in each method are substantially different. Films cast using the conventional DMAc method are normally has higher mechanical properties compared to the ones cast by TFA-cast membranes. TFA-cast films require a polymer of higher inherent viscosity to produce mechanically stable membranes. The directly casted films by TFA method are much rubberier and softer, however, conductivity of these films are higher compared to the ones prepared with conventional method. On the other hand, PPA-cast membranes have acid doping levels higher than two other methods, as high as 20-40 mol phosphoric acid per repeat unit of PBI. The resulting membranes achieve conductivity of 0.2 $S.cm^{-1}$ at 160-180^{0}C. They also have acceptable tensile strength (up to 3.5MPa) [75]. Sol-gel behaviors of the membranes depend highly on the polymer structure and molecular weight in PPA-casting method.

2.5.2. Membrane Modifications

Acid doping level is the major parameter that affects the conductivity of PBI based membranes. As the acid doping level of the membrane increases, the mechanical strength decreases. Also acid leaching from the membrane in case of direct contact of the membrane with water or water vapor is another major concern. In literature, certain methods to overcome this problem have been developed including preparation of composite membranes, ionic cross-linking and covalent cross-linking. In this section, these methods will be covered in detail.

2.5.2.1. Composite Membranes of PBI

Preparation of composites with inorganic fillers is the focus of recent attempts to develop better performing PEMs. Addition of hygroscopic filler to an ionomer for example is found to increase water retention and acid retention as well as make membranes stiffer [77]. In case that the inorganic filler is a solid proton conductor like zirconium phosphates enhances the proton conductivity of the membranes [77], thus the performance increase is expected. Introducing inorganic filler to the membrane matrix may also assist in improving the thermal stability, water absorption, reactant crossover resistance etc.

PBI and PBI blend composites have been widely studied in literature recently. Inorganic proton conductors such as zirconium phosphate [77],

phosphotungstic [78] acid, silicontungstic [79] acid and boron phosphate [80] have been studied with PBI matrix. It was observed that higher conductivity values, up to 0.2 S cm^{-1} can be obtained by addition of inorganic proton conductors [77].

Acid retention of the nanocomposite membranes were studied by Maity et al. [81] and Özdemir et al. [77]. The findings showed that acid leaching decreased with the introduction of nano particles.

Based on hexafluoro PBI and dodecylamine modified montmorillonite, Chuang et al. [82] developed nanocomposite membranes which show lower coefficient of thermal expansion, methanol cross over and decreased plasticizing effect after acid doping.

Lin et al. [83] prepared PBI-PTFE composite membranes. Nafion covered PTFE is used as filler matrix where Nafion serves as a coupling agent by an acid-base reaction with PBI. The thickness of the membrane was low as 22μm, however the gas permeability of the membrane was low, thus OCV was found low in this study.

2.5.2.2. Ionically Cross-linked Membranes of PBI

Ionic cross-linking of PBI can be brought by mixing PBI with a polymeric sulfonic in minor amounts, or phosphonic acid, by sulfonation or by grafting of vinyl-phosphonic acid side chains onto PBI. Flexible ionomer networks can be prepared from acid-base polymers by ionically cross-linking of polymeric acids and polymeric bases. PBI being a basic polymer, it can be combined with acidic polymers that are studied in literature such as SPSF [84], SPEEK [85], SPPO [86] and SPOP [87]. Additionaly, Hobson et al. [88] coated Nafion with PBI to reduce methanol permeability [74]. Durability improvement at OCV operation was reported by Zhai et al. [89]. However, the test duration was relatively short (480-720 h). It could be proven that by ionic cross-linking of PBI, chemical stability of PBI could be significantly improved [90]. Dissolution of PBI upon acid doping could also be minimized by ionic cross-linking. On the other hand, in most of the cases, ionically cross-linked membranes suffer from poor thermal stability in aqueous media since the ionic cross-link breaks at elevated temperatures [16].

2.5.2.3. Covalently Cross-linked Membranes of PBI

In a US Patent issued in 1977, David and Thomas [91] claimed that imidazole groups of the PBI membrane can be cross-linked by an organic acid or its halide with two or more functional groups per molecule. The polybenzimidazole is covalently cross-linked by mean of an amide-type linkage. Covalently cross-linked PBI is tougher and has higher compaction resistance under high pressures. EGDE [92], [93] (TPA), tetracarboxylic dianhydride (TCDA) [94], divinyl sulphone [95], DBpX [96], 3,4-dichloro-tetrahydro-thiophene-1,1-dioxide [97], dichloromethyl phpshonic acid [23] are common examples of many other cross-linkers used in the literature.

Covalently cross-linked membranes become brittle as they dry further. Kerres et al. [98] introduced a covalent cross-linker (1,4-diiodobutane, DIB) into ionically cross-linked blend. The product was covalently-ionically cross-linked and showed high proton conductivity, reduced swelling and improved thermal stability.

CHAPTER 3

EXPERIMENTAL STUDIES

3.1. Materials

The materials, which are required for PBI synthesis; PBI based cross-linked membrane preparation and membrane electrode assemblies, are the following.

Diaminobenzidine tetrachloride hydrate (DAB.4HCl.2H_2O, 98%), isophatalic acid (IPA, 99%), polyphosphoric acid (PPA, 115%), and phosphoric acid (PA, 85%) were obtained from Sigma-Aldrich (USA) and N-N Dimethylacetamide (DMAc, Merck) was used as received. Cross-linkers BADGE, TPA and DBpX were purchased from Sigma Aldrich (USA). Cross-linker EGDE was obtained from TCI (Tokyo Chemical Industry, Japan). De-ionized water was purchased from Sigma-Aldrich (USA) and used as received. All solvents used were high-grade reagents.

For the catalyst ink preparation 20 wt. % Pt on carbon (E-tek) was used as the catalyst and polyvinylidenefluorid (PVDF) (Sigma Aldrich) as the binder. Gas diffusion layer was purchased from Sigracet® GDL (SGL Carbon).

Gases used were nitrogen (99.999% pure) and hydrogen (99.999% pure) from Linde (Turkey). Dry air was fed through a compressor and a dryer to the fuel cell system.

3.2. Polybenzimidazole Synthesis

In this work PBI polymers were synthesized by solution polymerization method that was introduced by Iwakura et al. [11]. Synthesis was conducted using the method according to Iwakura et al. [11]. The monomers used were

DAB.4HCl.2H_2O and IPA, while the solvent was PPA. The experimental set-up consisted of a four-necked glass flask, mechanical stirrer, heating mantle, nitrogen inlet and CaCl2 drying tube. The system temperature was controlled by the thermocouple which was connected to a temperature controller. The reaction was conducted for 18 hours, at 200^0C, under a constant nitrogen flow. Polymerization reaction shown in **Figure 12**. The PBI polymer obtained was later characterized by C-NMR.

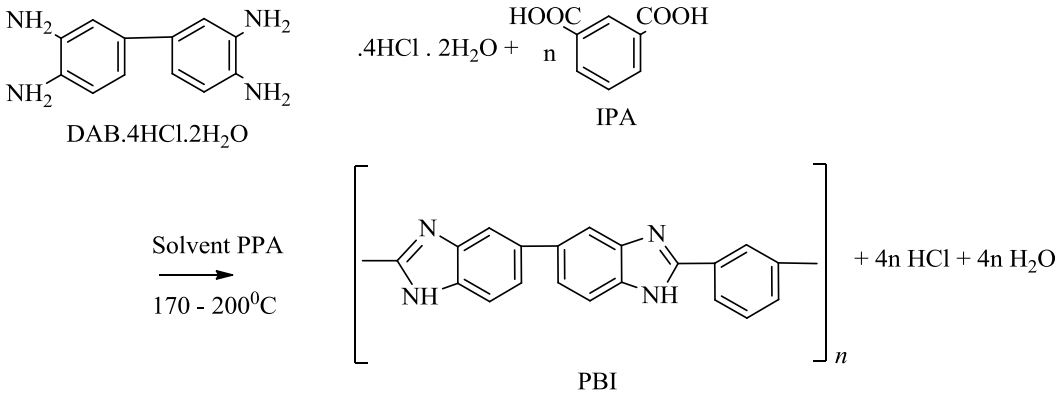

Figure 12 Solution Polymerization of PBI

For the synthesis of PBI; the reactor was a four-necked glass flask equipped with a mechanical overhead stirrer (WiseStir HS 100D, DAIHAN), nitrogen inlet and a $CaCl_2$ drying tube. The system temperature was adjusted by a heating mantel (ISOLAB) equipped with a temperature controller (GEMO, DT 109A) and a thermocouple (Pt 100). The picture of the set-up for polymer synthesis is given in **Figure 13**

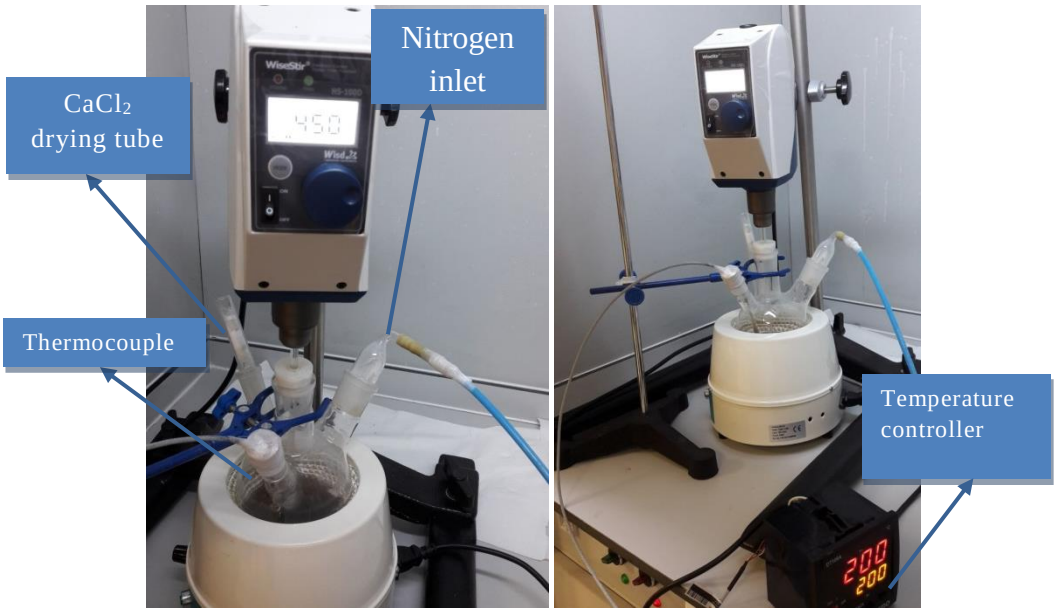

Figure 13 Experimental set-up for PBI synthesis

Firstly, a specific amount of PP, decided according to the polymer amount wanted, was heated to 140^0C and stirred till the viscosity of the PPA decreased to a point that stirring become easier. First monomer, DAB.4HCl.$2H_2O$ was added to hot PPA. Solution of monomer in PPA produces HCl gas bubbles, and this step of reaction was continued till the bubble formation stopped, which lasted for approximately 2 hours. Afterwards, an equimolar amount of IPA was added to the reactor and temperature was increased up to 170^0C for the first 5 hours and then to 200^0C for the rest of the polymerization reaction for 18-24 hours. The reaction mixture developed a blue-violet color and it started to get viscous as the reaction proceeds. After several hours, PBI polymer was isolated as yellowish-brown fibers in DI water. In order to remove all the PPA, the obtained polymer fibers were washed with DI water several times. Precipitate treated with sodium bicarbonate to neutralize the fibers completely. Purification is an important step to get soluble PBI polymer for membrane preparation. Afterwards PBI dried in the oven at 150^0C, for 24 hours. The schematic representation of PBI fibers and crushed PBI polymer were given in **Figure 14**.

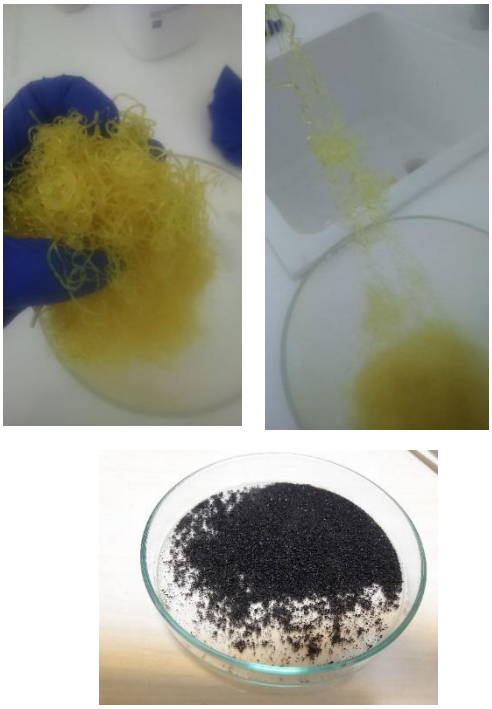

Figure 14 PBI fibers and crushed PBI polymer

3.3. Membrane Preparation

In this study, membranes were prepared by using PBI polymer purchased from DPS with molecular weights ranging between 39000 - 82000 g/mol. The PBI polymer batches synthesized in our laboratory were found to be insoluble in solvent like DMAc or DMSO, only soluble in acidic solvents like H_3PO_4 and PPA.

In this study, for membrane preparation, 2.5 wt. % PBI polymer was dissolved in 10 mL solvent (DMAc), at 80 ^{0}C temperature. Pristine PBI membrane was prepared by pouring the solution into petri dish and drying at 80 ^{0}C to evaporate the remaining solvent. The membrane was stripped from the petri dish after 24 hours of drying and washed in boiling water to remove the solvent completely. Cross-linked membranes were prepared by adding cross-linkers to the PBI solution. Cross-linkers were mixed with 1 mL DMAc and then they were mixed with PBI solution. The mixture was later poured onto a petri dish and dried at 80 ^{0}C for 24 hours. In order to complete the cross-linking reaction, the membranes were further heat treated. The duration and temperature of the heat treatment process was determined according to previous literature reports on TPA, EGDE [93], DBpX [23] and BADGE [25]. PBI-TPA and PBI-EGDE

membranes were kept at 150 ^{0}C for 3 hours. For PBI-BADGE membranes, thermal treatment was at 135 ^{0}C for an hour and for PBI-DBpX membranes, 160 ^{0}C for 18 hours. The content of BADGE, EGDE and TPA resins in cross-linked PBI-EGDE and PBI-TPA membranes was 5 wt. %. The amount of DBpX in PBI-DBpX membranes was 3 wt. %. PBI-BADGE membranes were prepared with three different BADGE resin amounts, 2.5 wt %, 5 wt % and 7.5 wt %. List of the membranes prepared was given in Table 3.1.

Table3.1. List of Membranes Prepared

Membrane Name	**Cross linker**	**Cross linker amount**
1st set of membranes		
PBI	-	-
PBI-TPA-5	TPA	5 wt. %
PBI-EGDE-5	EGDE	5 wt. %
PBI-DBpX-3	DBpX	3 wt. %
2nd set of membranes		
PBI-BADGE-2.5	BADGE	2.5 wt. %
PBI-BADGE-5	BADGE	5 wt. %
PBI-BADGE-7.5	BADGE	7.5 wt. %

A schematic representation of preparation of cross-linked PBI membranes is given in **Figure 15**.

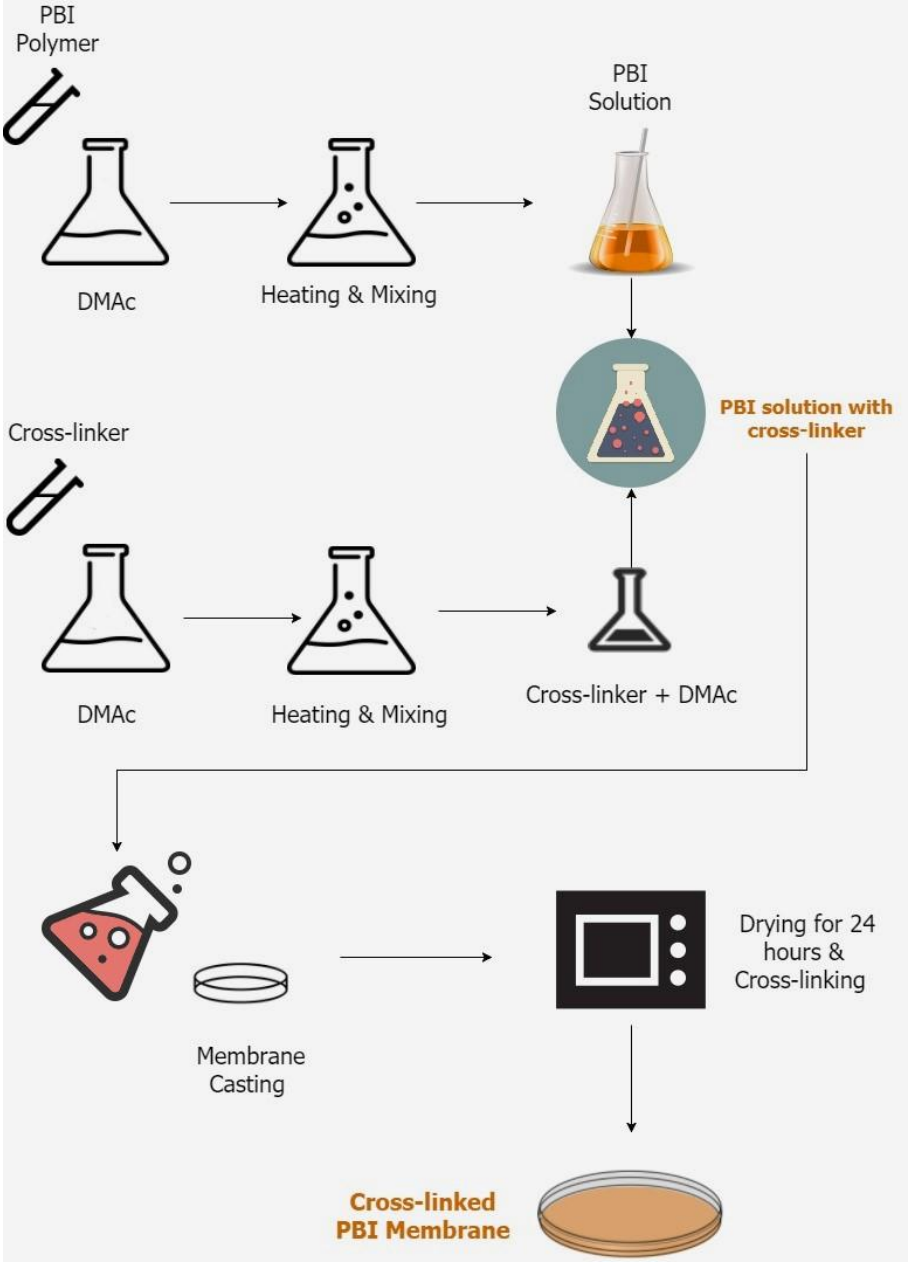

Figure 15 Schematic representation of membrane casting

The chemical structures of the cross-linked membranes are given in **Figure 15**.

As can be seen in the **Figure 16**, BADGE and EGDE cross-linking reactions occurred between the epoxy groups of the cross-linkers and the terminal amino groups of PBI. Cross- linking reaction in PBI-TPA membranes takes place between the formyl groups of TPA and the N-H groups of PBI. PBI-DBpX

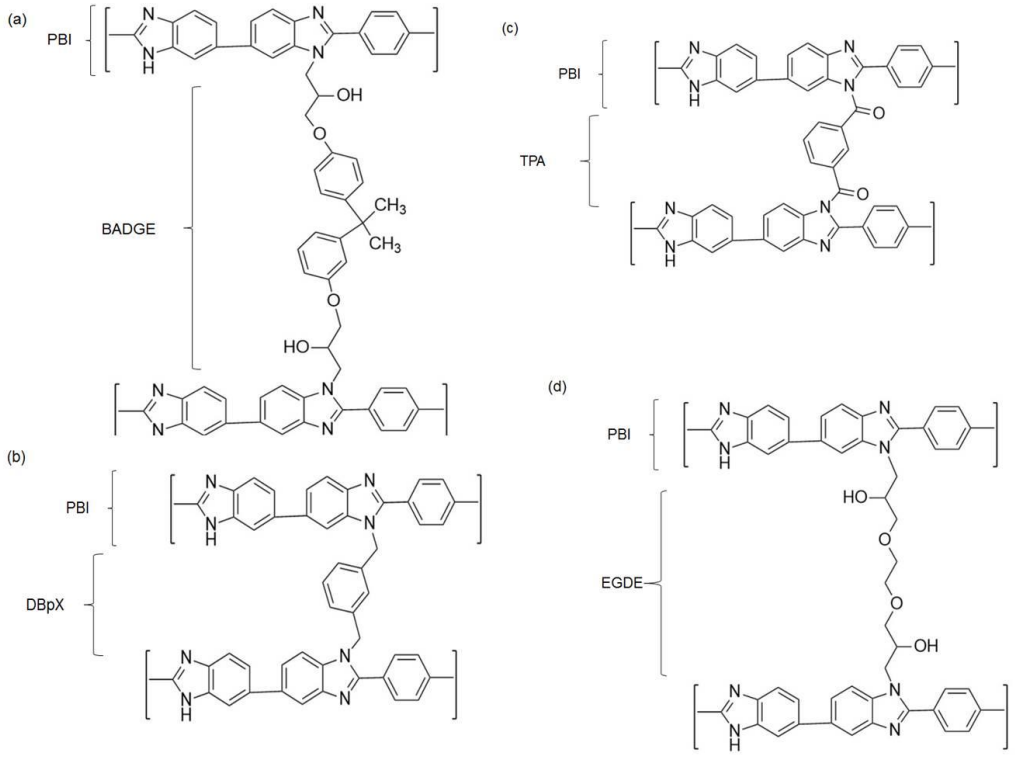

Figure 16 Cross-linking mechanism of (a) PBI-BADGE, (b) PBI-DBpX, (c) PBI-TPA, (d) PBI-EGDE [23,25,93]

cross- linked membrane was formed by reaction between -Br groups of DBpX and the N-H groups of PBI.

3.4. Acid Doping of the Membranes

PBI matrix needs to incorporate a large volume of PA to achieve high proton conductivity values. The pristine PBI and cross-linked PBI membranes were doped in phosphoric acid solution. The membranes were removed from the acid solution and wiped with a tissue before weighing. The weight gain due to both acid and water was estimated by comparing the weight before and after acid doping. Acid is absorbed in the matrix due to the strong interaction between PBI and PA [100]. PA doping level of the membrane is expressed as the number of H_3PO_4 moles per PBI repeat unit. Acid doping levels of the membranes are calculated according to the following equation:

$$\text{Acid Doping Level} = \frac{W_{PA}}{W_{dry}} \text{ x } \frac{\text{MW of PBI Repeat Unit}}{\text{MW of } H_3PO_4} \quad (3.1)$$

Where W_{PA} is the weight of acid doped membrane and W_{dry} is the dry membrane weight [99]. A sample calculation of acid doping level and the time vs doping level plot is given in Appendix A.

3.5. Preparation of Membrane Electrode Assembly

Membrane electrode assemblies (MEAs) with PBI and cross-linked PBI membranes were fabricated by Ultrasonic Coating Technique as it was described in literature [100]. The Pt/C is used as an anode and cathode side catalyst. The widely preferred Nafion polymer binder in LT-PEMFC, is not practical for HT-PEMFCs operating at higher temperatures because at higher temperatures humidity decreases drastically. Nafion is not conductive under non-humidified conditions therefore it blocks of the catalyst sites for hydrogen oxidation and oxygen reduction [106]. Thus, catalyst ink composed of 70 wt. % Pt on Vulcan XC-72 and PTFE was pulverized on gas diffusion layer (GDL). The catalyst ink was prepared by dispersing catalyst powder into a mixture of DMAc and PBI. The mixture was ultrasonicated for about 40 min before usage. The used commercial GDL was based on carbon paper coated with a carbon microporous layer (Freudenberg-H2315C2). The catalyst ink was ultrasonic-sprayed onto the GDLs at 80 °C by the Sono-Tek 'Exacta-coat' ultrasonic spray instrument (120 kHz). The catalyst ink was inserted in a syringe pump before atomization in the nozzle (Accumist) and sprayed at a flow rate up to 0.5 ml min^{-1}. A catalyst loading of 0.6 mg cm^{-2} was used for all MEAs, both in the anode and the cathode side. In the final step of MEA preparation the electrodes were hot pressed onto both sides of the phosphoric acid doped PBI and cross-linked PBI membranes at 150 °C and 172 $N.cm^{-2}$ for 5 min.

3.6. Characterization of PBI Polymer

3.6.1. Nuclear Magnetic Resonance (NMR)

Nuclear magnetic resonance is a physical phenomenon in which magnetic nuclei in a magnetic field absorb and re-emit electromagnetic radiation. The energy emitted during this process is at a specific resonance frequency depending on the strength of the magnetic field nuclei resides in and the magnetic properties of the isotope of the atoms [9]. The common studied nuclei are ^{1}H and ^{13}C. The chemical structure of the polymer synthesized was

characterized by ^{13}C CPMAS NMR. Bruker Superconducting FT-NMR Spectrometer was used at a spin rate of 8500 Hz and with a 4mm MAS probe.

3.6.2. Determination of the Molecular Weight

It is well known that one of the most important parameters in synthesizing polymers is correct determination of molecular weight of the polymer. Ubbelohde viscometer is a useful instrument to determine the viscosity of the polymer solution. In this study, to determine the viscosity of polymer solution, a clean viscometer was used firstly to measure retention time of pure solvent (H_2SO_4, 98 vol. %) named as t_0. After the measurement viscometer is cleaned and dried carefully and this time flow time of different concentrations (to give 2-5 g L^{-1} solid content typically), named as t, and was measured. Using the obtained retention time values t_0 and t, the relative viscosity (η_{rel}) and the specific viscosity (η_{sp}) should be determined at different concentrations according to (3.2) and (3.3) [74].

$$\eta_{rel} = \frac{t}{t_0} \tag{3.2}$$

$$\eta_{sp} = \frac{(t-t_0)}{t_0} \tag{3.3}$$

The specific viscosities were measured for a series of polymer solutions of different concentrations. The specific viscosity values obtained were then divided by the respective concentration, to get the reduced viscosity $\eta_{red.}$ Intrinsic viscosity ([η]) of the polymer solution can be obtained by plotting ‘’η_{inh}’’ vs. ‘’c’’ graph where ‘’c’’ is the concentration of the polymer solution. Intrinsic viscosity was obtained by the interception of this graph.

In order to calculate instrinsic viscosity both Huggin’s and Kraemer’s equations can be used. In Huggin’s equation reduced viscosity and intrinsic viscosity are directly proportional with each other while in Kramer’s equation inherent viscosity and intrinsic viscosity are directly proportional with each other. Equation 3.4 and 3.5 gives Huggin’s and Kramer’s equation.

$$\eta_{red} = \frac{\eta_{sp}}{c} = [\eta] + k_H.[\eta]^2.C \quad \text{(Huggins's equation) (3.4)}$$

$$\eta_{inh} = \frac{\ln \eta_{rel}}{c} = [\eta] - k_K.[\eta]^2.C \quad \text{(Kramer's equation) (3.5)}$$

After calculating intrinsic viscosities using both equations, the intrinsic viscosity can be calculated by taking mean value of the results obtained by both equations [101].

Three solutions of PBI with concentrations, 0.25, 0.5 and 0.7 g dL^{-1} were prepared with 98 vol. % H_2SO_4. Retention times of the solutions in viscometer were measured with the help of a chronometer. Flow times were measured at 30^0C. The temperature was stabilized by immersing the bottom part of the viscometer in a water bath that is kept at 30 ^{0}C. Molecular weight of the polymer was calculated by Mark Houwink equation (3.6) given below:

$$[\eta] = K(M_w)^a \quad (3.6)$$

Where '*K*' and '*a*' are constants depending on the polymer solvent and the temperature. The values for PBI were taken from literature: $K = 1.94 \times 10^{-4}$ and $a = 0.791$ [102]

3.7. Characterization of the Membranes

3.7.1. Thermal Gravimetric Analysis

Thermal stability of the membranes was examined using a Thermal Gravimetric Analyzer (Perkin Elmer Pyris 1 TGA). Temperature range was 25°C - 800°C, at a heating rate of 10°C min^{-1} under nitrogen atmosphere.

3.7.2. Scanning Electron Microscopy Analysis

The surface morphologies of the membranes were carried out by Scanning Electron Microscope (SEM), QUANTA 400F Field Emission SEM system equipped with an energy dispersive X-ray (EDX) spectrometer. To view the cross-section of the membranes, all the membrane samples were quenched in liquid nitrogen, and subsequently they were fractured. The fractured surfaces of the samples were coated with a layer of gold to avoid charging effect during SEM analysis.

3.7.3. Mechanical Tests

Tensile tests were conducted in order to decide on mechanical performances of the membranes. These tests were carried out according to ASTM 638.

A universal test machine Instron 3367 instrument was used (**Figure 17**) and the test speed was determined as 5 mm min^{-1}.

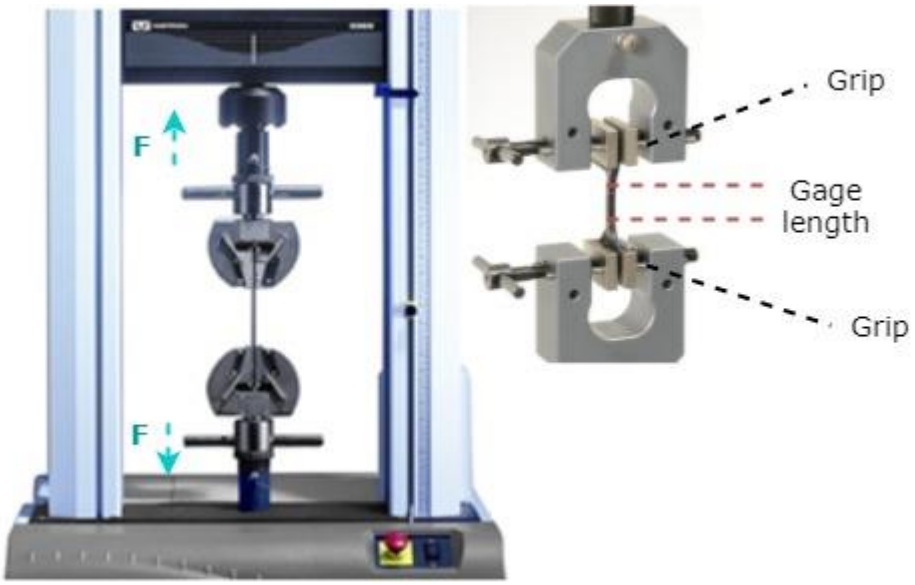

Figure 17 Instron 3367 tensile machine and a representative apparatus[103]

Dog-bone shaped samples were cut for the test and they were tested using universal tensile test machine illustrated in Figure3.6. Afterwards, the load (F) is applied to the dog-bone shaped sample gripped symmetrically. With the help of extensometer, the change in the length of the specimen (Δl) is measured with original length as reference (l_0). The equations (3.7) and (3.8) give Engineering Stress and Engineering Strain calculations.

$$Engineering\ Stress\ (MPa),\ S = \frac{F}{A_0} \tag{3.7}$$

$$Engineering\ Strain\ (\%),\ e = \frac{\Delta l}{l_0} \tag{3.8}$$

Where A_0 is the cross-sectional area of the dog-bone sample before test begins.

The tests were carried out for three times and the results are represented as the mean values of these three runs.

3.7.4. Acid Leaching Tests

In order to determine the acid retention capability of the membranes prepared, acid leaching tests were conducted. The procedure from literature was used to determine the effect of cross-linker used on the acid leaching [81]. The membranes were kept in direct contact with water vapor for five hours and weight loss due to the PA leaching from the membrane was determined by weighing the membrane in every hour. Acid leaching percentages of the membranes were calculated according to the following equation (3.9):

$$\text{Acid Loss Percentage} = \frac{W_{\text{PA doped}} - W_{\text{initial}}}{W_{\text{acid}}} \times 100\ \% \qquad (3.9)$$

A sample calculation of loss percentage is given in Appendix A.

3.7.5. Proton Conductivity Analysis

Electrochemical Impedance Spectroscopy (EIS) is the small-signal measurement of the linear electrical response of a material and the subsequent analysis of the response to yield useful information about the physiochemical properties of the system [104]. Currently, EIS has been widely used as a technique to characterize interfacial and transport properties of polymer films, organic-inorganic coatings, and self-assembled monolayers adsorbed on the surface of an electrode. The estimation of important parameters such as diffusion coefficient and charge transfer resistance that can explain the kinetics at interfaces becomes easier and more accurate compared to other techniques. Basically, a small amplitude AC signal is imposed on the system under study and the impedance measurements are taken at various frequencies of the applied AC signal [105]. Data depending on the frequency is fitted using equivalent circuits. Proton conductivities of the membranes were determined by electrochemical impedance spectroscopy, four probe method, with ZIVE SP2 (WonATech, Korea) Electrochemical Workstation test machine which is shown in **Figure 18**.

Figure 18 ZIVE SP2 Electrochemical Workstation

Four-probe method consists of four equally spaced – 1 cm for each space - Pt probes. Membranes were cut to fit in the measurement cell so that it interacts with all four probes. AC impedance was measured between 65 MHz and 65 mHz for all membranes. Measurements were done at three different temperatures, 140°C, 165°C and 180°C. In order to confirm relaibility of these results, at each temperature, data were collected for about an hour in every ten minutes. The results were fitted to Randel's Circuit model which is given for conducting polymer models in the program database. The model and the best fitted curve was given in **Figure 19**.

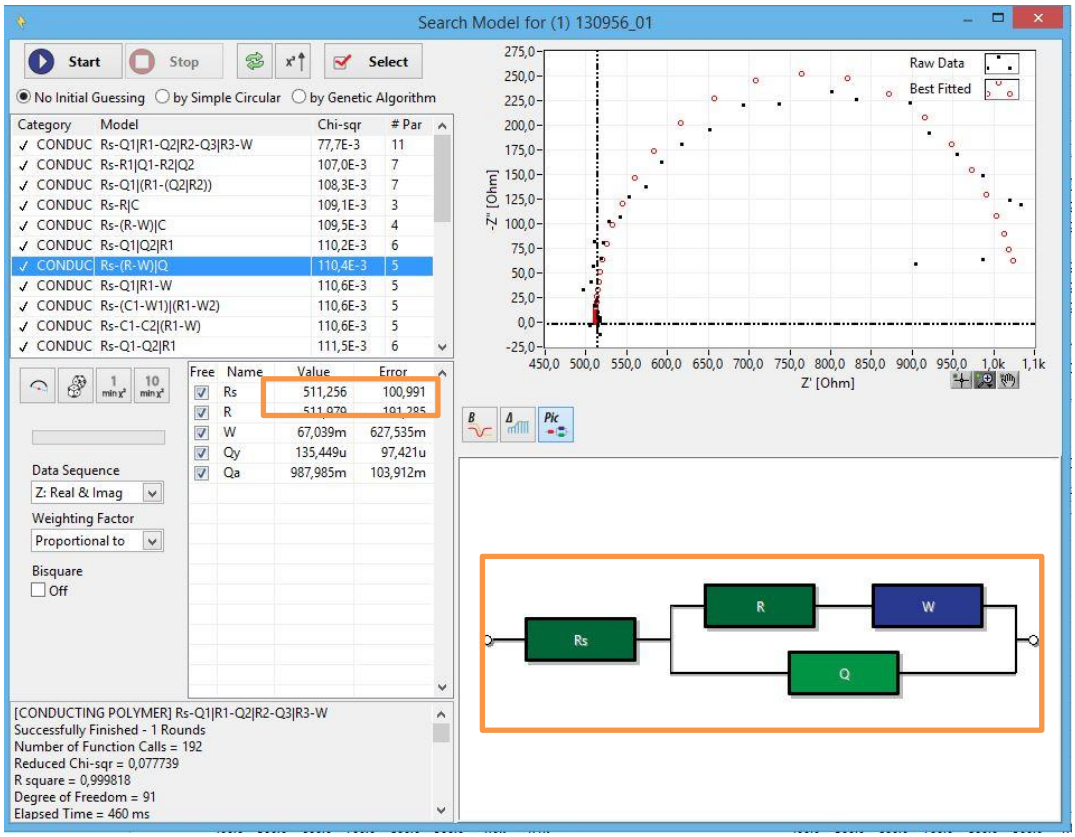

Figure 19 Randel's Circuit Model

The conductivity of the membranes was calculated using the following equation (3.11).

$$\sigma = \frac{L}{r \times w \times t} \qquad (3.11)$$

Where σ is the proton conductivity of the membrane (S cm^{-1}), r is the R_s (resistance) value obtained for the membrane (Ω) from the software output, w is membrane width (cm), t is the membrane thickness (cm) and L is the gap between two probes of the impedance cell (cm).

In order to decide on the proton conductivity mechanism, conductivity data is used to calculate the activation energies, using Arrhenius equation shown below in equation (3.11) [106].

$$ln(\sigma.T) = ln\sigma_0 - \frac{E_a}{RT} \qquad (3.10)$$

In this equation, σ is the proton conductivity of the membrane (S cm^{-1}), σ_0 is the pre-exponential factor (S cm^{-1}), E_a is the proton conducting activation energy (J mol^{-1}), R is universal gas constant (J mol^{-1} K^{-1}) and T is the absolute temperature (K).

The experimental set-up used for proton conductivity analysis is given in **Figure 20**.

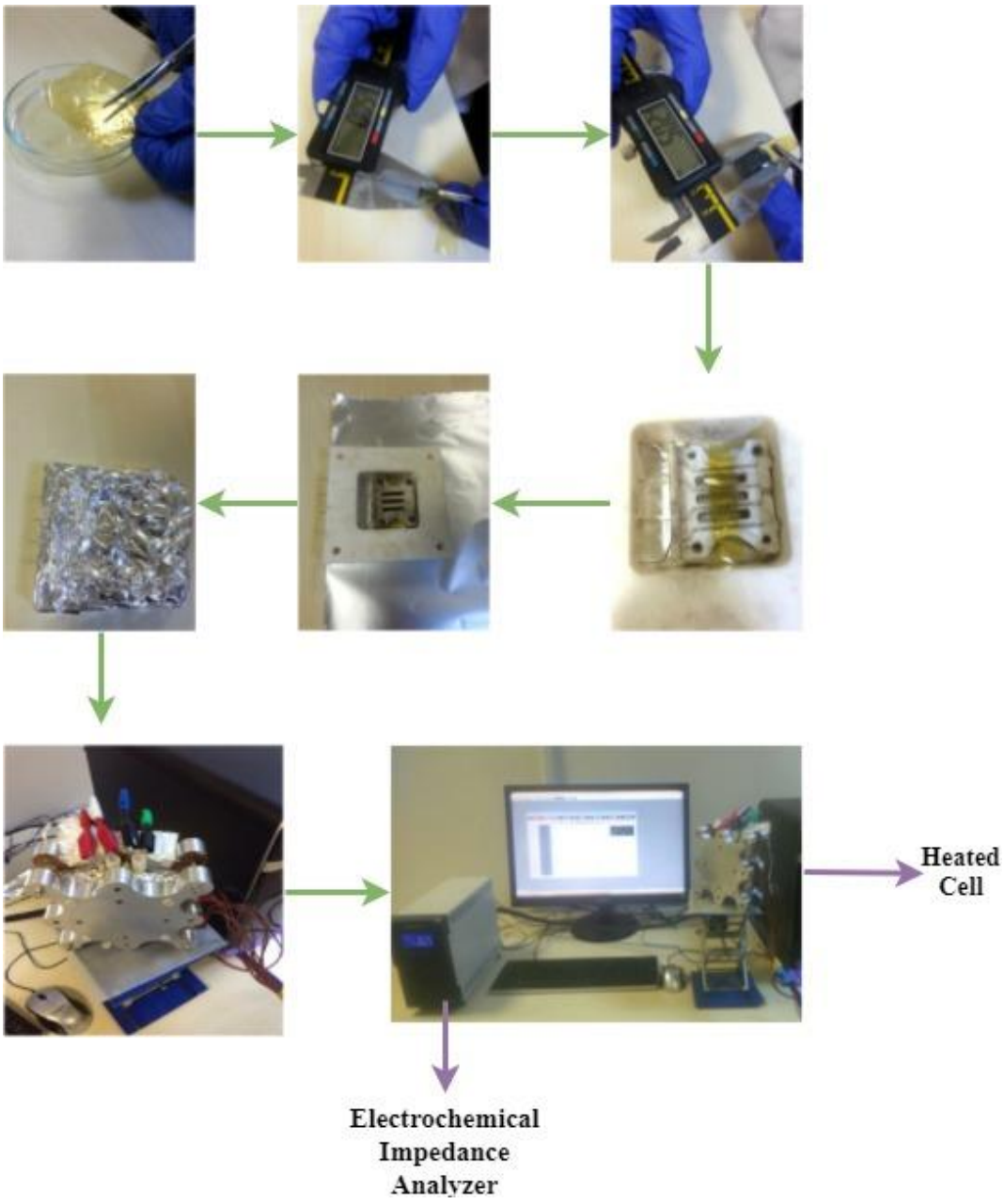

Figure 20 Experimental set-up for proton conductivity analysis.

3.8. HT-PEMFC Performance Tests

The best way to determine the performance of a HT-PEMFC is to perform performance tests that give information about currents density, voltage and maximum power density that can be obtained. There are three common ways to analyze the performance of a HT-PEMFC. These control current, voltage or power. Power control is the uncommon way of performing performance tests since it depends on both voltage and current density. In the current control method, current is controlled at corresponding voltage values to understand the correlation between them. As for the voltage control, the same method is followed but voltage is controlled at corresponding current values this time. In order to determine the HT-PEMFC performances of the fabricated MEA's, measurements was undertaken via the HT- PEMFC (TECHSYS Fuel Cell Test Kit) test station in Atılım University Hydrogen Energy Research Laboratory. The MEAs were tested in a single cell having 5 cm^2 active area. The flow field plates were made of graphite and the geometry of the flow channel was of the serpentine type. The single cell PEMFC sealing is a very important parameter as well. If the sealing had failed, oxygen and hydrogen would be mixed and this would result in the burning of the MEA [107]. Viton gaskets were used to prevent sealing failures and mixing the reactant gases. The performance of the fabricated MEAs was evaluated after conditioning for 5 h at 0.6 V. The current and voltage of the cell were monitored and logged throughout the operation of the cell by the fuel cell test software (TECHSYS-HYGO). Once the steady state was achieved, starting with the OCV value, the current–voltage data was collected by changing the voltage values from the load.

The test was performed with the following reactant gas flow rates and stoichiometric ratios:

- H_2: 0.05 slpm (standard liters per minute), at 1.5 stoichiometry (%99.995 H_2)
- Compressed Dry Air: 0.12 slpm (standard liters per minute), at 2.5 stoichiometry (Directly fed from compressor/dryer unit as shown in **Figure 21**)

The polarization curves were recorded at atmospheric pressure using dry air and hydrogen at 165 ^{0}C. HT-PEMFC test duration for the membranes was

approximately 40 hours for each. Table 3.2 gives important parameters of single HT-PEMFC. **Figure 21** shows the test station and experimental setup for HT-PEMFC tests.

Table3.2. HT-PEMFC Single Cell Properties

Active area	**5 cm^2**
Sealing	Viton Gaskets
Gas diffusion layer	Freudenberg H2315
Current collector	Gold Coated Copper
Bipolar plate	Composite Graphite
Flow channel	Serpentine Type
Connections	Stainless steel (Teflon connections were preffered for inlet and outlet connections to protect the Graphite plates)
Compression	1.7 Nm (Measured by a Torque Wrench)

It is important to note that, while collecting the cell, correct installation of the mechanical parts is very important. Gaskets must be placed so that the membrane is not in contact with graphite plates and the graphite plates do not touch each other, which results in short circuit. Additionally, damaged gaskets may cause leakage of hydrogen. While the cell is compressed at 1.7Nm, it is crucial to apply even out the pressure on each corner of the cell, so that the gaskets and the membrane do no get damaged. Finally, since graphite plates are fragile, the inlet and outlet gas connections should be chosen as Teflon, or if stainless steel they should be covered with Teflon tape.

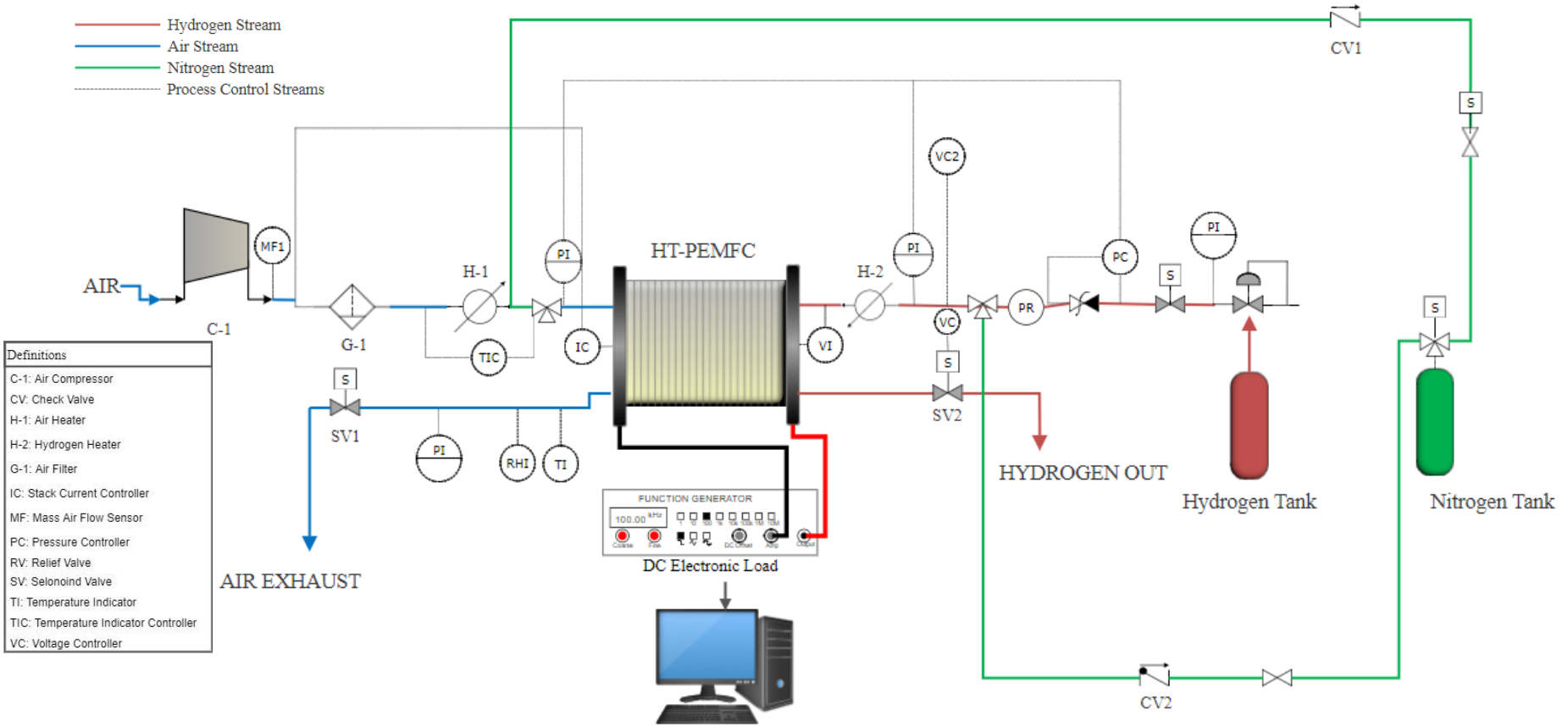

Figure 21 HT-PEMFC Test Station Set-up

CHAPTER 4

RESULTS AND DISCUSSION

In Chapter 4, the experimental results obtained in this study are given.

PBI polymer was synthesized with solution polycondensation method as described in Chapter 3. The synthesized and isolated PBI polymer which is in fiber form was characterized by C-NMR method.

The membranes studied in these experiments were casted by using PBI polymer. Membranes prepared with different cross-linkers and different cross-linking degrees were characterized to optimize HT-PEMFC performance of the membranes and determine the best performing cross-linker. In this sense, the cross-linked membranes were prepared by cross-linkers TPA (5 wt. %), BADGE (5 wt. %), DBpX (3 wt. %) and EGDE (5 wt. %). They were later characterized by TGA, SEM, FTIR, tensile tests, acid doping level, acid leaching level, DMAc extraction, and proton conductivity and finally HT-PEMFC performances of the membranes were measured. Furthermore, the investigations with BADGE cross-linker were carried out by changing the cross-linker amount to decide on the optimum BADGE amount for better HT-PEMFC performance. Cross-linked PBI membranes with 2.5 wt. %, 5 wt. % and 7.5 wt. % BADGE were prepared by solution casting method described in the previous chapter. These membranes were also characterized by following the same procedures.

4.1. Characterization of the Synthesized PBI Polymer

4.1.1. Nuclear Magnetic Resonance Spectra

The ^{13}C CPMAS NMR spectra of the pure PBI are shown in **Figure 22**.

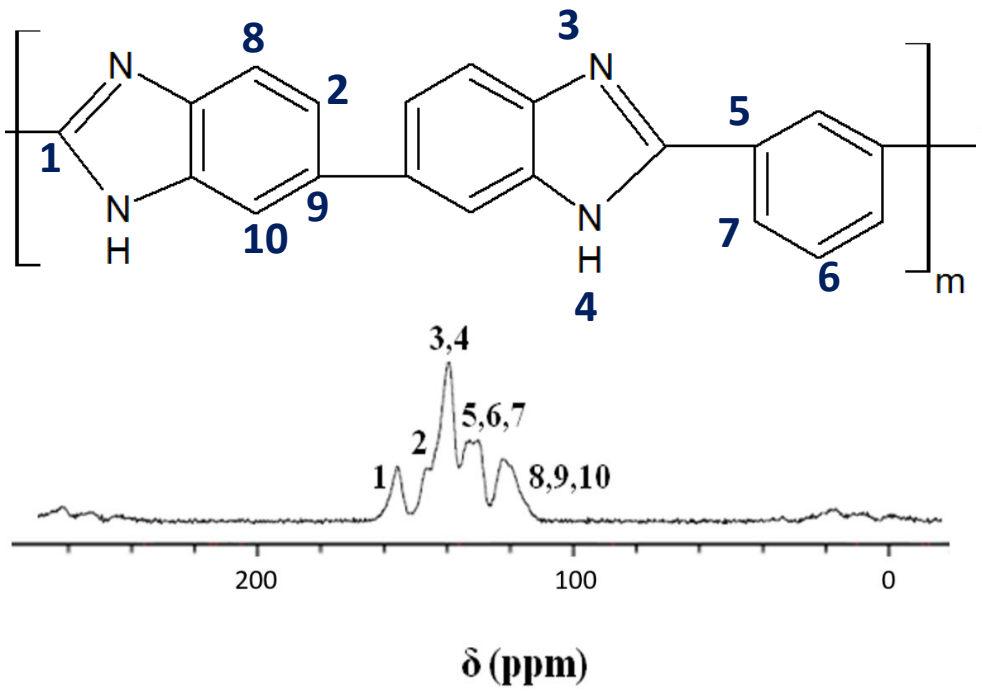

Figure 22 ^{13}C-NMR spectra of PBI polymer

The spectrum of PBI consists of several lines that can be identified, carbons of imidazole rings attached to phenylene rings (154 ppm), the carbons that connect benzimidazole rings in bibenzimidazole group (145 ppm). Aromatic carbons bound to the nitrogen atoms are represented with the third line (139 ppm). There are two remaining lines that must be assigned (133 ppm, 118 ppm). These are attributed to protonated carbons of PBI with a contribution from the non-protonated carbons of the phenylene ring to the line centered at 123 ppm [108,109].

4.1.2. Determination of Molecular Weight

Molecular weight of the PBI polymer synthesized was determined by Ubbelohde viscometer method (Section 3.5.2). For this test, the PBI solutions with different concentrations were prepared using H_2SO_4 as solvent. PBI solutions with approximate concentrations 0.25, 0.5 and 0.7 g dL^{-1} were prepared in sulphuric acid by diluting. The retention times of the solutions and pure solvent were measured through the Ubbelohde viscometer. The

measurements were done three times for confirmation. After completing each measurement viscometer cleaned and dried thoroughly.

Equation 3.2 and 3.3 were used to calculate η_{sp} and η_{red}. Concentration versus reduced viscosity was plotted as shown to obtain [η] based on Huggins' Equation (**Figure 23**). And inherent viscosity versus concentration graph is plotted to obtain [η] based on Kramer's Equation (**Figure 23**).

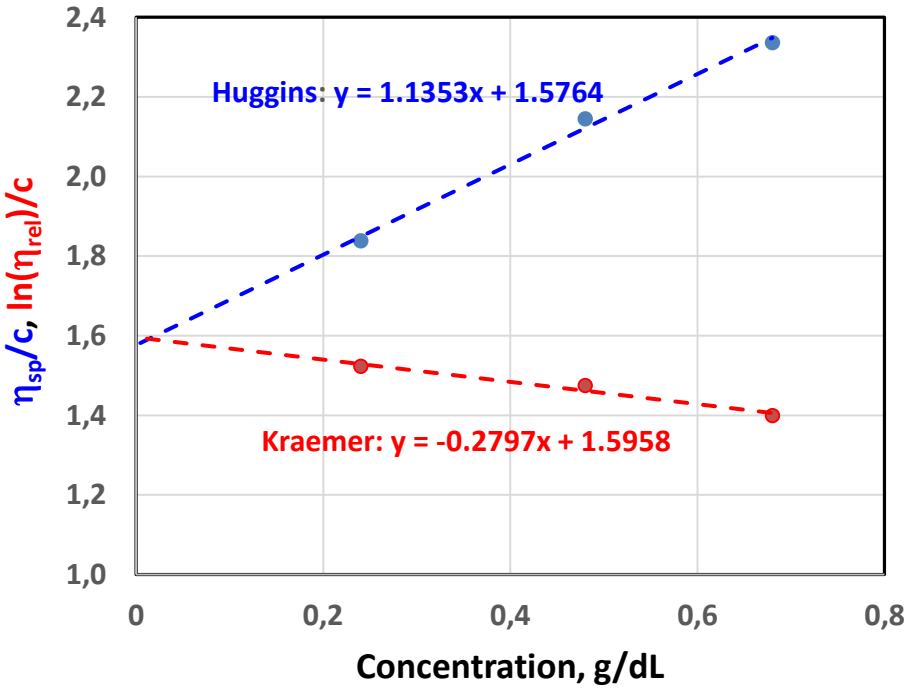

Figure 23 Reduced and inherent viscosity vs. concentration graphs.

Both values obtained by Huggins' equation (3.4) and Kramer's equation (3.5) were close to each other, thus [η] is calculated by taking the mean value of these two results. As a result, [η] was found as 1.586 g/dL. Calculated average molecular weight of the polymer was determined as 88.400 g/mol according to Equation 3.6.

In this study, the PBI was synthesized at different temperatures (185^0C - 200^0C) for different durations (16 hours - 24 hours) as it was studied in literature [110]. All the synthesized batches of PBI did not dissolve in DMAc and DMSO. The polymer synthesized with 88.400 g/mol at 190^0C for 19 hours was expected to

have better solubility but it was not used in the membrane preparation as well since it was found to be very hard to dissolve in organic solvents DMAc and DMSO. Ergün observed that with LiCl as the stabilizer, PBI tends to dissolve easier. Even with LiCl it was not possible to dissolve the polymer with the conventional dissolving methods. It is known that molecular weights of the PBI are limited due to the inherent solubility issues in organic solvents. Conventional synthesis and casting method used in this study is extremely time consuming for higher molecular weights. In literature [111,112], there are alternative methods to synthesize higher molecular weight PBI and cast membranes easier, however, these alternative methods were not within the scope of this study and they are not further investigated. Polymer with a molecular weight of 39000 g/mol was found to be very easy to solve and it has higher purity than in-house synthesized polymer. Thus, it was used for preparing the membranes that were tested on HT-PEMFC.

4.2. Characterization of the Membranes

4.2.1. Scanning Electron Microscopy Analysis (SEM)

The surface morphologies of the PBI based membranes before and after crosslinking were analyzed using SEM.

Figure 24 (a, b, c) shows the cross-sectional SEM images of PBI membranes with x2000, x5000 and x50000 magnifications. As seen from **Figure 24** (a,b,c) the cross-section of the pure PBI membrane shows a smooth surface without any cracks or pinholes, indicating the fine quality of the membrane. The EDX spectrum of the pristine PBI is shown in **Figure 24** (d). The spectrum shows the presence of carbon (C), oxygen (O) and nitrogen (N). Au and Pd peaks can be attributed to the coating before the measurement.

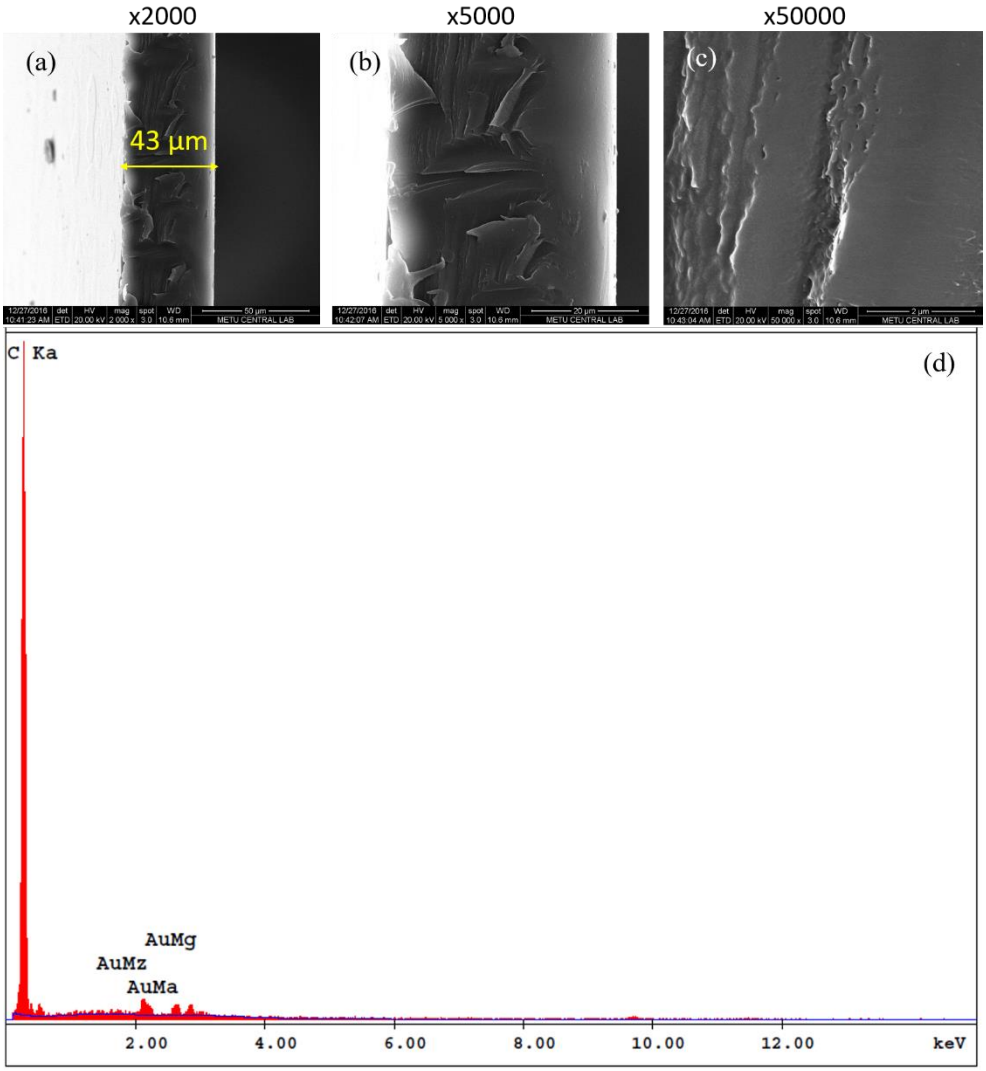

Figure 24 The cross-sectional SEM images of the pristine PBI membrane at x2000, x5000 and x50000 magnifications (a,b,c); the EDX analysis of pristine PBI membrane (d)

Figure 25 shows the cross-sectional SEM images of the cross-linked PBI-DBpX-3 membrane at x2000, x5000 and x50000 magnifications. As can be seen from **Figure 25** (a,b,c), the cross-sectional images of the PBI-DBpX-3 membrane shows smooth surface without any cracks or pinholes similar to the pristine PBI membrane. However, some agglomerated particles were observable. These particles can be attributed to unreacted DBpX particles. The EDX spectrum of aforementioned membrane shows similar peaks to the pristine PBI membrane, which can be interpreted as the homogeneity of the membrane was protected during the cross-linking reactions.

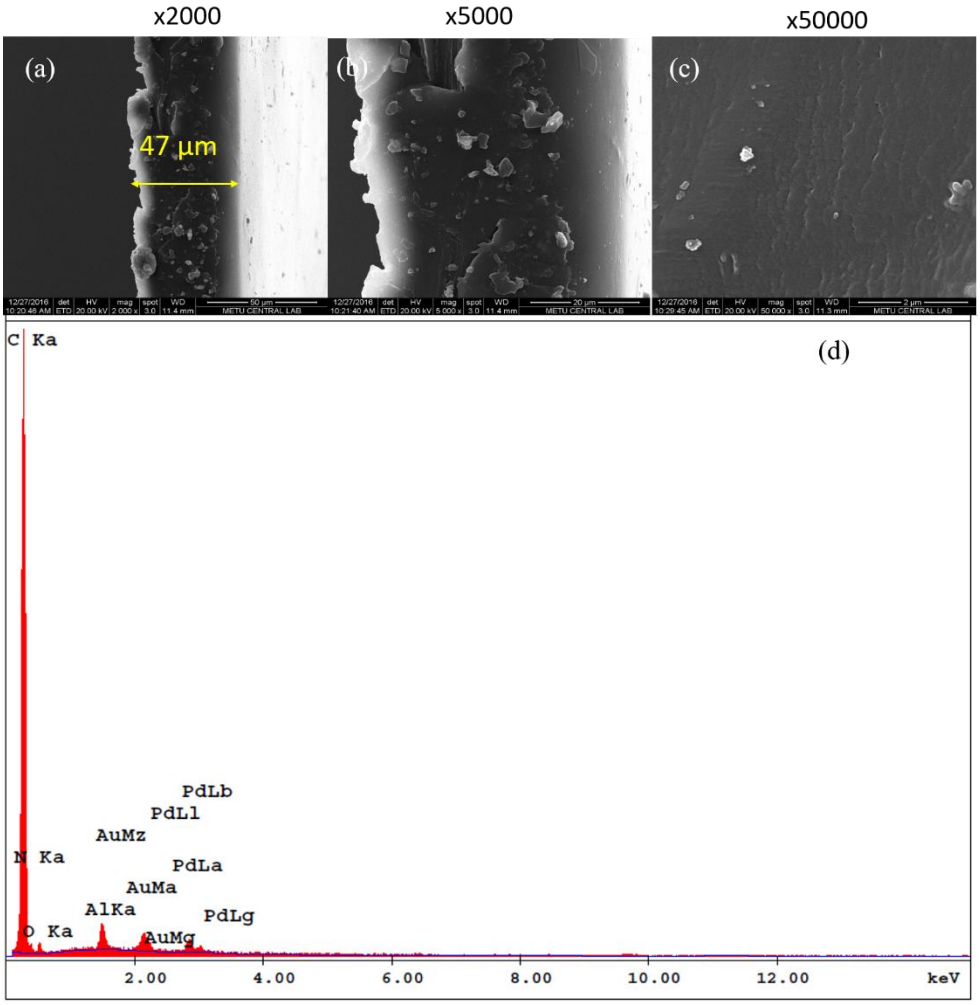

Figure 25 The cross-sectional SEM images of thr PBI-DBpX-3 membrane at x2000, x5000 and x50000 magnifications (a,b,c); the EDX analysis of the PBI-DBpX-3 membrane (d)

Figure 26 shows the cross-sectional SEM images of the cross-linked PBI-TPA-5 membrane at x2000, x5000 and x50000 magnifications. As seen from Figures 4.6 (a,b,c), the PBI-TPA-5 membrane shows agglomerated particles which can be attributed to unreacted TPA particles. The EDX spectrum of the membrane shows similar peaks to the pristine PBI membrane. The Spot EDX analysis was conducted in order to identify the agglomerated particles observed on the cross-section of the membrane. **Figure 26** (e) shows the spot EDX analysis result taken from the part with agglomerated particles. It was seen that there are C and O elements, which are present in both PBI and TPA. This result indicates that the immiscible particles are unreacted TPA which means that the cross-linking reaction with TPA was not effectively completed.

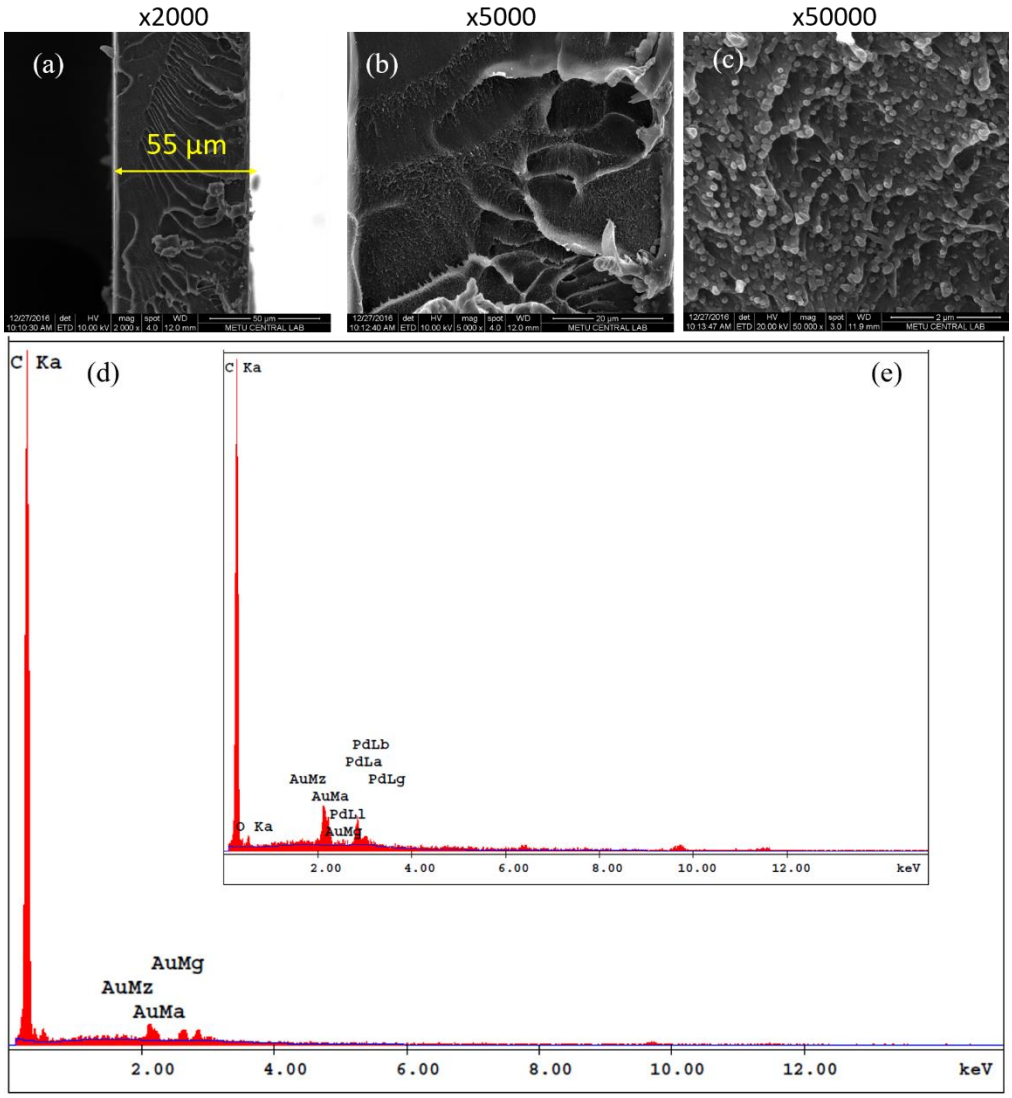

Figure 26 The SEM cross-sectional images of the PBI-TPA-5 membrane at x2000, x5000 and x50000 magnifications (a,b,c); the EDX analysis of PBI-TPA-5 membrane (d)

Figure 27 shows the cross-sectional SEM images of the cross-linked PBI-BADGE-5 membranes at x2000, x5000 and x50000 magnifications. The agglomerated particles were observable but not as much in the PBI-TPA-5 membrane. The EDX spectrum showed similar peaks compared to the other membranes, which shows the homogeneity in the membrane matrix.

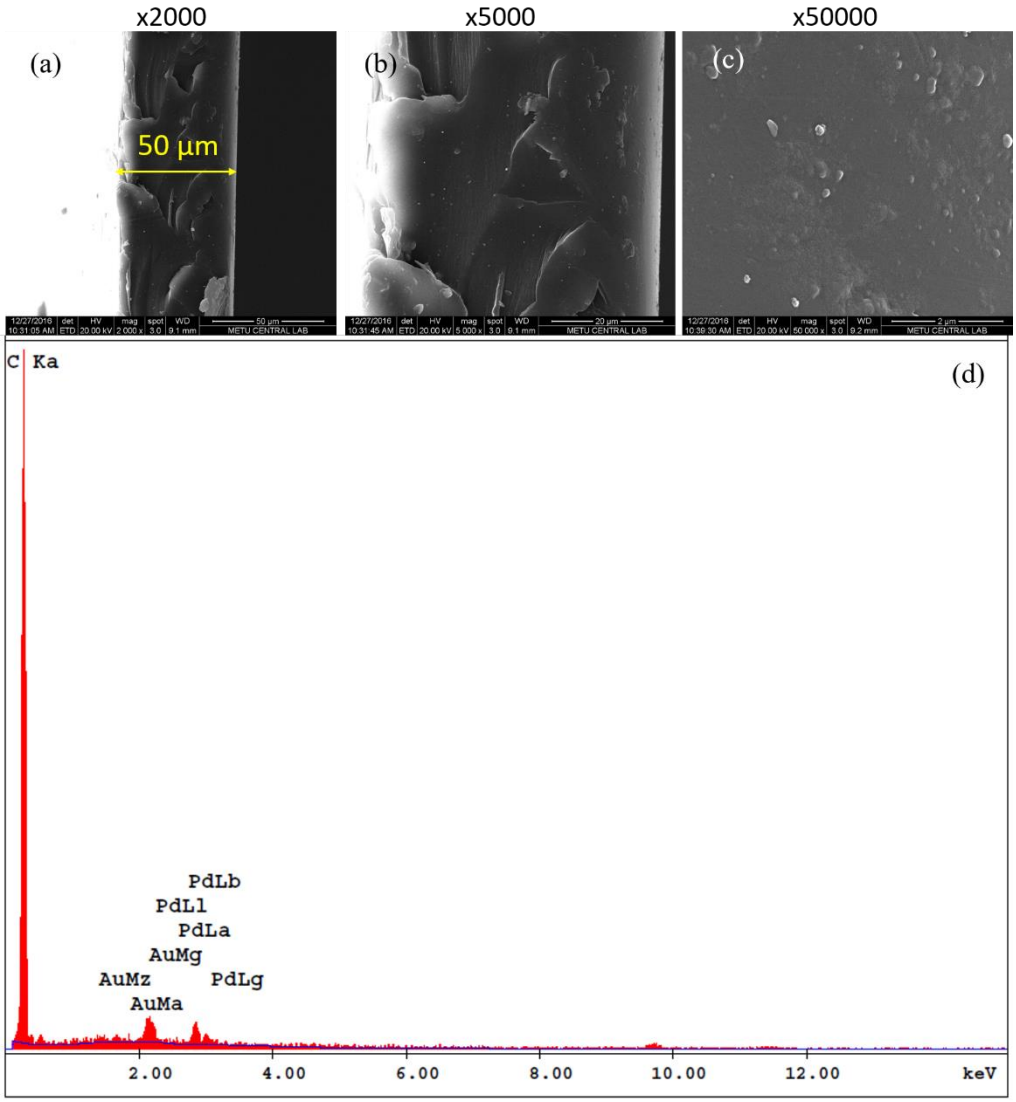

Figure 27 The SEM cross-sectional images of the PBI-BADGE-5 membrane at x2000, x5000 and x50000 magnifications (a,b,c), the EDX analysis of PBI-BADGE-5 membrane (d)

Figure 28 shows the cross-sectional SEM images of the cross-linked PBI-EGDE-5 membrane at x2000, x5000 and x50000 magnifications. The EGDE cross-linker was added in the liquid phase, thus immiscibility problem was not experienced with the PBI-EGDE-5 membrane. The SEM images shows no agglomeration as expected. The Membrane surface is smooth with no cracks or pinholes. In **Figure 28** (d) the EDX analysis of the membrane was given. It confirms homogeneous membrane matrix.

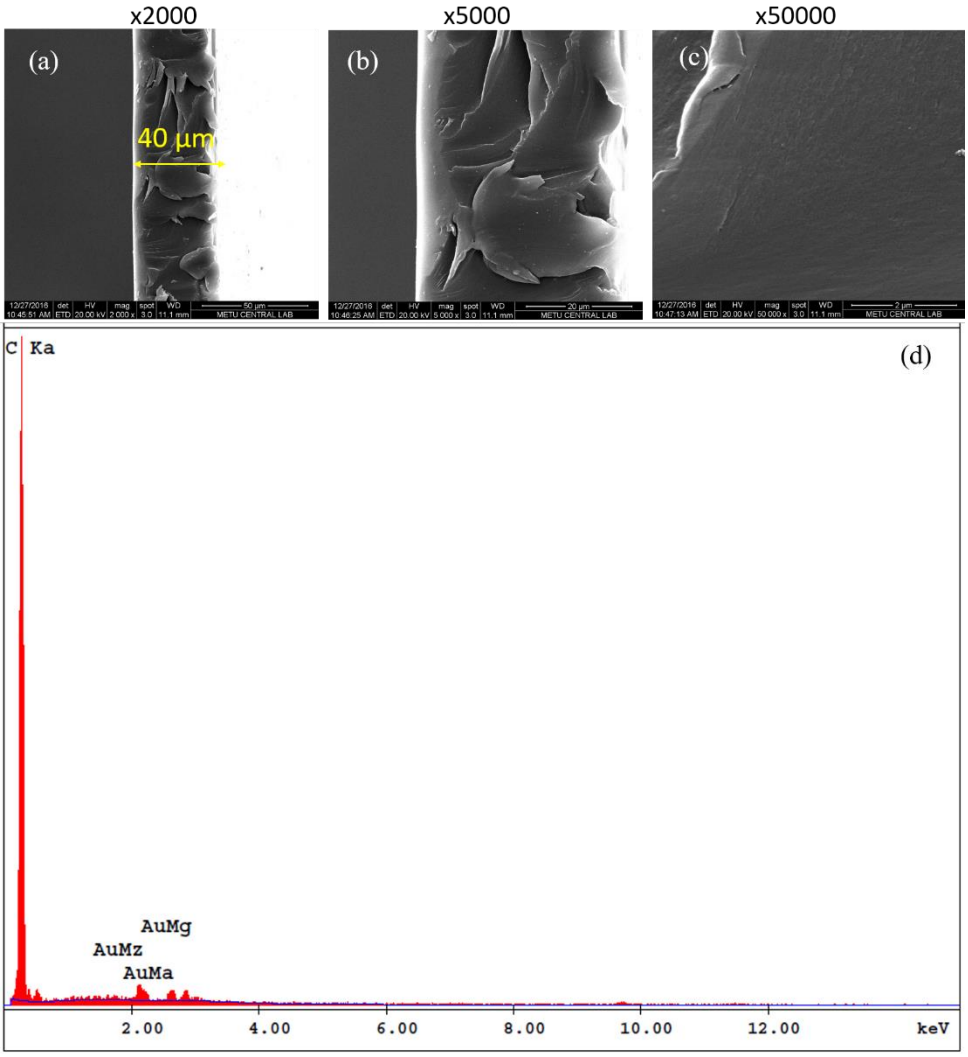

Figure 28 The cross-sectional SEM images of the PBI-EGDE-5 membrane from cross-section at x2000, x5000 and x50000 magnification (a,b,c); the EDX analysis of PBI-EGDE-5 membrane (d)

The SEM images also showed that the thicknesses of membranes stayed in the desired range between 40µm-55µm.

4.2.2. Thermogravimetric Analysis (TGA)

The thermal stability of the membranes was investigated to measure the effect of the cross-linking on thermal behavior of the PBI. TGA analysis conducted by heating samples first from room temperature to 100^0C. The membranes were held at 100^0C and then heated to 900^0C with a ramping rate of 10^0C min^{-1} with dry N_2 flowing. Figure 4.9 shows the thermal gravimetric analyses of the membranes with different cross-linkers while Figure 4.10 shows the TGA results of the covalently cross-linked PBI membranes with different amounts

of BADGE cross-linker. As can be seen from **Figure *29*** and **Figure *30***, three weight loss steps were observed for all membranes.

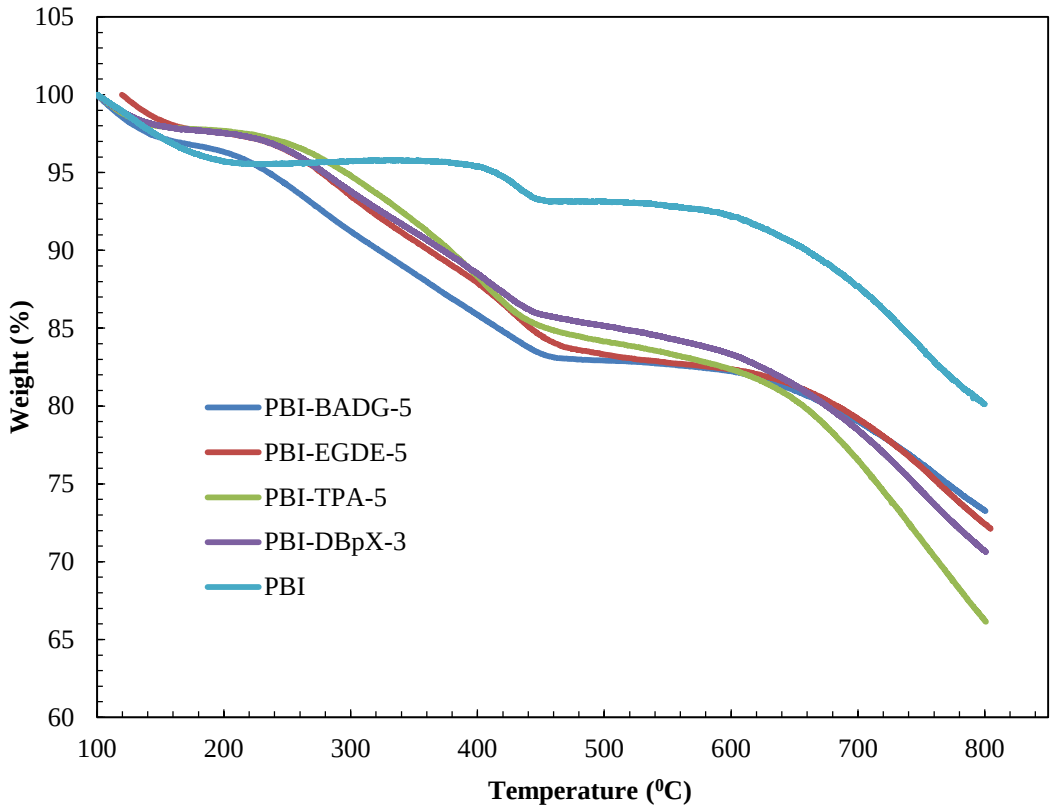

Figure 29 TGA graph of PBI membranes with different cross-linkers

The weight loss between 100^0C–150^0C is due to the evaporation of the remaining solvent and abundant water in the membrane. The pristine PBI membrane showed good thermal stability up to 600^0C, compatible with literature values [113]. However, a significant weight loss was observed at about 400^0C, which is attributed to non-specific cross-linking reactions which results in completely insoluble polymer [114]. It was stated in the literature that all of the weight loss cases up to 400^0C, were found to be mainly because of water. The polymer itself however, was thermally stable [8]. The cross-linked PBI membranes showed varying thermal stabilities. The second weight loss region was found to be different in all membranes. The membranes prepared with TPA cross-linker showed better thermal stability from the membranes PBI-DBpX, PBI-BADGE and PBI-EGDE. This is because of the more stable structure of residual TPA [93]. The PBI-DBpX membranes showed good thermal stability up to 217^0C while PBI-BADGE exhibited high thermal

stability up to 205^{0}C. The pristine PBI membranes lost 20 % of their initial weight during the experiment. PBI-TPA and PBI-EGDE membranes lost up to 33 % of their initial weights while PBI-BADGE lost approximately 36 %. PBI/ DBpX showed 29 % weight loss during the experiment.

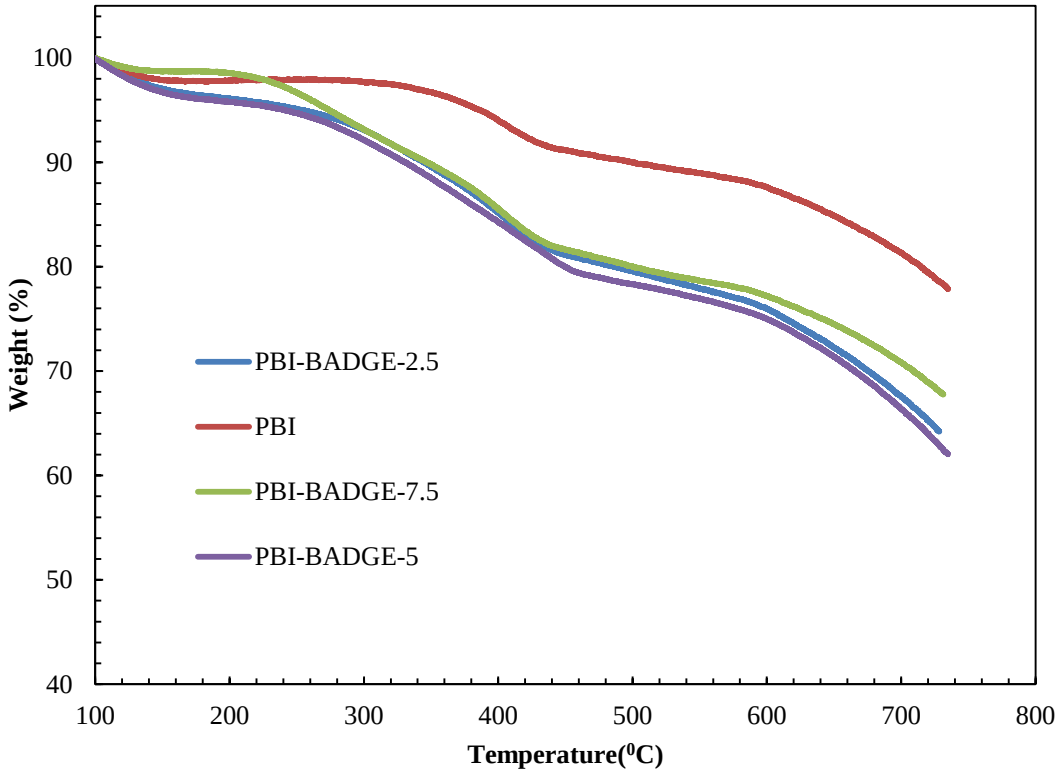

Figure 30 TGA graph of PBI membranes with BADGE cross-linker at different amounts

Figure 30 shows the effect of cross-linker amount on thermal stability of the covalently cross-linked PBI membrane. In **Figure 30**, the PBI-BADGE membranes exhibited the second weight loss around 225^{0}C independently of cross-linker amount. Pristine PBI membrane showed the highest thermal stability similar to the results in **Figure 29**. The Pure PBI membrane lost around 23 % of its initial weight. The PBI-BADGE-7.5 lost approximately 36% of its weight at 720^{0}C due to the degradation of cross-linked structure. Because of the same degradation mechanism, PBI-BADGE-2.5 and PBI-BADGE-5 lost 36% of their initial weight at 720^{0}C.

Excluding the loss of the volatiles, no significant weight loss was observed for the membranes prepared up to 200^{0}C which is high enough for fuel cell applications. All the membranes prepared are thermally stable at the fuel cell

operating temperatures. Therefore, they can be used in HT-PEMFC applications.

4.2.3. FTIR Analysis

FTIR analyses were conducted to validate the successful blending of the cross-linkers with the PBI matrix. **Figure 31** shows the IR spectrum for the first set of membranes: PBI, PBI-BADGE-5, PBI-TPA-5, PBI-DBpX-3, and PBI-EGDE-5. **Figure 32** shows the IR spectrums of PBI-BADGE-2.5, PBI-BADGE-5 and PBI-BADGE-7.5. IR spectrum of pristine PBI (**Figure 31**) and of BADGE from literature (Appendix B) is also given for comparison.

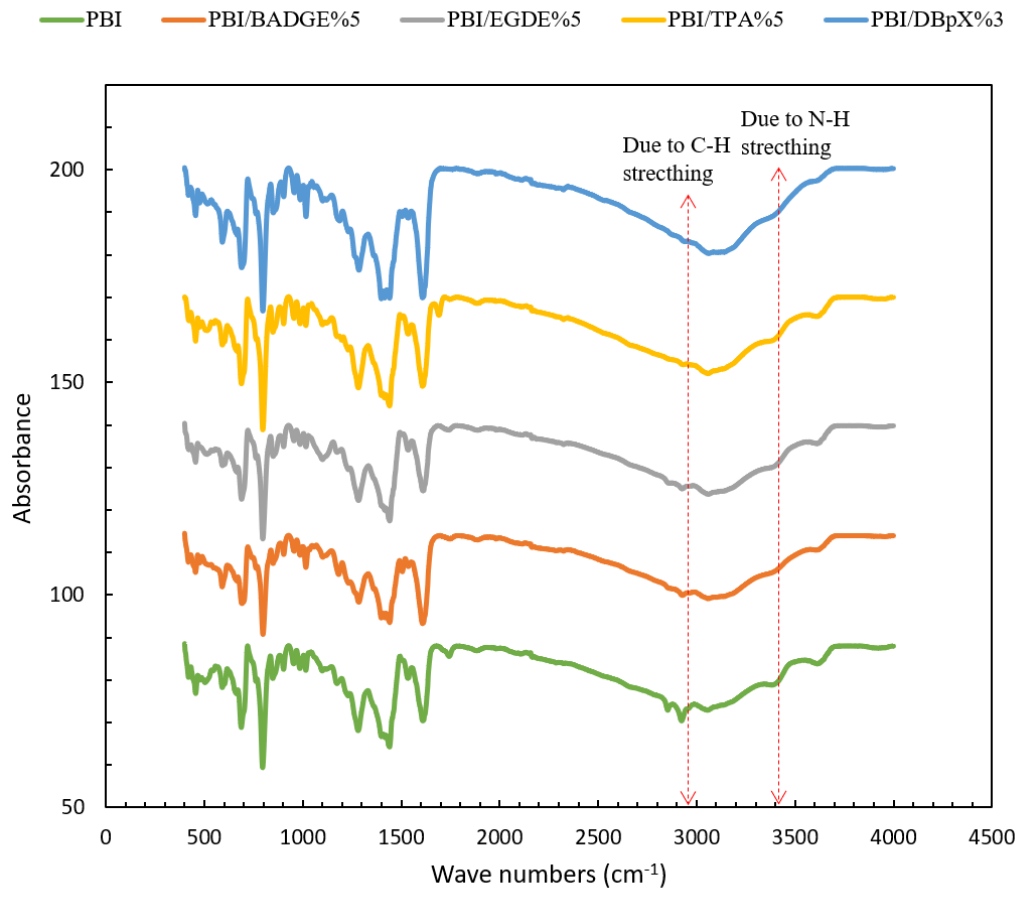

Figure 31 FTIR spectrums for pristine PBI, PBI-BADGE-5, PBI-TPA-5, PBI-DBpX-3, and PBI-EGDE-5.

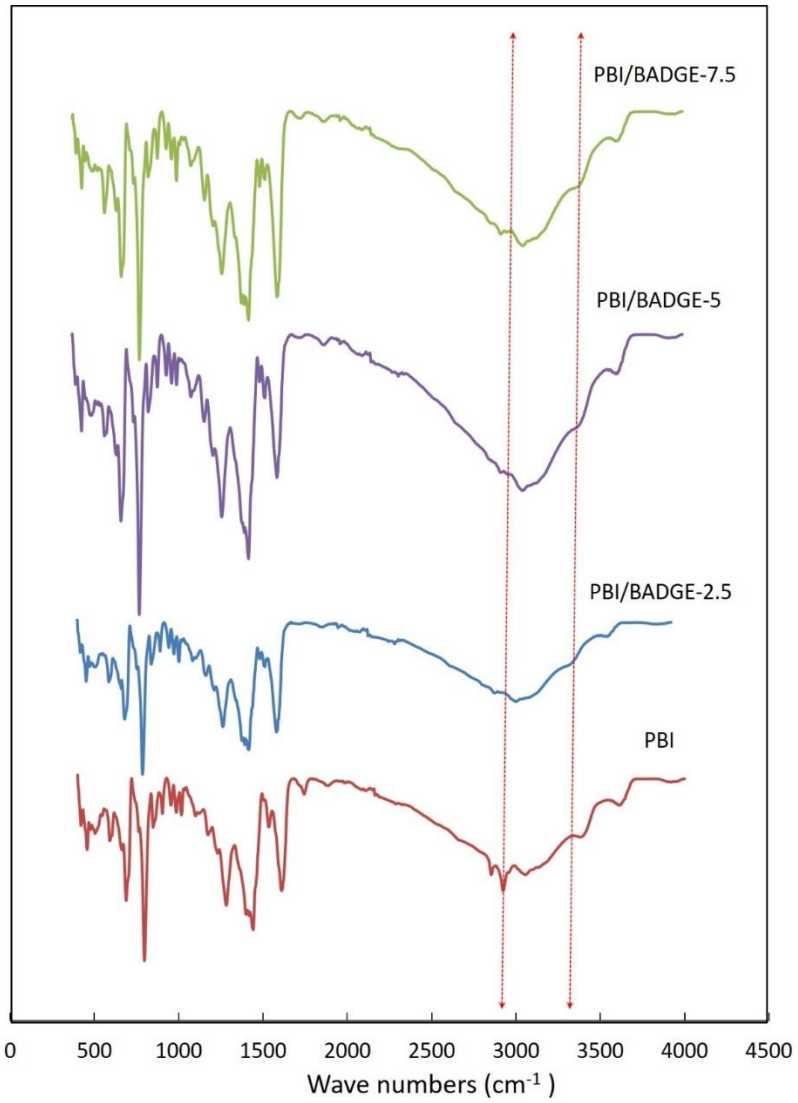

Figure 32 FTIR spectrums of pristine PBI, PBI-BADGE-2.5, PBI-BADGE-5 and PBI-BADGE-7.5.

The FTIR spectra of all PBI and cross-linked PBI membranes exhibited the typical bands corresponding to the benzimidazole of PBI (1430, 1600 and 1620 cm^{-1}). It is evident that the cross-linker added affected the free non-hydrogen bonded N-H stretching band at 3386 cm^{-1} and C-H stretching band at 2938 cm^{-1}. The N-H stretching band present in the pristine PBI, revealed substantial broadening and decrease in the intensity as the cross-linkers added. This peak broadening and reducing in intensity after blending can be interpreted as indications of interactions between PBI and cross-linkers added [120].

FTIR absorption frequencies reference tables and IR spectrum of BADGE are also given in Appendix B.

4.2.4. Acid Doping

The PA doping level of the cross-linked membranes determines the conductivity. All membranes were doped with 85% PA for one week. Before doping, the membranes were washed with boiling water to remove the remaining solvent and to increase the acid doping capacity of the membranes. Acid doping levels (ADL) for all membranes are shown in Table 4.5 and Table 4.6. The results showed that the highest doping level was obtained with PBI-DBpX-5 and pristine PBI membrane, both having ADL of approximately 14.

In the first series of the membranes prepared (Table 4.3) PBI-BADGE-5 membranes exhibited the lowest acid doping levels at approximately 10. PBI-EGDE-5 membranes showed slightly higher ADL than PBI-BADGE-5. At room temperature, ADL values are in good agreement with previously reported literature data [121]. All the cross-linked membranes showed lower ADL compared to the PBI-DBpX-3 and pristine PBI membranes. The cross-linked structure formed from the reaction of epoxide from imidazole -NH groups results in a decrease in the polymer free volume and a decrease in the excess free PA retained in the PBI cross-linked membranes [25].

In the second series of membranes, as the cross-linker amount increased, ADL decreased. PBI-BADGE-2.5 exhibited the highest ADL with 14.3 PA doping level. This value dropped to 12.3 as the cross-linker amount increased to 5 wt. % with PBI-BADGE-5. Finally, PBI-BADGE-7.5 had the lowest ADL value with 10.7. These results prove that as the cross-link density increases, PA doping levels decreases [25].

4.2.5. Acid Leaching

In order to further investigate the acid trapping ability of the prepared membranes, acid leaching tests were conducted according to previous reports in the literature [122]. The PA doped membranes were dried with a tissue in order to remove the excess acid and water on the surface of the membrane. The membranes were kept hanging over hot boiling water (95^0C-100^0C) for 5 hours and the weight of the membranes every one hour was recorded. The acid leaching values for first series and second series of membranes are summarized in Table 4.5 and Table 4.6 respectively.

In the first series of the membranes, pristine PBI showed the lowest acid retention capability among all membranes, losing 85 % of PA doped. It was followed by PBI-TPA-5 with 82% PA loss and the lowest acid leaching value was obtained using PBI-BADGE with 73% PA loss.

In the second series of the membranes, PBI-BADGE-7.5 showed the lowest acid retention capability with a leaching value of 85 %. It was followed by PBI-BADGE-2.5 with 78 % PA loss and the lowest acid leaching value was obtained using PBI-BADGE-5 with 73 % PA loss.

These results prove that cross-linking is an effective method to decrease acid leaching from the PA doped PBI membranes in a humid environment. Lower acid leaching values that obtained with cross-linked membranes may be explained by the amount of water adsorbed in the membrane matrix. The adsorption and diffusion of water in polymeric materials depends on the free volume and polymer-water affinity. The amount of free-volume is related to molecular packing and is affected by cross-link density [123]. The physicochemical reason for this phenomenon requires further investigation; however, it may be connected to a lower diffusivity of phosphoric acid in the cross-linked membrane. It arguably would lead to lower ionic conductivity as well, but if conductivity to a large extent is taking place via the Grotthuss mechanism, then the long range mobility of the acid molecules is not crucial in this regard [124]. The lowest acid leaching value obtained with PBI-BADGE-5 in the first series of membranes may suggest that the most effective cross-linking was between PBI polymer matrix and BADGE.

In the second set of membranes, the effect of BADGE amount was investigated. The membrane that was expected to have higher cross-link density, PBI-BADGE-7.5, exhibited lowest acid retention capability. The reason for this phenomenon was not further investigated, however, it is possible that PBIBADGE-7.5 was not as effectively cross-linked as others or acid retention capability is not directly correlated to cross-linking degree and there are other correlations.

4.2.6. Solubility in DMAc Tests

Solubility in DMAc tests was conducted in order to determine the comparative degree of cross-linking. In order to investigate the stability of the membranes in hot DMAc, the extraction residue was measured. The results are presented in Tables 4.1 and 4.2.

As expected the pristine PBI membrane dissolved completely in DMAc at 130^0C while PBI-DBpX-3 and PBI-BADGE-5 remained as solid membranes in DMAc under the same conditions. The PBI-DBpX-3, PBI-BADGE-5, PBI-EGDE-5 membranes were found to preserve 98%, 93 % and 63% of their initial weights, respectively. Furthermore, the PBI-TPA-5 membrane was dissolved in hot DMAc; however, there were residuals of the membrane at the end of the test. The PBI-TPA-5 membrane preserved 2 % of its initial weight which was the lowest compared to PBI-DBpX-3, PBI-BADGE-5 and PBI-EGDE-5. This result shows that cross-linking with TPA was not efficient, suggesting that longer cross-linking times and higher amounts of TPA are required to enhance the cross-linking degree. However, this was not further investigated in this study.

Table4.1. Extraction in DMAc test results for 1st set of cross-linked membranes and pristine PBI

Membranes	**Extract Ratio (%)**
PBI	0
PBI-DBpX-3	98
PBI-BADGE-5	93
PBI-TPA-5	2
PBI-EGDE-5	63

As for the second set of membranes prepared with different amounts of BADGE, the highest chemical stability was obtained with PBI-BADGE-5

membrane, 90% of its initial weight was preserved. This indicates that the highest cross-link density was obtained with PBI-BADGE-5 membrane[8]. PBI-BADGE-7.5 exhibited very close extract ratio value to PBI-BADGE-5. Since the difference between two values is so small, the reliable comment for this result would be these two membranes are cross-linked effectively and cross-linking density of these two membranes are very close to each other. The question, which has the higher cross-link density, can be answered with acid doping values (Table 4.6) that indicates PBI-BADGE-7.5 has higher cross-linking density since ADL is lower than other two membranes. However, the small differences between test results could be due to the potential measurement errors so the question which membrane has the higher cross-linking density is arguable. The lowest cross-linking density, on the other hand, was unarguably observed with PBI-BADGE-2.5 membrane, which was expected.

Table 4.2. Extraction in DMAc test results for 2nd set of cross-linked membranes and pristine PBI

Membranes	**Extract Ratio (%)**
PBI-BADGE-2.5	83
PBI-BADGE -5	90
PBI-BADGE-7.5	88

4.2.7. Proton Conductivity Analysis

Electrochemical impedance spectroscopy (EIS) was conducted to determine the conductivities of the membranes. Impedance spectroscopy is the small-signal measurement of the linear electrical response of a material and the subsequent analysis of the response to yield useful information about the physiochemical properties of the system [104]. , **Figure 34**, , **Figure 36Figure 37** shows Nyquist plots for the pristine PBI, PBI-BADGE-5, PBI-DBpX-3, PBI-EGDE-5 and PBI-TPA-5 membranes at 165^0C.

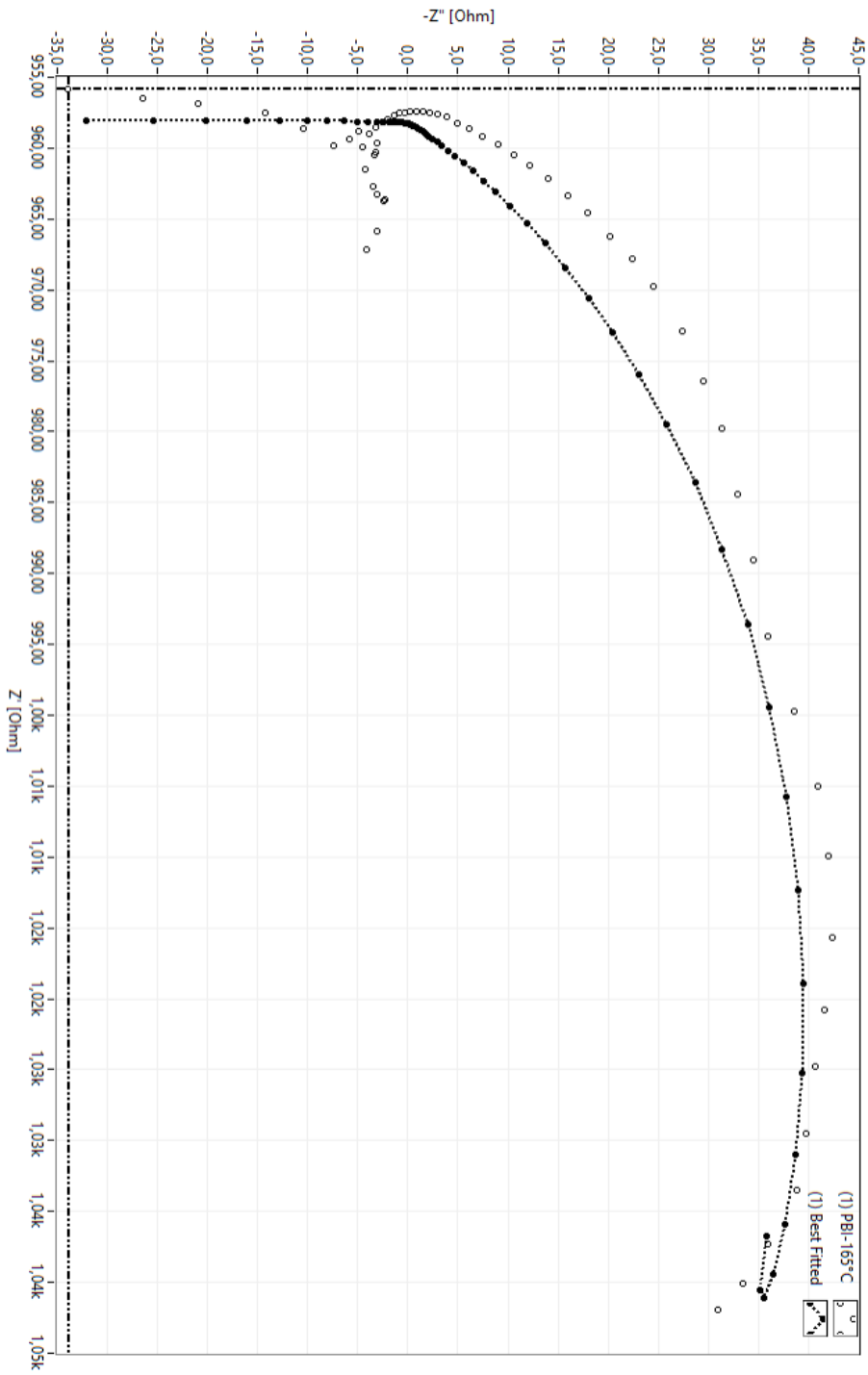

Figure 33 Nyquist plot for PBI

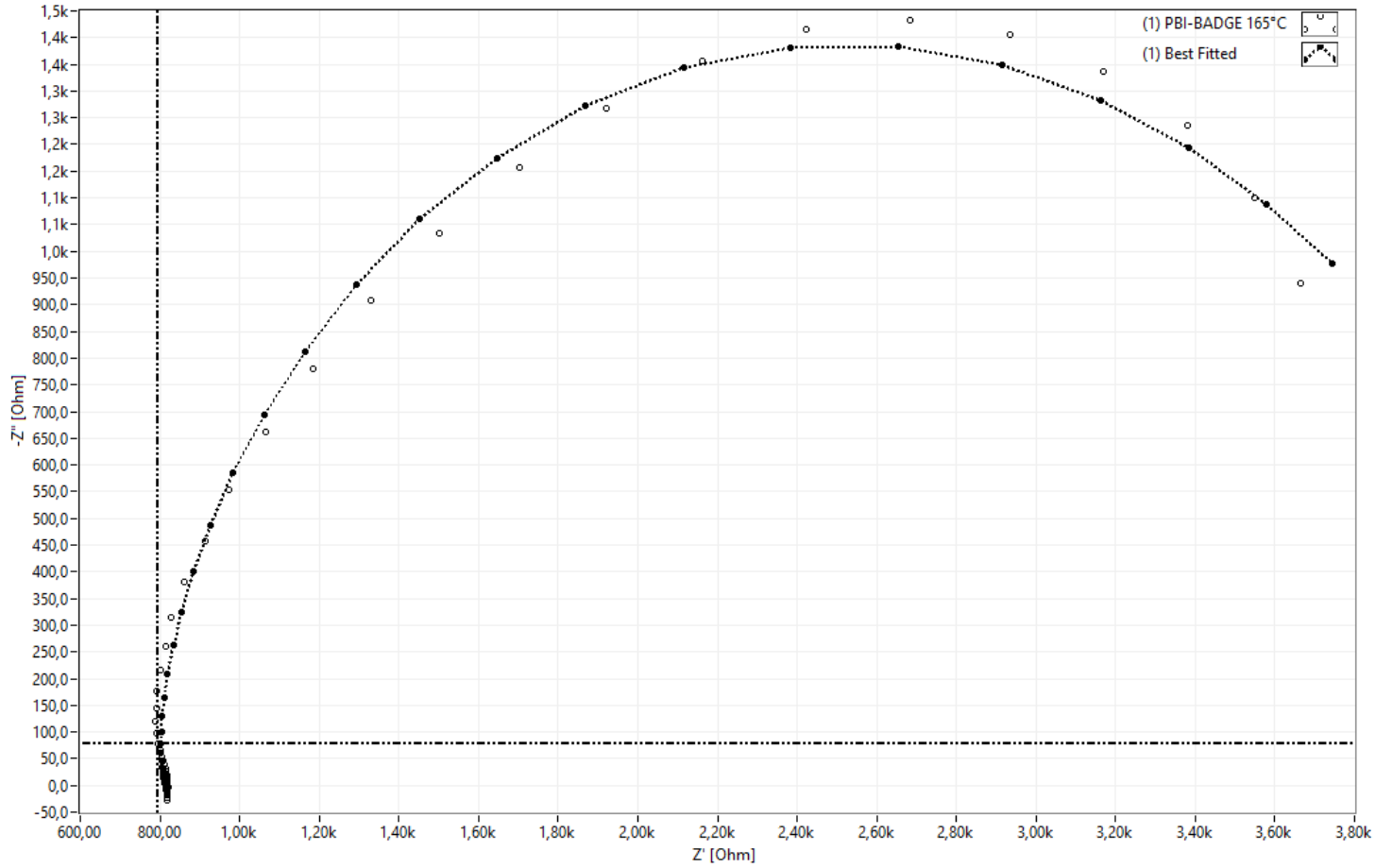

Figure 34 Nyquist plot for PBI-BADGE-5

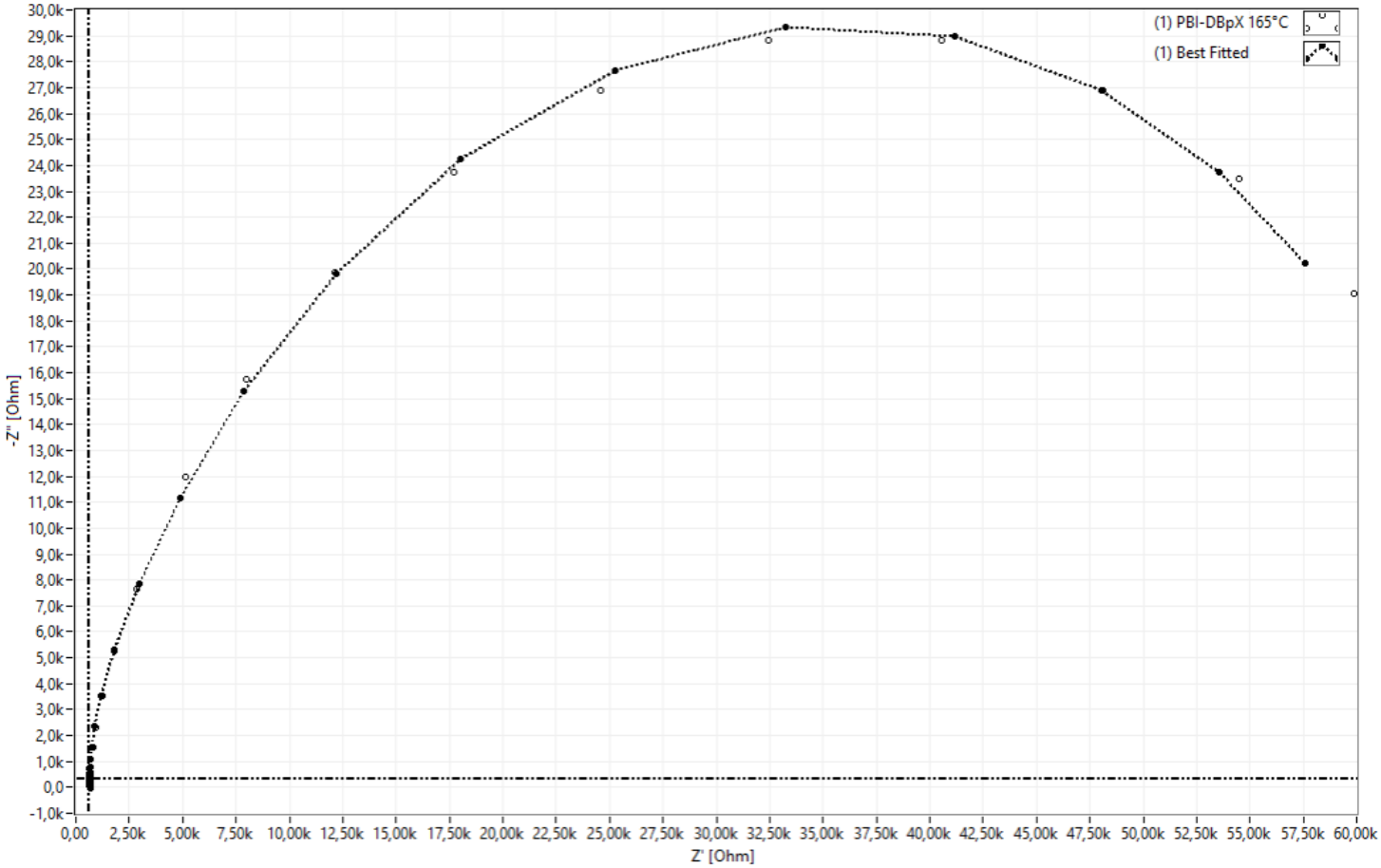

Figure 35 Nyquist plot for PBI-DBpX-3

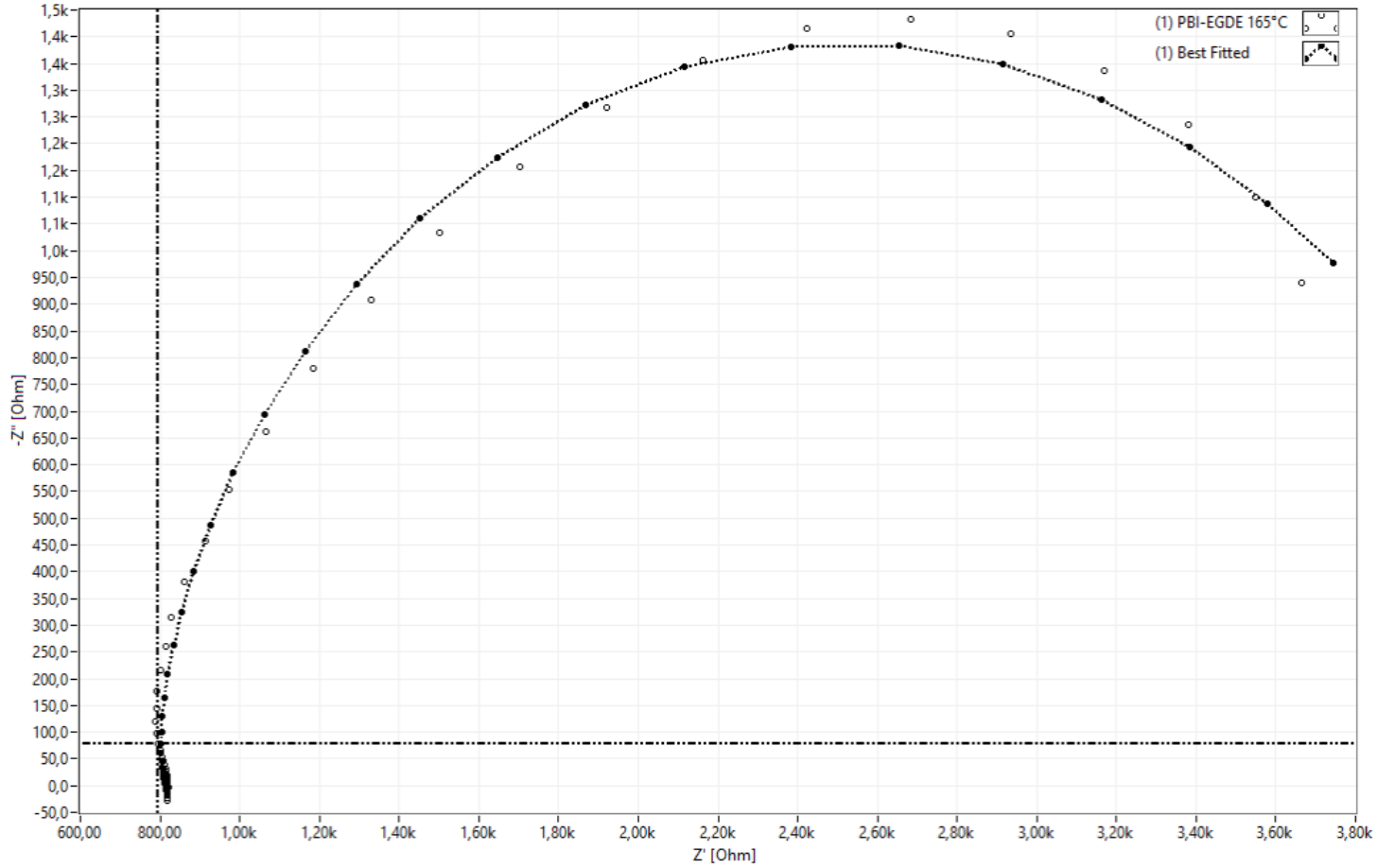

Figure 36 Nyquist plot for PBI-EGDE-5

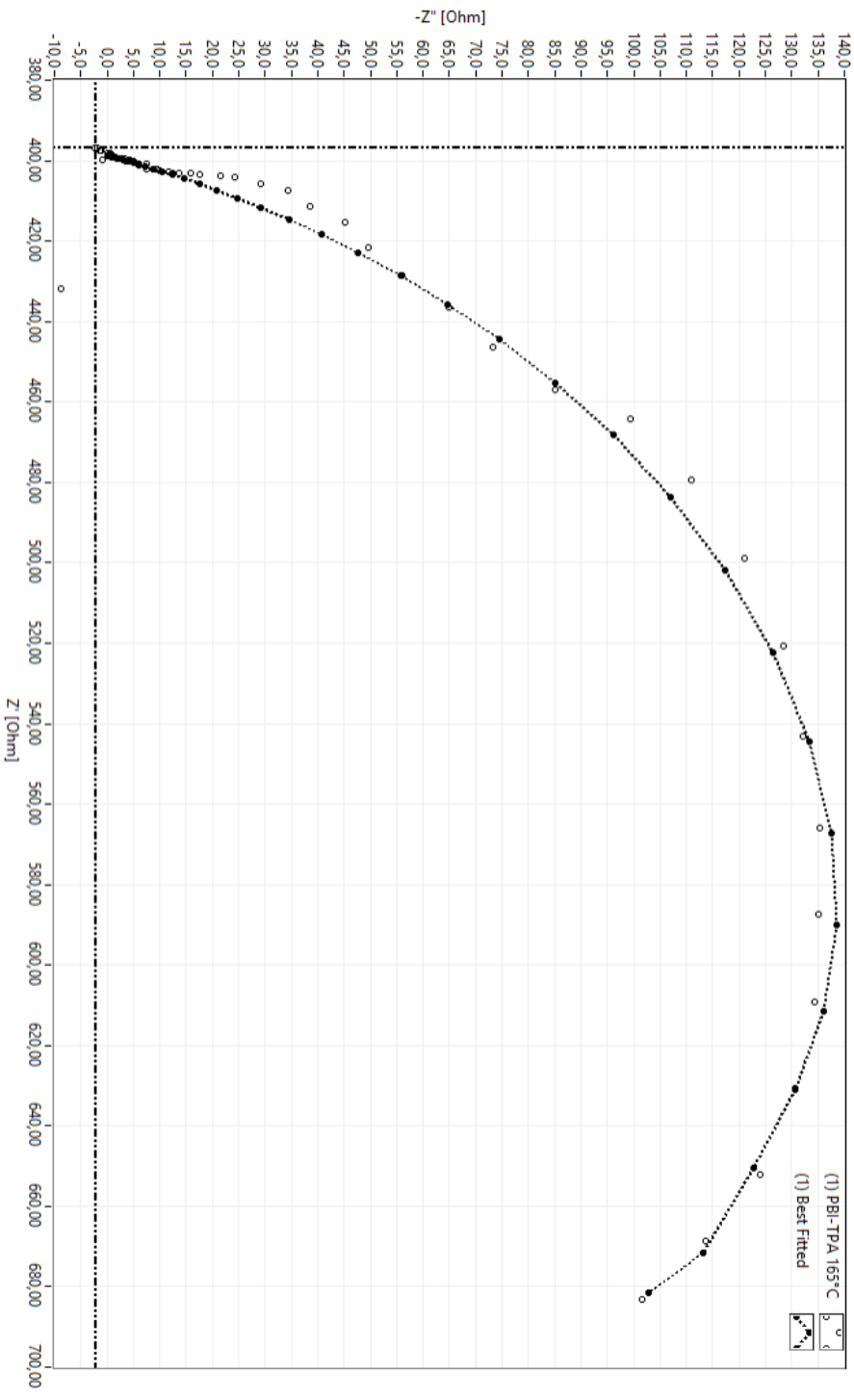

Figure 37 Nyquist plot for PBI-TPA-5

The software used for the impedance spectroscopy was used for model fitting to the Nyquist plots. A Randles circuit model was found to fit the experimental data for PBI and cross-linked PBI membranes. In the model, Rs is the bulk resistance, while R1 is charge transfer resistance, W is the Warburg impedance and Q is the constant phase element.

The proton conductivities of the PBI and cross-linked PBI membranes at different temperatures were measured. The proton conductivities, acid doping and acid leaching results of the membranes prepared are all tabulated in Table 4.3. As shown in Tables 4.3, the proton conductivities increase with increasing test temperatures. This trend may be attributed to the Grotthus proton conduction mechanism (discussed in detail in section 2.4) as studied previously in the literature [125]. **Figure 38** represents the proton conduction by Grotthus mechanism in acid doped PBI membranes, which takes place by means of a hydrogen bond chain with hopping from one site to another one.

Table 4.3. Proton conductivity results of cross-linked PBI membranes prepared with different cross-linkers (BADGE, EGDE, TPA and DBpX) and cross- linked PBI membranes prepared with different amounts of BADGE cross-linker.

Membrane Type	**Proton Conductivity (S cm^{-1})**			**Acid Leaching (%)**	**Acid Doping[a]**
	140°C	**165°C**	**180°C**		
PBI	0.0794	0.1030	0.1439	85	13.5
PBI-BADGE-5	0.0541	0.0590	0.0666	73	10
PBI-EGDE-5	0.0468	0.0682	0.0972	80	10.4
PBI-TPA-5	0.0631	0.0891	0.1172	82	13.5
PBI-DBpX-3	0.0711	0.1009	0.1513	80	15

2nd set of membranes	**Proton Conductivity (S cm^{-1})**					**Acid Leaching (%)**	**Acid Doping[a]**
	125ºC	**140ºC**	**150ºC**	**165ºC**	**180ºC**		
PBI-BADGE-2.5	0.041	0.049	0.058	0.072	0.097	78	14.3
PBI-BADGE-5	0.059	0.072	0.082	0.115	0.123	73	12.3
PBI-BADGE-7.5	0.044	0.045	0.051	0.056	0.069	85	10.7

[a] Molecules of H_3PO_4/repeating unit of PBI.

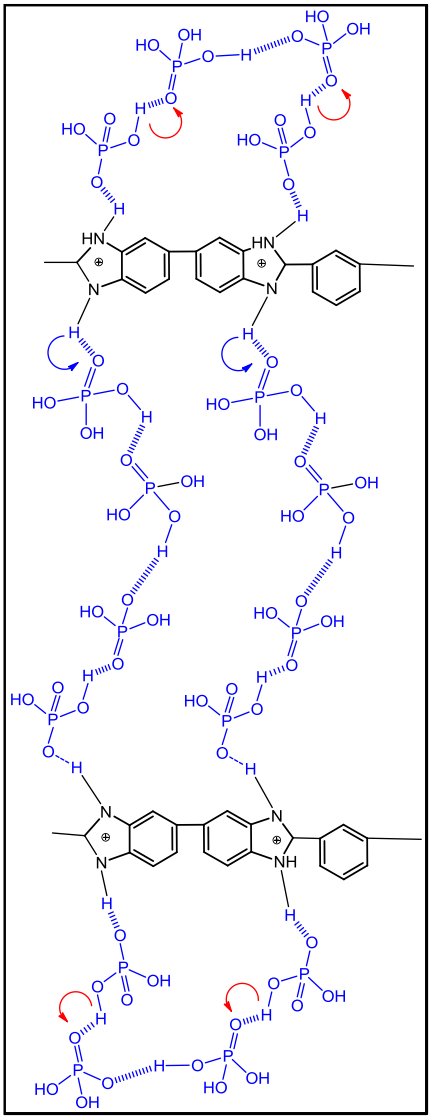

Figure 38 Proton conduction by Grotthus mechanism in PBI-H3PO4 system.

The PBI-DBpX-3 membrane showed the highest proton conductivity at 180^{0}C with 0.151 S.cm^{-1}, which is 4.8% higher than the proton conductivity of pristine PBI at the same temperature. The PBI-BADGE-5 had the lowest proton conductivity values at 165^{0}C and 180^{0}C, with 0.059 and 0.067 S.cm^{-1} proton conductivity values, respectively. This value is relatively high compared to the literature values obtained by Lin. et al. [25] The proton conductivity of PBI-EGDE-5 at 140^{0}C was observed as 0.047 S. cm^{-1}, which was the lowest for this temperature. The PA interacted with the imidazole groups. The excess free PA and the free imidazole groups that are not bound by PA are the key factors that affect proton conductivity. Thus, the membranes having lower ADLs showed lower proton conductivity values. Xu et al. [93] stated that the membranes they

have prepared with EGDE had a lower acid doping and thus, proton conductivity values compared to TPA. This is consistent with our case.

2nd set of membranes were tested with the same procedure for proton conductivity. Results showed that as the temperature increased, proton conductivity of the membranes increased as well. The PBI-BADGE-5 membrane exhibited the highest proton conductivity values among the cross-linked membranes which can be explained by the relatively high ADL of the membrane. Also it is observed that as the temperature increased, proton conductivity of the PBI-BADGE-5 membrane increased more, compared to the other membranes prepared by BADGE. This may indicate that the hoppin mechanism dominating proton conductivity mechanism regarding this membrane. Even though, the PBI-BADGE-2.5 membrane had the highest ADL among these three membranes, its proton conductivity findings were lower than that of the PBI-BADGE-5 membrane. As the cross-linking density increases, the dimensional stability and acid retention capability of the membranes increase as well. These improvements are the main reasons of the difference between proton conductivity of the membranes. As the findings of Table 4.4. shows, the cross-link density is highest with PBI-BADGE-5 membrane. These results given in Table 4.5 also shows that the most efficient cross-linker ratio was 5 wt. % for the BADGE epoxy resin.

4.2.8. Mechanical Analysis

The determination of the mechanical properties of the PBI based cross-linked membranes is one of the critical parameters in determining if the membrane is mechanically stable to be tested in HT-PEMFC. Adequate mechanical strength is essential for PEM fuel cell application to possess to withstand fabrication of the membrane electrode assembly, which is conducted by applying hot press at 150 °C and 172 $N.cm^{-2}$ (1.72 MPa), and also operation in fuel cell. Tensile tests were performed to determine the effect of DBpX and BADGE on the mechanical properties of PBI membranes since these two cross-linkers reacted most effectively with PBI to give cross-linked structure. The membranes should possess enough mechanical strength to withstand the stresses formed during the fabrication of membrane electrode assemblies and form mechanically strong PEMFC assemblies. In addition, mechanical stability is

important in deciding acid doping duration of the membranes. As the acid doping level increases, mechanical properties of the membranes is decreasing. Keeping a mechanically unsufficient membrane in acid for too long may result in deteroriation of the membrane.

The mechanical properties of the membranes prepared are shown in Table 4.4. It was expected that the cross-linked membranes would have better mechanical properties compared to the pristine PBI membrane [23]. Via the cross-linking route a large, stable network of anchored polymeric chains is achieved, which stabilizes the membrane and improves its mechanical properties [23]. The tensile strength of the PBI-DBpX-3 membrane was found to be the highest, as expected. However, the membrane with BADGE showed the lowest tensile strength and elongation at break values. This was attributed to the brittle structure of this epoxide type cross-linker [126]. As a result of the mechanical tests, the membranes are found to be mechanically stable enough to be used in the HT-PEMFC applications.

Table4.4. Mechanical test results for PBI, PBI-DBpX-3 and PBI-BADGE-5

Membranes	**Tensile Strength (MPa)**	**Elongation at Break (%)**
PBI	133±7.09	65±17
PBI-BADGE-5	90±11.5	79±17
PBI-DBpX-3	88±2.25	26±13

4.3. HT-PEMFC Test Results

The results of the HT-PEMFC tests were given in **Figure 39** and **Figure 41** whilst OCV values are presented with graphs given in **Figure 40** and **Figure 42**.

Figure 39 shows the performance alteration of the HT-PEMFC single cell equipped with pristine PBI membrane and the cross-linked membranes of first

set of the membranes for 40 hours of operation time. **Figure 40** concludes the OCV values obtained with first set of the membranes.

The HT-PEMFC tests displayed open circuit voltage (OCV) for PBI and PBI crosslinked membranes approximately 0.93-0.95 V. The OCV values were quite satisfactory for PBI, PBI-BADGE-5, and PBI-DBpX-3 MEAs. However, PBI-TPA-5 gave rise to a very low OCV value, of approximately 0.75 V, which may indicate H_2 crossover through the membrane or difficulties with MEA preparation such as pin-hole formation, noncompatibility between the ionomer used and polymer membrane, etc. [127]. A morphological study of the PBI-TPA membrane indicates that the membrane had agglomerated particles in the cross-section. This may result in higher hydrogen crossover rates due to the nonhomogeneous porous structure of the membrane. In this study, all of the fuel cell tests were conducted after proper short-circuit tests. Thus, pin holes caused by material flaws introduced during MEA processing would have been detected before HT-PEMFC tests. Conditions imposed during fuel cell tests can also lead to pin-hole formation and pose low OCV values. Noncompatibility between membrane and ionomer used in preparation of the electrodes can also result in lower reaction rates, thus lower OCV values. The adverse effect of this problem is reflected on the performance curve of MEA prepared with a PBI-TPA-5 membrane. However, it is not further investigated in this study.

The pristine PBI membrane reached to 0.085 $W.cm^{-2}$ maximum power density and 0.081 A. cm^{-2} current density at 0.6 V which is slightly higher than PBI-TPA-5 membrane. The current density for PBI-BADGE-5 was found to be 0.121 A. cm^{-2} and maximum power density was determined as 0.123 W. cm^{-2}. This is the highest performance obtained in this study which is interesting because the PBI-BADGE-5 membrane gave the lowest proton conductivity. This finding can be related to the low acid leaching value presented by the PBI-BADGE-5 membrane. The second best performing membrane was found to be the PBI-DBpX-3 membrane with 0.106 W. cm^{-2} maximum power density. The PBI-DBpX-3 was the membrane having highest ADL. High performance of this MEA can be attributed to high proton conductivity of the membrane. It can be said for PBI-BADGE-5 and PBI-DBpX-3 membranes have less activation loss

compared to the pristine PBI membrane which is also a sign of better contact between the electrolyte and electrocatalyst [118].

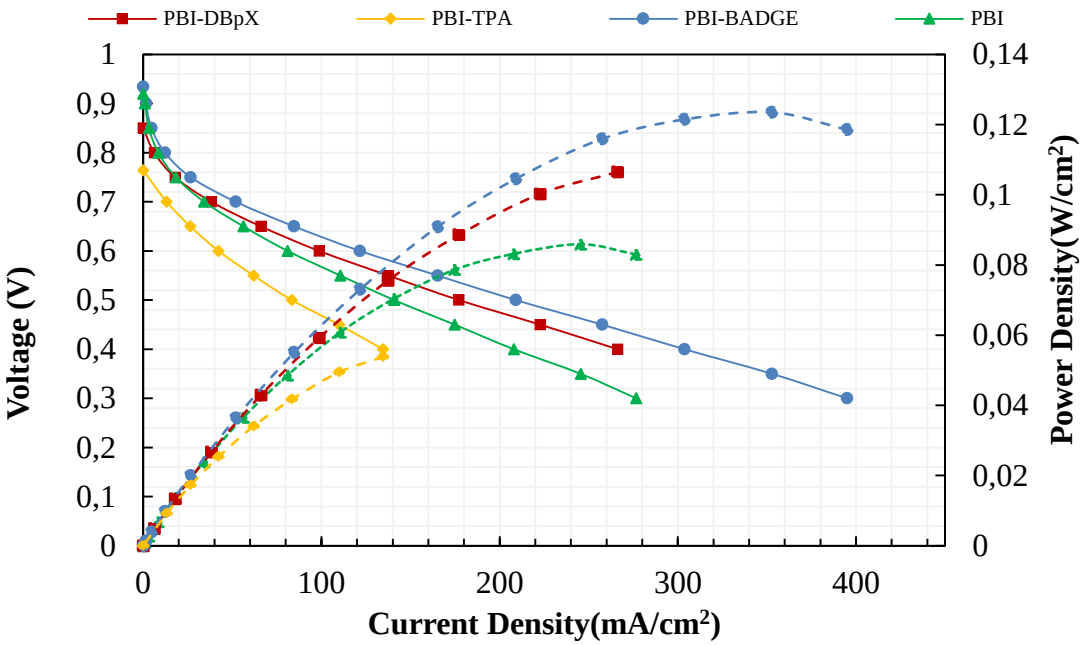

Figure 39 The HT-PEMFC performance curves of base PBI and PBI-BADGE-5, PBI-DBpX-3, PBI-EGDE-5 and PBI-TPA-5 membranes (First set of membranes). Operating conditions: H2 and air stoichiometry of 1.5 and 2.5, respectively; H2 and air RH of 0; 1650C cell temperature

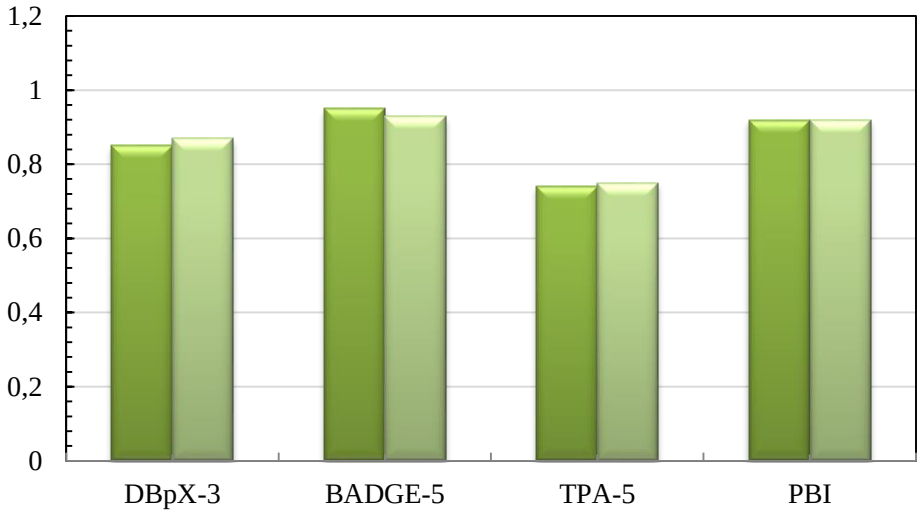

Figure 40 OCV values (V) of cross-linked PBI membranes (1st set of membranes) and pristine PBI membrane

In the literature, Lin et al.[25] obtained 0.172 $W.cm^{-2}$ power density with a PBI-BADGE membrane with higher cross-linker amount. One of the best performances given in the literature with PA doped blend membranes was 0.457 $W.cm^{-2}$ peak power density at 180^0C [8]. According to the information given literature, it can be concluded that although the power density is not explicitly high, the overall performance of PBI-BADGE-5 and PBI-DBpX-3 membranes were found to be higher than a pristine PBI membrane which gives indications for suitability for medium to HT-PEMFC applications. The cell performance was quite stable with the average constant power output during the test. The PBI-BADGE-5 membrane performed better than the pristine PBI membrane. Performance decay for the PBI-BADGE-5 membrane was approximately 3%. The Pristine PBI membrane showed 15% power loss at the end of the test duration. Results revealing that the cross-linked PBI membrane possesses a higher stability are consistent with literature. Improved acid retention characteristics were found to show significant contribution to the short-term stability of the HT-PEMFCs by Sondergaard et al. [124]. As a future work, HT-PEMFC equipped with cross-linked membranes will be optimized to improve the long-term stability of HT-PEMFC.

Figure 41 shows the performance alteration of the HT-PEMFC single cell equipped with the pristine PBI membrane and the second set of the cross-linked membranes for 40 hours of operation time.

The best HT-PEMFC performance was obtained using the PBI-BADGE-5 membrane. The second best performing membrane was the pristine PBI one. The PBI-BADGE-7.5 membrane performed poorly compared to the other membranes. It showed maximum power density of 0.019 W cm^{-2}. The highest maximum power density reached was 0.121 W cm^{-2} with the PBI-BADGE-5 membrane. The OCV values were between 0.85-1 V for all the membranes except PBI-BADGE-2.5. The low OCV value by this membrane can be associated with high H_2 crossover rate from the membrane or difficulties with MEA preparation such as pin-hole formation, no compatibility between the ionomer used and polymer membrane, etc.

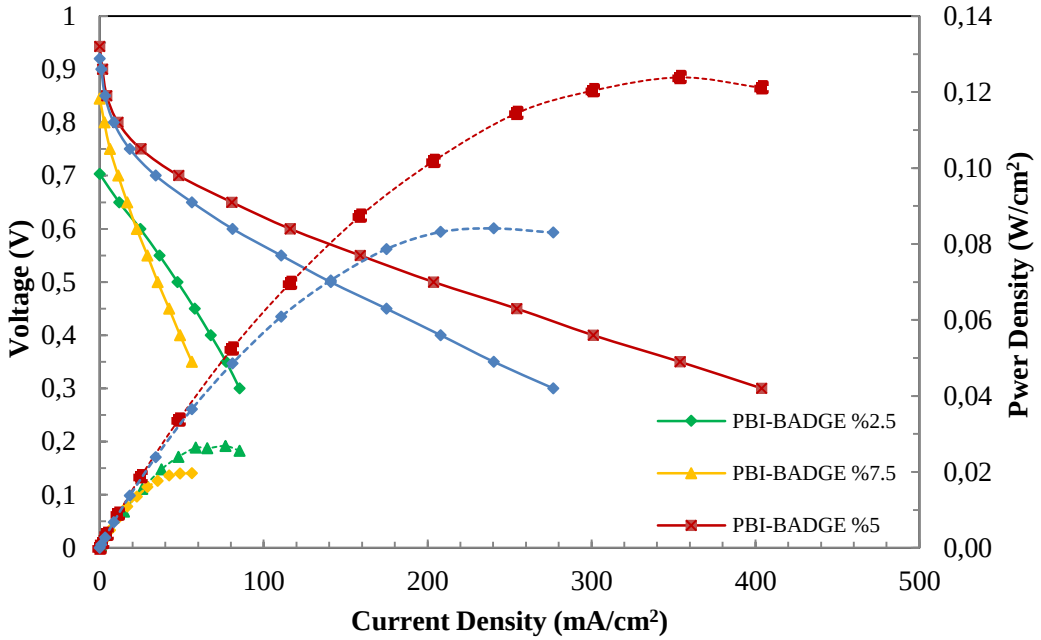

Figure 41 The HT-PEMFC performance curves of base PBI and PBI-BADGE-5, PBI-DBpX-3, PBI-EGDE-5 and PBI-TPA-5 membranes (First set of membranes). Operating conditions: H2 and air stoichiometry of 1.5 and 2.5, respectively; H2 and air RH of 0; 165^{0}C cell temperature

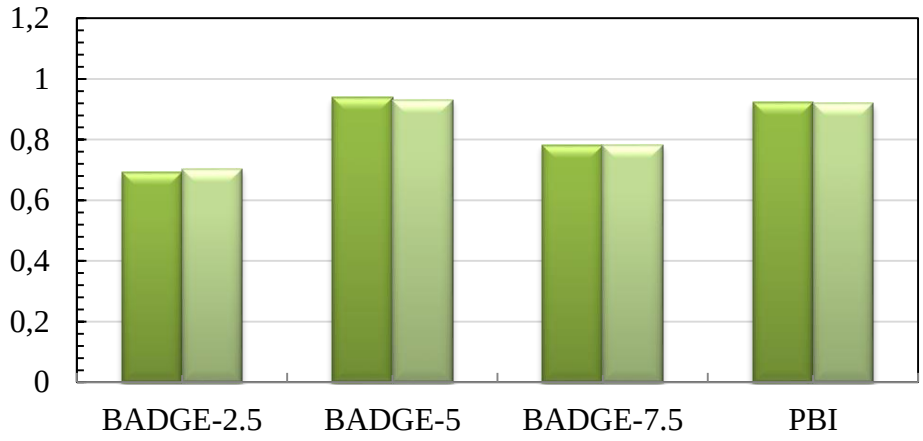

Figure 42 The OCV values (V) of PBI-BADGE cross-linked membranes (2nd set of membranes) and pristine PBI membrane

These results suggest that the acid leaching has adverse effects on the HT-PEMFC performance of PBI based membranes. The PBI-BADGE-7.5 membrane was found to be the worst performing membrane in terms of acid leaching and proton conductivity. The influences of low proton conductivity and high acid loss percentage can be observed in these HT-PEMFC test results. Also, the highest performance was achieved with the PBI-BADGE-5 membrane

which also had the lowest acid loss and second highest proton conductivity. The interesting result here is that pristine PBI membrane which showed the highest proton conductivity performed worse than the PBI-BADGE-5 membrane which proves the importance of acid leaching from the membranes. According to the HT-PEMFC tests, it can be concluded that although the power density is not explicitly high, the overall performance of PBI-BADGE-5 membrane was found to be the best among other cross-linked membranes and gives indications of being a promising alternative for conventional membranes.

CHAPTER 5

CONCLUSIONS AND RECOMMENDATIONS

The aim of this study was to develop novel cross-linked PBI membranes for HT-PEMFCs operating between 150^0C-180^0C. Two sets of membranes were prepared to have a better understanding of covalent cross-linking mechanism of PBI and its effects on HT-PEMFC performance. Membranes were prepared by using PBI with molecular weight of 39000 g mol^{-1}. PBI was also synthesized in-house and characterized by C-NMR spectrum. However, the obtained PBI polymer was found to be very hard to dissolve in organic solvents such as DMAc and DMSO. Thus, the polymer by DPS was used to cast pristine and cross-linked PBI membranes. The first sequence of membranes involving PBI-BADGE-5, PBI-DBpX-3, PBI-TPA-5 and PBI-EGDE-5 were later imbibed in concentrated H_3PO_4. The acid doping of the membranes was lasted for approximately 2 weeks for every membrane. Afterwards, the acid doped membranes were tested for acid doping capability, acid leaching, and proton conductivity by EIS while dry membranes were characterized with TGA, FTIR and SEM. The results showed that the acid doping level of the PBI-DBpX-3 membrane reached 15 which is the highest value among all membranes. It was followed by pristine PBI and PBI-TPA-5 which both revealed ADL of 13.5. The lowest acid doping capability was observed with the PBI-BADGE-5 membrane. This membrane revealed ADL of 10, which is the lowest value obtained in this set of membranes. The acid leaching test results proved that the cross-linking is an effective way to decrease acid loss from the membranes. The PBI-BADGE-5 membrane was found to have the best acid retention capability under hydrous conditions while its proton conductivity values were poor. The PBI-EGDE-5 membrane revealed poor performance in terms of acid dopig, acid leaching and proton conductivity values. It reached proton conductivity of 0.0972 S cm^{-1} at

180^0C. At 165^0C which is the operation temperature of single cell HT-PEMFC in this study, the proton conductivity of the PBI-EGDE-5 membrane was found as 0.0682 S cm^{-1}. When high acid leaching value, low acid doping value and low proton conducutivity of the membrane at 165^0C taken into consideration, the PBI-EGDE-5 membrane was not analyzed in single cell HT-PEMFC tests.

TGA analysis indicated that all the membranes had very good thermal stabilities at the HT-PEMFC operating temperatures. At higher temperatures, the decompositon of the cross-linked structure of the membranes were observed. SEM analysis indicated that the membrane PBI-TPA-5 showed some agglomerated TPA particles inside of the membrane matrix. This reveals that the cross-linking reaction in this membrane was not as effectively completed as the other membranes. The extraction in DMAc tests and FTIR anaylsis were conducted to confirm the cross-linked structure obtained. The Extraction in DMAc tests revealed that the most effective cross-linking was obtained with the PBI-BADGE-5 and PBI-DBpX-3 membranes whilst the PBI-TPA-5 membrane lost its shape and rigidty during the test. The extraction results fort he PBI-TPA-5 membrane shows that the cross-linking reaction was not successfully completed.

Regarding the HT-PEMFC tests, the PBI-BADGE-5 membrane was the best performing membrane with a current density of 0.121 A cm^{-2} at 0.6 V and a maximum power density of 0.123 Wcm^{-2}. The second best performing membrane was found to be the PBI-DBpX-3 membrane with 0.106 W. cm^{-2} maximum power density. These results validated that both acid doping level and acid retention capability have significant importance on the performance of the membranes. The performance results obtained were compatible with the literature values and this is accepted as an indication of usage of these membranes in commercial HT-PEMFCs.

Second set of membranes were prepared by using BADGE as the cross-linker in different amounts. Since the BADGE membrane showed the lowest acid leaching and the highest performance, it was studied further to decide on the optimum amount of BADGE to be added to the PBI matrix. For this aim, PBI-BADGE cross-linked membranes were prepared with 2.5 wt. %, 5 wt. % and 7.5 wt. % weight percent of BADGE. TGA analysis showed that the membranes' thermal durabilities were high enough to be tested in HT-PEMFC

tests. The acid doped membranes were tested with the same sequence of the characterization methods used for the first set of the membranes. Acid doping level of PBI-BADGE-2.5 was found as the highest (14.3) whilst acid doping level of PBI-BADGE-7.5 was the lowest (10.7). These results are coherent with literature. It was concluded that as the cross-linking density increases, the acid capture capability decreases. On the other hand, the acid leaching value of PBI-BADGE-7.5 was found to be the highest. This behavior suggests that the acid leaching is not directly correlated to cross-linking degree of the membranes. However, other effects were not further investigated in this study. The proton conductivity analysis revealed that PBI-BADGE-5 had the highest proton conductivity values at all temperatures with the lowest acid leaching value as well. The highest proton conductivity of 0.1227 S cm^{-1} was reached at 180^0C.

Single cell HT-PEMFC tests were conducted with the PBI-BADGE-2.5 and PBI-BADGE-7.5 membranes initially and the results were compared with the results obtained for pristine PBI and PBI-BADGE-5 before. The best performing membrane was again PBI-BADGE-5 membrane whilst PBI-BADGE-7.5 and PBI-BADGE-2.5 membranes performed poorly during the tests revealing 0.019 W cm^{-2} and 0.025 W cm^{-2} power densities, respectively. These values are very low compared to literature. The reasons for the poor performance results were discussed in Chapter 4.

Recommendations

- The reasons behind the low performances of PBI-BADGE-2.5 and PBI-BADGE-7.5 can be investigated.
- High acid leaching PBI-BADGE-7.5 exhibited can be studied to have a better understanding the correlation between acid leaching and cross-linking density.
- Tests can be lasted longer, and test set-up can be adjusted to conduct a life-time test for the cross-linked membranes.

REFERENCES

[1] Vassiliev A. High temperature PEM fuel cells and organic fuels : Ph. D. thesis. DTU Energy Conversion, Department of Energy Conversion and Storage; 2014.

[2] Barbir F. PEM fuel cells : theory and practice. Academic Press; 2013.

[3] KnowledgePublications - Learning a Little More Every Day n.d. http://knowledgepublications.com/fuelcells/fuel_cells_for_public_utility_and_industrial_power_detail.htm (accessed November 5, 2017).

[4] Mench MM. Introduction to Fuel Cells. Fuel Cell Engines, Hoboken, NJ, USA: John Wiley & Sons, Inc.; n.d., p. 1–28. doi:10.1002/9780470209769.ch1.

[5] Wang Y, Chen KS, Mishler J, Cho SC, Adroher XC. A review of polymer electrolyte membrane fuel cells: Technology, applications, and needs on fundamental research. Appl Energy 2011;88:981–1007. doi:10.1016/j.apenergy.2010.09.030.

[6] NFCRC Homepage n.d. http://www.nfcrc.uci.edu/3/default.aspx (accessed November 5, 2017).

[7] DoITPoMS - TLP Library Fuel Cells n.d. https://www.doitpoms.ac.uk/tlplib/fuel-cells/printall.php (accessed November 5, 2017).

[8] Li Q, Aili D, Hjuler HA, Jensen JO. High Temperature Polymer Electrolyte Membrane Fuel Cells. Cham: Springer International Publishing; 2016. doi:10.1007/978-3-319-17082-4.

[9] Xu C. Development of membranes for low and intermediate temperature polymer electrolyte membrane fuel cell. 2013.

[10] Vogel H, Marvel CS. Polybenzimidazoles, new thermally stable polymers. J Polym Sci 1961;50:511–39. doi:10.1002/pol.1961.1205015419.

[11] Iwakura Y, Uno K, Imai Y. Polyphenylenebenzimidazoles. J Polym Sci Part A Gen Pap 1964;2:2605–15. doi:10.1002/pol.1964.100020611.

[12] Christopher B. Shogbon †, Jean-Luc Brousseau ‡, Haifeng Zhang †, Brian C. Benicewicz † and, Yvonne A. Akpalu* †. Determination of the Molecular Parameters and Studies of the Chain Conformation of Polybenzimidazole in DMAc/LiCl 2006. doi:10.1021/MA0609836.

[13] Wainright JS. Acid-Doped Polybenzimidazoles: A New Polymer Electrolyte. J Electrochem Soc 1995;142:L121. doi:10.1149/1.2044337.

[14] Kerres J, Atanasov V. Cross-linked PBI-based high-temperature membranes: Stability, conductivity and fuel cell performance. Int J Hydrogen Energy 2015;40:14723–35. doi:10.1016/j.ijhydene.2015.08.054.

[15] Hajdok I, Bona A, Werner H-J, Kerres J. Synthesis and characterization of fluorinated and sulfonated poly(arylene ether-1,3,4-oxadiazole) derivatives and their blend membranes. Eur Polym J 2014;52:76–87. doi:10.1016/j.eurpolymj.2013.12.003.

[16] Kerres JA, Katzfuß A, Chromik A, Atanasov V. Sulfonated poly(styrene)s-PBIOO® blend membranes: Thermo-oxidative stability and conductivity. J Appl Polym Sci 2014;131:n/a-n/a. doi:10.1002/app.39889.

[17] Atanasov V, Gudat D, Ruffmann B, Kerres J. Highly phosphonated polypentafluorostyrene: Characterization and blends with polybenzimidazole. Eur Polym J 2013;49:3977–85. doi:10.1016/j.eurpolymj.2013.09.002.

[18] Thomas OD, Peckham TJ, Thanganathan U, Yang Y, Holdcroft S. Sulfonated polybenzimidazoles: Proton conduction and acid-base crosslinking. J Polym Sci Part A Polym Chem 2010;48:3640–50. doi:10.1002/pola.24147.

[19] Ng F, Péron J, Jones DJ, Rozière J. Synthesis of novel proton-conducting highly sulfonated polybenzimidazoles for PEMFC and the effect of the type of bisphenyl bridge on polymer and membrane properties. J Polym Sci Part A Polym Chem 2011;49:2107–17. doi:10.1002/pola.24630.

[20] Angioni S, Villa DC, Barco SD, Quartarone E, Righetti PP, Tomasi C, et al. Polysulfonation of PBI-based membranes for HT-PEMFCs: a possible way to maintain high proton transport at a low H_3PO_4 doping level. J Mater Chem A 2014;2:663–71. doi:10.1039/C3TA12200J.

[21] Gillham JK. Polymer Structure: Cross-Linking of a Polybenzimidazole. Science (80-) 1963;139.

[22] Han M, Zhang G, Liu Z, Wang S, Li M, Zhu J, et al. Cross-linked polybenzimidazole with enhanced stability for high temperature proton exchange membrane fuel cells. J Mater Chem 2011;21:2187–93. doi:10.1039/C0JM02443K.

[23] Qingfeng Li *, Chao Pan, Jens Oluf Jensen, Pernille Noyé and, Bjerrum NJ. Cross-Linked Polybenzimidazole Membranes for Fuel Cells 2007. doi:10.1021/CM0627793.

[24] Noyé P, Li Q, Pan C, Bjerrum NJ. Cross-linked polybenzimidazole membranes for high temperature proton exchange membrane fuel cells with dichloromethyl phosphinic acid as a cross-linker. Polym Adv Technol 2008;19:1270–5. doi:10.1002/pat.1123.

[25] Lin H-L, Chou Y-C, Yu TL, Lai S-W. Poly(benzimidazole)-epoxide crosslink membranes for high temperature proton exchange membrane fuel cells. Int J Hydrogen Energy 2012;37:383–92. doi:10.1016/j.ijhydene.2011.09.049.

[26] Yuan S, Yan G, Xia Z, Guo X, Fang J, Yang X. Preparation and properties of covalently cross-linked sulfonated poly(sulfide sulfone)/polybenzimidazole blend membranes for fuel cell applications. High Perform Polym 2014;26:212–22. doi:10.1177/0954008313507589.

[27] Han M, Zhang G, Liu Z, Wang S, Li M, Zhu J, et al. Cross-linked polybenzimidazole with enhanced stability for high temperature proton exchange membrane fuel cells. J Mater Chem 2011;21:2187–93. doi:10.1039/C0JM02443K.

[28] Li Q, Jensen JO, Savinell RF, Bjerrum NJ. High temperature proton exchange membranes based on polybenzimidazoles for fuel cells. Prog Polym Sci 2009;34:449–77. doi:10.1016/j.progpolymsci.2008.12.003.

[29] Hoogers G. Fuel cell technology handbook. CRC Press; 2003.

[30] Devrim Y, Devrim H, Eroglu I. Development of 500 W PEM fuel cell stack for portable power generators. Int J Hydrogen Energy 2015;40:7707–19.

doi:10.1016/J.IJHYDENE.2015.02.005.

[31] Wannek C, Glüsen A, Stolten D. Materials, manufacturing technology and costs of fuel cell membranes. Desalination 2010;250:1038–41. doi:10.1016/J.DESAL.2009.09.102.

[32] Zawodzinski TA, Derouin C, Radzinski S, Sherman RJ, Smith VT, Springer TE, et al. Water Uptake by and Transport Through Nafion® 117 Membranes. J Electrochem Soc 1993;140:1041. doi:10.1149/1.2056194.

[33] Alonso RH, Estevez L, Lian H, Kelarakis A, Giannelis EP. Nafion–clay nanocomposite membranes: Morphology and properties. Polymer (Guildf) 2009;50:2402–10. doi:10.1016/J.POLYMER.2009.03.020.

[34] Devrim Y, Albostan A. Enhancement of PEM fuel cell performance at higher temperatures and lower humidities by high performance membrane electrode assembly based on Nafion/zeolite membrane. Int J Hydrogen Energy 2015;40:15328–35. doi:10.1016/J.IJHYDENE.2015.02.078.

[35] Şengül E, Erdener H, Akay RG, Yücel H, Baç N, Eroğlu İ. Effects of sulfonated polyether-etherketone (SPEEK) and composite membranes on the proton exchange membrane fuel cell (PEMFC) performance. Int J Hydrogen Energy 2009;34:4645–52. doi:10.1016/J.IJHYDENE.2008.08.066.

[36] Devrim Y, Erkan S, Baç N, Eroğlu I. Preparation and characterization of sulfonated polysulfone/titanium dioxide composite membranes for proton exchange membrane fuel cells. Int J Hydrogen Energy 2009;34:3467–75. doi:10.1016/j.ijhydene.2009.02.019.

[37] Wilkinson DP, Johnson MC, Colbow KM, Campbell SA. United States Patent: 5874182, 1997.

[38] Steele BCH, Heinzel A. Materials for fuel-cell technologies. Nature 2001;414:345–52. doi:10.1038/35104620.

[39] Debe MK. Electrocatalyst approaches and challenges for automotive fuel cells. Nature 2012;486:43–51. doi:10.1038/nature11115.

[40] Chen Z, Waje M, Li W, Yan Y. Supportless Pt and PtPd Nanotubes as Electrocatalysts for Oxygen-Reduction Reactions. Angew Chemie Int Ed 2007;46:4060–3. doi:10.1002/anie.200700894.

[41] Bliznakov S, Vukmirovic M, Yang L, Sutter E, Adzic RR. Pt Monolayer on Electrodeposited Pd Nanostructures-Advanced Cathode Catalysts for PEM Fuel Cells. ECS Trans., vol. 41, The Electrochemical Society; 2011, p. 1055–66. doi:10.1149/1.3635638.

[42] Kuttiyiel KA, Sasaki K, Su D, Vukmirovic MB, Marinkovic NS, Adzic RR. Pt monolayer on Au-stabilized PdNi core–shell nanoparticles for oxygen reduction reaction. Electrochim Acta 2013;110:267–72. doi:10.1016/J.ELECTACTA.2013.04.037.

[43] Debe MK, Steinbach AJ, Hendricks SM, Kurkowski MJ, Vernstrom GD, Atanasoski RT, et al. Advanced Cathode Catalysts and Supports for PEM Fuel Cells, DOE Hydrogen Program FY 2010 Annual Progress Report n.d.

[44] Van der Vliet D, Wang C, Debe M, Atanasoski R, Markovic N, Stamenkovic VR. Platinum-alloy nanostructured thin film catalysts for the oxygen reduction reaction. Electrochim Acta 2011;56:8695–9. doi:10.1016/J.ELECTACTA.2011.07.063.

[45] Serov A, Artyushkova K, Atanassov P. Fe-N-C Oxygen Reduction Fuel Cell Catalyst Derived from Carbendazim: Synthesis, Structure, and Reactivity. Adv Energy Mater 2014;4:1301735. doi:10.1002/aenm.201301735.

[46] Salim RI, Noura H, Nabag M, Fardoun A. Modeling and Temperature Analysis of the Nexa 1.2 kW Fuel Cell System. J Fuel Cell Sci Technol 2015;12:61006. doi:10.1115/1.4032061.

[47] Li Q, He R, Jensen JO, Bjerrum NJ. PBI-Based Polymer Membranes for High Temperature Fuel Cells– Preparation, Characterization and Fuel Cell Demonstration. Fuel Cells 2004;4:147–59. doi:10.1002/fuce.200400020.

[48] Li Q, He R, Jensen JO, Bjerrum NJ. Approaches and Recent Development of Polymer Electrolyte Membranes for Fuel Cells Operating above 100 °C. Chem Mater 2003;15:4896–915. doi:10.1021/cm0310519.

[49] Li MQ, Shao ZG, Scott K. A high conductivity Cs2.5H0.5PMo12O40/polybenzimidazole (PBI)/H3PO4 composite membrane for proton-exchange membrane fuel cells operating at high temperature. J Power Sources 2008;183:69–75.

doi:10.1016/j.jpowsour.2008.04.093.

[50] Peighambardoust SJ, Rowshanzamir S, Amjadi M. Review of the proton exchange membranes for fuel cell applications. vol. 35. Elsevier Ltd; 2010. doi:10.1016/j.ijhydene.2010.05.017.

[51] Motupally S, Becker AJ, Weidner JW. Diffusion of Water in Nafion 115 Membranes. J Electrochem Soc 2000;147:3171. doi:10.1149/1.1393879.

[52] Rikukawa M, Sanui K. Proton-conducting polymer electrolyte membranes based on hydrocarbon polymers. Prog Polym Sci 2000;25:1463–502. doi:10.1016/S0079-6700(00)00032-0.

[53] Smitha B, Sridhar S, Khan AA. Solid polymer electrolyte membranes for fuel cell applications—a review. J Memb Sci 2005;259:10–26. doi:10.1016/J.MEMSCI.2005.01.035.

[54] Donoso P, Gorecki W, Berthier C, Defendini F, Poinsignon C, Armand MB. NMR, conductivity and neutron scattering investigation of ionic dynamics in the anhydrous polymer protonic conductor PEO(H3PO4)x). Solid State Ionics 1988;28–30:969–74. doi:10.1016/0167-2738(88)90313-X.

[55] Petty-Weeks S, Zupancic JJ, Swedo JR. Proton conducting interpenetrating polymer networks. Solid State Ionics 1988;31:117–25. doi:10.1016/0167-2738(88)90295-0.

[56] Stevens JR, Wieczorek W, Raducha D, Jeffrey KR. Proton conducting gel/H3PO4 electrolytes. Solid State Ionics 1997;97:347–58. doi:10.1016/S0167-2738(97)00036-2.

[57] Tanaka R, Yamamoto H, Shono A, Kubo K, Sakurai M. Proton conducting behavior in non-crosslinked and crosslinked polyethylenimine with excess phosphoric acid. Electrochim Acta 2000;45:1385–9. doi:10.1016/S0013-4686(99)00347-3.

[58] Steininger H, Schuster M, Kreuer KD, Kaltbeitzel A, Bingöl B, Meyer WH, et al. Intermediate temperature proton conductors for PEM fuel cells based on phosphonic acid as protogenic group: A progress report. Phys Chem Chem Phys 2007;9:1764–73. doi:10.1039/B618686F.

[59] Glipa X, Bonnet B, Mula B, Jones DJ, Rozière J. Investigation of the conduction properties of phosphoric and sulfuric acid doped polybenzimidazole. J Mater Chem 1999;9:3045–9. doi:10.1039/a906060j.

[60] Savadogo O, Xing B. Hydrogen/oxygen polymer electrolyte membrane fuel cell (PEMFC) based on acid-doped polybenzimidazole (PBI). J New Mater Electrochem Syst 2000;3:343–7. doi:10.1016/S1388-2481(00)00107-7.

[61] Rozière J, Jones DJ, Marrony Ma, Glipa X, Mula B. On the doping of sulfonated polybenzimidazole with strong bases. Solid State Ionics 2001;145:61–8. doi:10.1016/S0167-2738(01)00914-6.

[62] Jang MY, Yamazaki Y. Preparation, characterization and proton conductivity of membrane based on zirconium tricarboxybutylphosphonate and polybenzimidazole for fuel cells. Solid State Ionics 2004;167:107–12. doi:10.1016/J.SSI.2003.12.003.

[63] Kohama S, Gong J, Kimura K, Yamazaki S, Uchida T, Shimamura K, et al. Morphology control of poly(2,2′-phenylene-5,5′-bibenzimidazole) by reaction-induced crystallization during polymerization. Polymer (Guildf) 2008;49:1783–91. doi:10.1016/J.POLYMER.2008.02.016.

[64] Bae JM, Honma I, Murata M, Yamamoto T, Rikukawa M, Ogata N. Properties of selected sulfonated polymers as proton-conducting electrolytes for polymer electrolyte fuel cells. Solid State Ionics 2002;147:189–94. doi:10.1016/S0167-2738(02)00011-5.

[65] Glipa X, El Haddad M, Jones DJ, Rozière J. Synthesis and characterisation of sulfonated polybenzimidazole: a highly conducting proton exchange polymer. Solid State Ionics 1997;97:323–31. doi:10.1016/S0167-2738(97)00032-5.

[66] Kawahara M, Rikukawa M, Sanui K, Ogata N. Synthesis and proton conductivity of sulfopropylated poly(benzimidazole) films. Solid State Ionics 2000;136–137:1193–6. doi:10.1016/S0167-2738(00)00596-8.

[67] Asensio JA, Borrós S, Gómez-Romero P. Proton-conducting polymers based on benzimidazoles and sulfonated benzimidazoles. J Polym Sci Part A Polym Chem 2002;40:3703–10. doi:10.1002/pola.10451.

[68] Bouchet R, Siebert E, Vitter G. Acid-Doped Polybenzimidazole as the Membrane of Electrochemical Hydrogen Sensors. J Electrochem Soc 1997;144:L95. doi:10.1149/1.1837622.

[69] Bouchet R, Siebert E, Vitter G. Polybenzimidazole-Based Hydrogen Sensors I. Mechanism of Response with an E-TEK Gas Diffusion Electrode. J Electrochem Soc 2000;147:3125. doi:10.1149/1.1393869.

[70] Rathod D, Vijay M, Islam N, Kannan R, Kharul U, Kurungot S, et al. Design of an "all solid-state" supercapacitor based on phosphoric acid doped polybenzimidazole (PBI) electrolyte. J Appl Electrochem 2009;39:1097–103. doi:10.1007/s10800-008-9764-3.

[71] Asensio JA, Sánchez EM, Gómez-Romero P. Proton-conducting membranes based on benzimidazole polymers for high-temperature PEM fuel cells. A chemical quest. Chem Soc Rev 2010;39:3210. doi:10.1039/b922650h.

[72] Trouw NS. United States Patent: 4693825, 1985.

[73] Moaddel H. Development and Characterization of Polybenzimidazole as a Solid Polymer. 1996.

[74] Li Q, Jensen JO, Savinell RF, Bjerrum NJ. High temperature proton exchange membranes based on polybenzimidazoles for fuel cells. Prog Polym Sci 2009;34:449–77. doi:10.1016/j.progpolymsci.2008.12.003.

[75] Lixiang Xiao †, Haifeng Zhang, Eugene Scanlon, L. S. Ramanathan, Eui-Won Choe, Diana Rogers, et al. High-Temperature Polybenzimidazole Fuel Cell Membranes via a Sol−Gel Process 2005. doi:10.1021/CM050831+.

[76] Xiao L, Zhang H, Jana T, Scanlon E, Chen R, Choe E-W, et al. Synthesis and Characterization of Pyridine-Based Polybenzimidazoles for High Temperature Polymer Electrolyte Membrane Fuel Cell Applications. Fuel Cells 2005;5:287–95. doi:10.1002/fuce.200400067.

[77] Özdemir Y, Üregen N, Devrim Y. Polybenzimidazole based nanocomposite membranes with enhanced proton conductivity for high temperature PEM fuel cells. Int J Hydrogen Energy 2017;42:2648–57. doi:10.1016/j.ijhydene.2016.04.132.

[78] Staiti P, Minutoli M, Hocevar S. Membranes based on phosphotungstic acid and polybenzimidazole for fuel cell application. J Power Sources 2000;90:231–5. doi:10.1016/S0378-7753(00)00401-8.

[79] He RH, Li Q, Xiao G, Bjerrum NJ. Proton conductivity of phosphoric acid doped polybenzimidazole and its composites with inorganic proton conductors. J Memb Sci 2003;226:169–84. doi:10.1016/J.MEMSCI.2003.09.002.

[80] Zaidi SMJ. Preparation and characterization of composite membranes using blends of SPEEK/PBI with boron phosphate. Electrochim Acta 2005;50:4771–7. doi:10.1016/J.ELECTACTA.2005.02.027.

[81] Maity S, Singha S, Jana T. Low acid leaching PEM for fuel cell based on polybenzimidazole nanocomposites with protic ionic liquid modified silica. Polym (United Kingdom) 2015;66:76–85. doi:10.1016/j.polymer.2015.03.040.

[82] Chuang S-W, Hsu SL-C. Synthesis and properties of a new fluorine-containing polybenzimidazole for high-temperature fuel-cell applications. J Polym Sci Part A Polym Chem 2006;44:4508–13. doi:10.1002/pola.21555.

[83] Lin H-L, Yu TL, Chang WK, Cheng CP, Hu CR, Jung GB. Preparation of a low proton resistance PBI/PTFE composite membrane. J Power Sources 2007;164:481–7. doi:10.1016/J.JPOWSOUR.2006.11.036.

[84] Xing D, Kerres J. Improved performance of sulfonated polyarylene ethers for proton exchange membrane fuel cells. Polym Adv Technol 2006;17:591–7. doi:10.1002/pat.758.

[85] Kerres J, Ullrich A. Synthesis of novel engineering polymers containing basic side groups and their application in acid–base polymer blend membranes. Sep Purif Technol 2001;22–23:1–15. doi:10.1016/S1383-5866(00)00146-5.

[86] Kosmala B, Schauer J. Ion-exchange membranes prepared by blending sulfonated poly(2,6-dimethyl-1,4-phenylene oxide) with polybenzimidazole. J Appl Polym Sci 2002;85:1118–27. doi:10.1002/app.10632.

[87] Wycisk R, Lee JK, Pintauro PN. Sulfonated Polyphosphazene-Polybenzimidazole Membranes for DMFCs. J Electrochem Soc

2005;152:A892. doi:10.1149/1.1874692.

[88] Hobson LJ, Nakano Y, Ozu H, Hayase S. Targeting improved DMFC performance. J Power Sources 2002;104:79–84. doi:10.1016/S0378-7753(01)00875-8.

[89] Zhai Y, Zhang H, Zhang Y, Xing D. A novel H3PO4/Nafion–PBI composite membrane for enhanced durability of high temperature PEM fuel cells. J Power Sources 2007;169:259–64. doi:10.1016/J.JPOWSOUR.2007.03.004.

[90] Li QF, Rudbeck HC, Chromik A, Jensen JO, Pan C, Steenberg T, et al. Properties, degradation and high temperature fuel cell test of different types of PBI and PBI blend membranes. J Memb Sci 2010;347:260–70. doi:10.1016/j.memsci.2009.10.032.

[91] Davis HJ, Thomas NW. Chemical modification of polybenzimidazole semipermeable, 1975.

[92] Yamamoto T. Method for producing bridged polymer membrane and fuel cell, 2000.

[93] Xu H, Chen K, Guo X, Fang J, Yin J. Synthesis of hyperbranched polybenzimidazoles and their membrane formation. J Memb Sci 2007;288:255–60. doi:10.1016/j.memsci.2006.11.022.

[94] Sheratte MB. Linear and cross-linked polybenzimidazoles. US4154919 A, 1976.

[95] Sansone MJ. Crosslinking of polybenzimidazole polymer with divinyl sulfone. US4666996 A, 1986.

[96] Wang KY, Xiao Y, Chung T-S. Chemically modified polybenzimidazole nanofiltration membrane for the separation of electrolytes and cephalexin. Chem Eng Sci 2006;61:5807–17. doi:10.1016/J.CES.2006.04.031.

[97] Young JS, Long GS, Espinoza BF. Cross-linked polybenzimidazole membrane for gas separation, 2004.

[98] Kerres J. Covalent-Ionically Cross-linked Poly(Etheretherketone)-Basic Polysulfone Blend Ionomer Membranes. Fuel Cells 2006;6:251–60. doi:10.1002/fuce.200500207.

[99] Ergun D, Devrim Y, Bac N, Eroglu I. Phosphoric acid doped polybenzimidazole membrane for high temperature PEM fuel cell. J Appl Polym Sci 2012;124:E267–77. doi:10.1002/app.36507.

[100] Devrim Y, Devrim H, Eroglu I. Polybenzimidazole/SiO2 hybrid membranes for high temperature proton exchange membrane fuel cells. Int J Hydrogen Energy 2016;41:10044–52. doi:10.1016/j.ijhydene.2016.02.043.

[101] Osuji C. ENAS 606 : Polymer Physics Size and Mass Characterization -Non Scattering 1 Viscosity Measurements. 2009.

[102] Buckley A, Stuetz DE, Serad G. Polybenzimidazoles. Encycl. Polym. Sci. Eng. Second Edition, Wiley-Interscience; 1988, p. 572–601.

[103] ASTM D638 - Standard Test Method for Tensile Properties of Plastics n.d. http://benttram.com/Standard_ASTMD638.html (accessed November 6, 2017).

[104] Bayer T, Bishop SR, Nishihara M, Sasaki K, Lyth SM. Characterization of a graphene oxide membrane fuel cell. J Power Sources 2014;272:239–47. doi:10.1016/j.jpowsour.2014.08.071.

[105] Vyas RN, Wang B. Electrochemical analysis of conducting polymer thin films. Int J Mol Sci 2010;11:1956–72. doi:10.3390/ijms11041956.

[106] Ghosh S, Maity S, Jana T. Polybenzimidazole/silica nanocomposites: Organic-inorganic hybrid membranes for PEM fuel cell. J Mater Chem 2011;21:14897. doi:10.1039/c1jm12169c.

[107] Bayrakçeken A, Erkan S, Türker L, Eroğlu İ. Effects of membrane electrode assembly components on proton exchange membrane fuel cell performance. Int J Hydrogen Energy 2008;33:165–70. doi:10.1016/J.IJHYDENE.2007.08.021.

[108] Hazarika M, Jana T. Proton Exchange Membrane Developed from Novel Blends of Polybenzimidazole and Poly(vinyl-1,2,4-triazole). ACS Appl Mater Interfaces 2012;4:5256–65. doi:10.1021/am301185b.

[109] Grobelny J, Rice DM, Karasz FE, MacKnight WJ. High-resolution solid-state carbon-13 nuclear magnetic resonance study of polybenzimidazole/polyimide blends. Macromolecules 1990;23:2139–44.

doi:10.1021/ma00210a007.

[110] Ergun D. HIGH TEMPERATURE PROTON EXCHANGE MEMBRANE FUEL CELLS. Middle East Technical University, 2009.

[111] Seel DC, Benicewicz BC, Xiao L, Schmidt TJ, Seel DC, Benicewicz BC, et al. High-temperature polybenzimidazol-based membranes. Handb. Fuel Cells, Chichester, UK: John Wiley & Sons, Ltd; 2010. doi:10.1002/9780470974001.f500019.

[112] Molleo M. Polybenzimidazole Membranes with Enhanced Mechanical Properties for Extended Lifetime Electrochemical Applications. University of South Carolina, 2013.

[113] Li X, Singh RP, Dudeck KW, Berchtold KA, Benicewicz BC. Influence of polybenzimidazole main chain structure on H2/CO2 separation at elevated temperatures. J Memb Sci 2014;461:59–68. doi:10.1016/j.memsci.2014.03.008.

[114] Aili D, Cleemann LN, Li Q, Jensen JO, Christensen E, Bjerrum NJ. Thermal curing of PBI membranes for high temperature PEM fuel cells. J Mater Chem 2012;22:5444. doi:10.1039/c2jm14774b.

[115] Xu C, Cao Y, Kumar R, Wu X, Wang X, Scott K. A polybenzimidazole/sulfonated graphite oxide composite membrane for high temperature polymer electrolyte membrane fuel cells. J Mater Chem 2011;21:11359. doi:10.1039/c1jm11159k.

[116] Matias TB, Asato GH, Ramasco BT, Botta WJ, Kiminami CS, Bolfarini C. Processing and characterization of amorphous magnesium based alloy for application in biomedical implants. J Mater Res Technol 2014;3:203–9. doi:10.1016/j.jmrt.2014.03.007.

[117] Arrieta C, David E, Dolez P, Vu-Khanh T. X-ray diffraction, Raman, and differential thermal analyses of the thermal aging of a Kevlar®-PBI blend fabric. Polym Compos 2011;32:362–7. doi:10.1002/pc.21041.

[118] Carollo A, Quartarone E, Tomasi C, Mustarelli P, Belotti F, Magistris A, et al. Developments of new proton conducting membranes based on different polybenzimidazole structures for fuel cells applications. vol. 160. 2006.

doi:10.1016/j.jpowsour.2006.01.081.

[119] Lu W, Zhang G, Li J, Hao J, Wei F, Li W, et al. Polybenzimidazole-crosslinked poly(vinylbenzyl chloride) with quaternary 1,4-diazabicyclo (2.2.2) octane groups as high-performance anion exchange membrane for fuel cells. J Power Sources 2015;296:204–14. doi:10.1016/j.jpowsour.2015.07.048.

[120] Rewar AS, Chaudhari HD, Illathvalappil R, Sreekumar K, Kharul UK. New approach of blending polymeric ionic liquid with polybenzimidazole (PBI) for enhancing physical and electrochemical properties. J Mater Chem A 2014;2:14449. doi:10.1039/C4TA02184C.

[121] Li Q, He R, Berg RW, Hjuler HA, Bjerrum NJ. Water uptake and acid doping of polybenzimidazoles as electrolyte membranes for fuel cells. Solid State Ionics 2004;168:177–85. doi:10.1016/j.ssi.2004.02.013.

[122] Pu H, Liu L, Chang Z, Yuan J. Organic/inorganic composite membranes based on polybenzimidazole and nano-SiO2. Electrochim Acta 2009;54:7536–41. doi:10.1016/j.electacta.2009.08.011.

[123] Abdelkader AF, White JR. Water absorption in epoxy resins: The effects of the crosslinking agent and curing temperature. J Appl Polym Sci 2005;98:2544–9. doi:10.1002/app.22400.

[124] Søndergaard T, Cleemann LN, Becker H, Aili D, Steenberg T, Hjuler HA, et al. Long-term durability of HT-PEM fuel cells based on thermally cross-linked polybenzimidazole. J Power Sources 2017;342:570–8. doi:10.1016/j.jpowsour.2016.12.075.

[125] Kulkarni M, Potrekar R, Kulkarni RA, Vernekar SP. Synthesis and characterization of novel polybenzimidazoles bearing pendant phenoxyamine groups. J Polym Sci Part A Polym Chem 2008;46:5776–93. doi:10.1002/pola.22892.

[126] Tripathi G, Srivastava D. Effect of carboxyl-terminated poly(butadiene-co-acrylonitrile) (CTBN) concentration on thermal and mechanical properties of binary blends of diglycidyl ether of bisphenol-A (DGEBA) epoxy resin. Mater Sci Eng A 2007;443:262–9. doi:10.1016/j.msea.2006.09.031.

[127] Vilekar SA, Datta R. The effect of hydrogen crossover on open-circuit voltage in polymer electrolyte membrane fuel cells. J Power Sources 2010;195:2241–7. doi:10.1016/j.jpowsour.2009.10.023.

[128] EXPERIMENT 2.3 FOURIER-TRANSFORM INFRARED SPECTROSCOPY. n.d.

[129] Bisphenol A diglycidyl ether n.d. http://webbook.nist.gov/cgi/cbook.cgi?ID=C1675543&Mask=80#IR-Spec (accessed November 7, 2017).

APPENDIX A

Phosphoric acid doping to PBI based membranes

Sample Calculation of acid doping level (ADL):

- Acid doping of PBI-BADGE-2.5 membrane

Initial weight of the membrane: 0.2667 g

After two weeks of doping, acid doped membrane weight: 1.4780 g

$$ADL = \frac{1.4780 - 0.2667}{0.2667} \times \frac{\frac{308gPBI}{RU\ of\ PBI}}{98g\ H_3PO_4/molH_3PO_4} = 14.3$$

Doping Level changing by time:

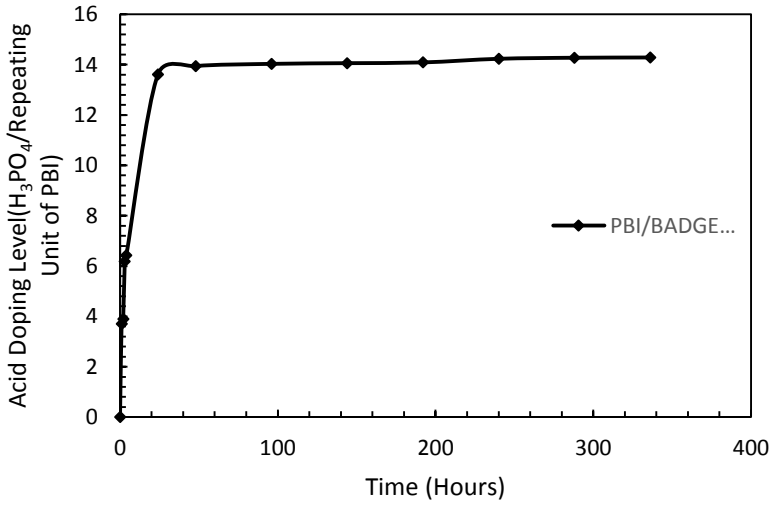

Acid Retention Tests of PBI based membranes

Sample Calculation of acid leaching percentage:

- Acid leaching of PBI-BADGE-2.5 membrane

Initial membrane weight: 0.2406g

Initial acid doped membrane weight: 1.2452g

Final membrane weight (After 5 hours of acid leaching test): 0.3921g

Loss of H_3PO_4: $1.2452 - 0.3931 = 0.7806g$

Amount H_3PO_4 doped initialy: $1.2452 - 0.2406 = 1.0046g$

$$Acid\ Leaching\ Percentage = \frac{0.7806g}{1.0046g} \times 100 = 77.7 \cong 78$$

APPENDIX B

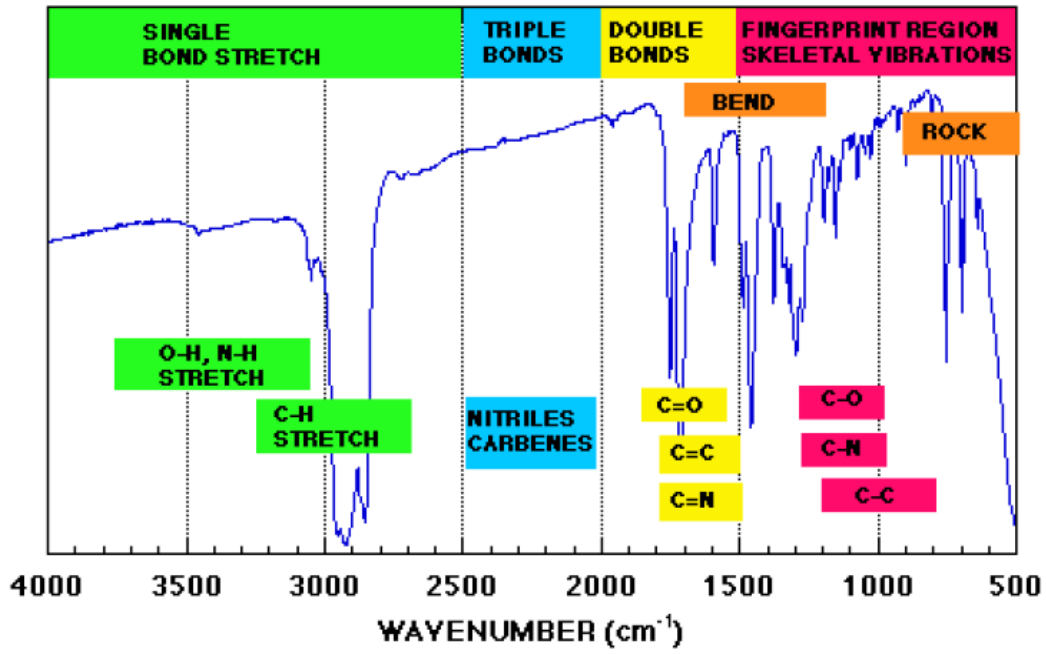

Figure 43 Spectrum map for bond responses [128]

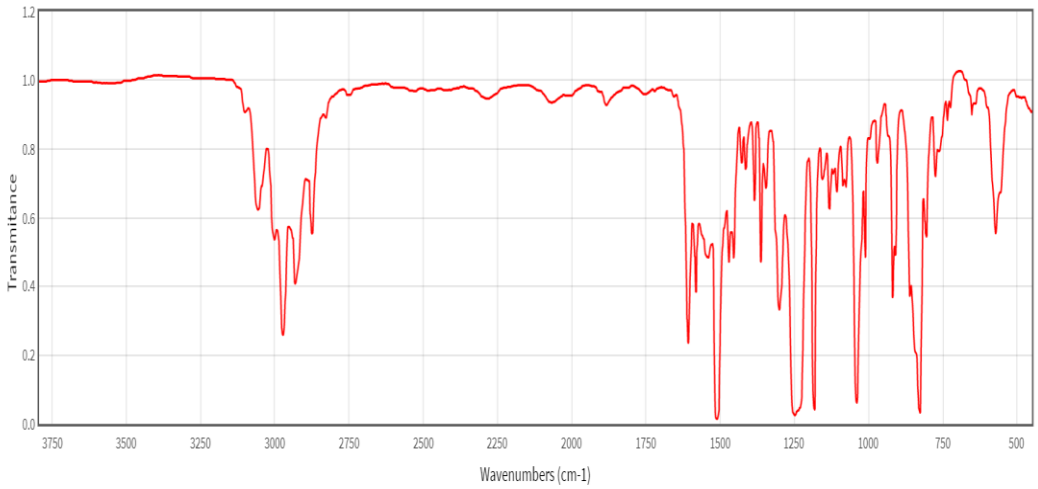

Figure 44 FTIR Spectrum of BADGE [129]